Polyurethane films, foams and nanocomposites prepared from vegetable oil-based polyols

by

Chaoqun Zhang

A dissertation submitted to the graduate faculty

in partial fulfillment of the requirements for the degree of

DOCTOR OF PHILOSOPHY

Major: Materials Science and Engineering

Program of Study Committee:
Michael R. Kessler, Major Professor
Xiaoli Tan
Jason S. Chen
Pranav Shrotriya
Samy Madbouly

Iowa State University

Ames, Iowa

2014

TABLE OF CONTENTS

ACKNOWLEDGEMENTS

I would like to express my sincere gratitude to my advisor Dr. Michael R. Kessler, for his guidance, support and patience throughout my PhD studies and research period. All his help made it possible for me to complete this project and this dissertation.

I appreciate my committee members Dr. Xiaoli Tan, Dr. Jason Chen, Dr. Pranav Shrotriya, and Dr. Samy Madbouly for their technique guidance and helpful suggestions. I would like to thank Dr. Shu Xu, Dr. Patrick A. Johnston, Jerry L. Amenson, Warren E, Straszheim, Tracey M, Pepper for their valuable technical support.

My sincere thanks also go to Dr. Ying Xia for helping me out at my early research period, and he taught me a lot of expertise and knowledge, which will benefit me for the whole life. I would also like to thank members of the polymer composites research group, Dr. Vijay Kumar, Dr. Hongyu Cui, Dr. Peter Hondred, Dr. Eliseo De León, Dr, Mahendra Thunga, Dr. James A Bergman, Ruqi Chen, Rui Ding, Danny Vennerberg, Yuzhan Li, and Hongchao Wu, for creating an enjoyable working environment.

Funding support from Kumho petrochemical is gratefully acknowledged.

Finally, I would like to thank my family for their loving support and encouragement. Last, but not the least, I would also like to thank my wife, Ling Yuan for her accompany, love and support.

ABSTRACT

Polyurethanes (PUs) have been widely used in coatings, adhesives, sealants, and foams. Historically, the raw materials of a PU, polyol and isocyanate, were derived from petroleum. Nowadays, the increasing concerns regarding the depletion of petroleum resources and environmental problems caused by fossil fuels, has triggered great interest in the development of monomers based on renewable resources for PU production. In this project, a novel solvent-free/catalyst-free method was developed to prepare polyols from epoxidized soybean oil and castor oil for PU production. The effects of reaction temperature, reaction time, and reaction ratios of carboxyl acid and epoxy groups on the properties of the resulting polyols were investigated. Moreover, the properties of final PUs were compared with that from castor oil and methoxylated soybean oil polyol.

To validate the versatility of this approach, this method was extended to other vegetable oils systems. Polyols with a broad functionality were prepared by castor oil fatty acid initiating ring opening reaction of various epoxidized vegetable oils, which were prepared with formic acid and hydrogen peroxide. The effect of the polyols' structure on the thermal, mechanical, and shape memory properties of the resulting PU was studied.

Possible catalysts (DBU, Pyridine) were found that could promote the ring opening reaction in this method by decreasing the reaction temperature and reaction time. The ring opening reaction kinetic for the vegetable oil systems was investigated by dynamic differential scanning calorimetry. The effect of DBU on the structure of polyols was studied as well as the properties of PU.

The polyols prepared by this novel method were used to prepare PU foam for potential application in automobile seat cushions. The compatibility between this vegetable oil-based polyol and a petroleum-based polyol was investigated by solution tests and theoretical prediction. The effect of bio-component on the physical, mechanical, thermal stability, and thermal conductivity of resulting PU was investigated.

Also, two approaches were proposed to modify lignin to compatibilize them with PU matrix for preparation of PU nanocomposites. The effects of this cheap and abundant renewable filler on the thermo-mechanical and dielectric properties of the final PU composites were studied.

In order to increase the hydroxyl numbers of vegetable oil-based polyols, another method was developed for high performance PUs. A strong reductant, $LiAlH_4$, was used to reduce the ether and epoxy groups in epoxidized vegetable oils to prepare high functionality bio-polyols. The properties of the final PU based on those novel polyols were characterized and compared with that from a petroleum-based polyol.

Finally, carbon nanotubes were incorporated into the PU matrix to improve the thermo-mechanical properties of nanocomposites. The surface of carbon nanotube was functionalized with an amine group, which formed a covalent bond with the PUs. The loading effect of carbon nanotube on the properties of the resulting PU was investigated.

CHAPTER 1: GENERAL INTRODUCTION

1.1 Introduction

Polyurethanes (PUs) are versatile polymeric material with various advantages, such as their excellent abrasion resistance, high toughness, chemical resistance, and low film-forming temperatures and has been widely used in coating, foam, adhesives, and composites[1-4]. Historically, petroleum has been the feedstock for polyols and isocyanates for the production of PU. Over the past decade, depleting fossil reserves, increasing petroleum prices, and environmental concerns have triggered growing interest in the development of biorenewable feedstocks (such as cellulose, starch, proteins, natural oils and sugar) to substitute petrochemically derived components in the production of PUs. Of these, vegetable oils are among the most promising because they are readily available in vast quantities, inherently sustainable, and available at relatively low cost[5-7].

Vegetable oils are triglycerides formed between glycerin and different fatty acids (structure shown in Figure 1.1), containing anywhere from 8 to 24 carbons and 0 to 7 carbon-carbon double bonds. The structures of the most common fatty acids found in vegetable oils are given in Table 1.1[7]. What distinguishes one vegetable oil from another is their fatty acid composition. Table 1.2 gives the fatty acid composition of selected vegetable oils, as well as the number of carbon-carbon double bonds per triglyceride.

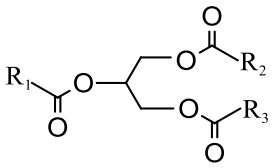

Figure 1.1 Triglyceride structure (R1, R2, R3 represents fatty acid side chains)

The (C *x*:*y*) nomenclature in Table 1.1 corresponds to the composition of the fatty acid, where *x* = the number of carbon atoms in the fatty acid chain; *y* = the number of carbon-carbon double bonds in the fatty acids. Different vegetable oils contain different composition of fatty acids depending on the plant type and climatic conditions of harvest.

Table 1.1 Six common fatty acids composition in vegetable oils

Fatty acids	Structure
Palmitc (C16:0)	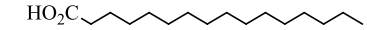
Stearic (C 18:0)	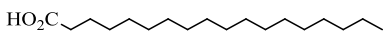
Oleic (C 18:1)	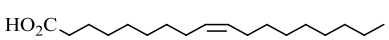
Linoleic (C 18:2)	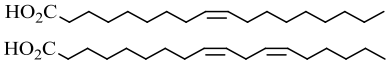
Linolenic (C 18:3)	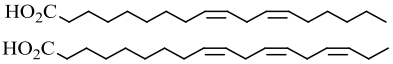
Ricinoleic (C18:1 OH)	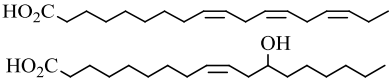

Table 1.2 Degree of unsaturation, composition of common vegetable oils

	Double bonds	Fatty acid composition (%)				
		C 16:0	C 18:0	C 18:1	C 18:2	C 18:3
Castor	3.0	1.5	0.5	5.0	4.0	0.5
Corn	4.5	10.9	2.0	25.4	59.6	1.2
linseed	6.6	5.5	3.5	19.1	15.3	56.6
Olive	2.8	13.7	2.5	71.1	10.0	0.6
Palm	1.7	42.8	4.2	40.5	10.1	-
Soybean	4.6	11.0	4.0	23.4	53.3	7.8
Canola	3.9	4.1	1.8	60.9	21.0	8.8

With the exception of castor oil, nearly all vegetable oils do not naturally contain the hydroxyl groups necessary to produce polyurethanes. Many methods were developed to incorporate hydroxyl groups to produce polyols for PU production. Generally, the reactive sites within vegetable oils, such as carbon-carbon double bonds and the ester functionality, allow for the introduction of such groups. For example, epoxidation of carbon carbon double bonds in backbone chains of vegetable oils, followed by oxirane ring opening is one of the most important and widely studied reactions to produce various polyols with different functionalities. The properties of polyols can be tailored by selection of appropriated ring opening agents, such as amines, carboxylic acids/halogenated acids, or alcohols[8-11]. Ozonolysis of carbon carbon double

bonds into ozonides, followed by reduction to alcohol, can create polyols containing primary hydroxyl groups with three times higher reactivity towards isocyanates than secondary groups. Moreover, the terminal hydroxyl groups prepared by this method would make all the backbone chains of polyols in the resulting polyurethane network and reduce the dangling chains of macromolecure, therefore resulting in better thermomechanical properties of polymer[12]. Primary hydroxyl groups can also be introduced by hydroformylation/reduction with syngas (CO/H_2) catalyzed by rhodium or cobalt carbonyl complexes[13, 14]. Some scientists found approaches to conduct transesterification of ether groups in vegetable oils with alcohols or amines. Also, the hydroxyl numbers of the final polyols could be tailored by choosing alcohols or amines or controlling the degree of transesterification[15, 16]. Nowadays, several methods combining strategies discussed above have been developed to prepared polyols with high functionalities. For example, The ring opening reaction of epoxy groups in epoxidized vegetable oils and transterification with triglyceride were spontaneous initiated by 1, 3-proprnediol[17]. Ring-opening polymerization of epoxidized methyl oleate followed by reduction of the ester groups were developed to prepare oligomeric polyether polyols[18].

Vegetable oil-based polyols are one of most promising monomer, which can react with diisocyanates to prepare PU coatings, foams, and adhesives. Due to the hydrophobic nature of the triglycerides from which they are derived, vegetable oil based PUs exhibit excellent physical and thermal stability properties, and therefore may find application in protective coatings, building construction, and medical device as partial or total replacements for petroleum-based counterparts in future[19-21].

1.2 Dissertation Organization

This dissertation is divided into nine chapters. Chapter two to chapter eight contains content that have either been published in or submitted to scholarly journals. Chapter one simply describes the general research background and research objective of the thesis. Chapter two covers the novel solvent-free/catalyst-free method developed to prepare 100% bio-based polyols for PU production. Chapter three studies the extension of this novel method to other vegetable oil systems for various PU with broad properties. Chapter four involves the reaction kinetic of the ring opening reaction in this novel method and the effect of possible catalysts on the properties of final polyols and PUs. Chapter five discusses the preparation of PU foam from blends of a vegetable oil-based polyol and a petroleum-based polyol. Chapter six presents the preparation of PU nanocomposites from polyols discussed above reinforced with modified lignin as fillers. Chapter seven presents another method to prepare high functionalities polyols using strong reducing agents for PU matrix. Chapter eight discusses the synthesis of PU/CNT nanocomposites from polyols developed in chapter seven. Chapter night gives general conclusions drawn through this project.

1.3 Research Objective

The primary objective of this thesis is to develop easy-processing methods to prepare novel vegetable oil-based polyols, which is promising in mass PU production, investigate the compatibility of these vegetable oil-based polyols with petroleum-based polyols currently used in polyurethane production, and evaluate the thermal and mechanical properties of the resulting PU films, and PU foams made from these bio-polyols or blends of bio-polyols with petroleum-based polyols. Also, this study investigates the effect of nano-fillers on the thermo-mechanical properties of PU composites for greener and stronger polymeric materials.

1.4 Reference

1. Z. S. Petrovic, *Polym Rev*, 2008, **48**, 109-155.
2. D. P. Pfister, Y. Xia and R. C. Larock, *Chemsuschem*, 2011, **4**, 703-717.
3. C. K. Williams and M. A. Hillmyer, *Polym Rev*, 2008, **48**, 1-10.
4. M. Desroches, M. Escouvois, R. Auvergne, S. Caillol and B. Boutevin, *Polym Rev*, 2012, **52**, 38-79.
5. J. Argyropoulos, P. Popa, G. Spilman, D. Bhattacharjee and W. Koonce, *J Coat Technol Res*, 2009, **6**, 501-508.
6. A. Gandini, *Macromolecules*, 2008, **41**, 9491-9504.
7. Y. Xia and R. C. Larock, *Green Chem*, 2010, **12**, 1893-1909.
8. A. Guo, Y. J. Cho and Z. S. Petrovic, *J Polym Sci Pol Chem*, 2000, **38**, 3900-3910.
9. X. Pan and D. C. Webster, *Chemsuschem*, 2012, **5**, 419-429.
10. D. S. Tathe and R. N. Jagtap, *J Am Oil Chem Soc*, 2013, **90**, 1405-1413.
11. C. S. Wang, L. T. Yang, B. L. Ni and G. Shi, *J Appl Polym Sci*, 2009, **114**, 125-131.
12. Z. S. Petrovic, W. Zhang and I. Javni, *Biomacromolecules*, 2005, **6**, 713-719.
13. U. Biermann, W. Friedt, S. Lang, W. Luhs, G. Machmuller, J. O. Metzger, M. R. Klaas, H. J. Schafer and M. P. Schneider, *Angew Chem Int Edit*, 2000, **39**, 2206-2224.
14. A. Guo, D. Demydov, W. Zhang and Z. S. Petrovic, *J Polym Environ*, 2002, **10**, 49-52.
15. A. Fridrihsone, U. Stirna, B. Lazdina, M. Misane and D. Vilsone, *Eur Polym J*, 2013, **49**, 1204-1214.
16. S. D. Miao, S. P. Zhang, Z. G. Su and P. Wang, *J Appl Polym Sci*, 2013, **127**, 1929-1936.
17. X. H. Kong, G. G. Liu, H. Qi and J. M. Curtis, *Prog Org Coat*, 2013, **76**, 1151-1160.
18. G. Lligadas, J. C. Ronda, M. Galia, U. Biermann and J. O. Metzger, *J Polym Sci Pol Chem*, 2006, **44**, 634-645.
19. Y. S. Lu and R. C. Larock, *Biomacromolecules*, 2008, **9**, 3332-3340.

20. L. Zhang, H. K. Jeon, J. Malsam, R. Herrington and C. W. Macosko, *Polymer*, 2007, **48**, 6656-6667.

21. N. Supanchaiyamat, P. S. Shuttleworth, A. J. Hunt, J. H. Clark and A. S. Matharu, *Green Chem*, 2012, **14**, 1759-1765.

CHAPTER 2: SOY-CASTOR OIL BASED POLYOLS PREPARED USING A SOLVENT-FREE AND CATALYST FREE METHOD AND POLYURETHANE THEREFROM

A paper published in Green Chemistry, 2013, 15, 1477-1484

Chaoqun Zhang[a], Ying Xia[a], Ruqi Chen[a], Seungmoo Huh[e], Patrick A. Johnston[c], Michael R. Kessler[a,b,d,*]

[a] Dept. of Materials Science and Engineering, Iowa State University, Ames, IA, USA

[b] Dept. of Mechanical Engineering, Iowa State University, Ames, IA, USA

[c] Center for Sustainable Environmental Technologies, Iowa State University, Ames, IA, USA

[d] Ames Laboratory, US Dept. of Energy, Ames, IA, United States

[e] Kumho Petrochemical R&BD Center, Daejeon, South Korea

[*] Author for correspondence

2.1 Abstract

Bio-based polyols from epoxidized soybean oil and castor oil fatty acid were developed using an environmentally friendly, solvent-free/catalyst-free method. The effects of the molar ratios of the carboxyl to the epoxy groups, reaction time, and reaction temperature on the polyols' structures were systematically studied. Subsequently, polyurethane films were prepared from these green polyols. Properties of the new, soy-castor oil based polyurethane films were compared with two other polyurethane films prepared from castor oil and methoxylated soybean oil polyol, respectively. Thermal and mechanical tests showed that the polyurethane films prepared from the new polyols exhibited higher glass transition temperatures, tensile strength, Young's modulus, and thermal stability because of the higher degree of crosslinking in the new polyols. Moreover, the novel polyols, prepared using the solvent-free and catalyst-free synthetic route, were 100%

bio-based and facilitate a more environmentally friendly and economical process than conventional soy-based polyols used for polyurethane production.

2.2 Introduction

Environmental concerns and the increasing price of crude oil have triggered great interest in the development of materials based on renewable resources, such as cellulose, starch, natural oils, and sugars. Vegetable oils are among the most promising options; they offer excellent properties, including ready availability, inherent sustainability, and relatively low cost.[1, 2] Vegetable oils are triglycerides, formed from glycerol and three fatty acids. The most common fatty acids are:

- Saturated: palmitic (C16:0)[1] and stearic (C18:0),
- Unsaturated: oleic (C18:1), linoleic (C18:2), and linolenic (C18:3).

Some fatty acids have specific functional groups, such as hydroxyl-containing ricinoleic acid (C18:1 OH). In all vegetable oils the general reactive sites are esters and carbon-carbon double bonds, which can be modified to give a variety of monomers.[3]

Polyurethanes (PUs) are an important class of polymers and exhibit an exceptionally versatile range of properties and applications. In order to meet specific requirements, their structures can be tailored by selecting appropriate polyols and polyisocyanates. In industry, only a few polyisocyanates are commonly used, while a variety of polyols are available. Therefore, the choice of polyol typically determines the properties of the created polyurethane.[4] In addition to petroleum-based polyols, vegetable oils, such as soybean oil,[5] canola oil,[6, 7] palm oil,[8, 9] sunflower oil, corn oil and linseed oil,[10-12] have been extensively studied as bases for various polyols used for the manufacture of PUs with high thermal stability and mechanical properties.

[1] In this notation, the first number represents the number of carbon atoms in the fatty acid chain and the second number represents the number of carbon-carbon double bonds in the fatty acid.

However, almost all these vegetable oil-based polyols were prepared using large amounts of solvents, which increases both process cost and environmental burden.

Soybean oil and castor oil are two important vegetable oils offering a wide range of advantages. Currently, the US is the top producer of soybean oil in the world.[3] Soybean oil contains a high number of double bonds, opening a variety of potential modification routes. Epoxidation and subsequent oxirane ring opening is a common method to prepare polyols from soybean oil using alcohols, inorganic acids, and hydrogenation for ring opening. For example, Petrovic et al. developed PUs ranging widely from soft and rubbery to hard and glassy using HX (X = -Br, -Cl, -CH_3O, -H) to open the epoxide rings in the oils.[13, 14] Wang prepared a series of polyols from epoxidized soybean oil (ESBO) using 1, 2-ethanediol and 1, 2-propanediol to open the epoxidized rings; they studied the effect of the OH numbers in these polyols on thermal and mechanical properties of the final cast PUs.[15] Organic acids were also utilized as ring opening agents. Pan reported the use of acetic acid, propionic acid, and 2-ethylhexanoic acid to initiate epoxide ring-opening reactions in epoxidized sucrose esters of soybean oil to prepare PUs.[16] However, almost all polyols were prepared by ring-opening of epoxidized vegetable oils with petroleum-based small molecules. Castor oil, on the other hand, naturally contains hydroxyl groups (approximately 2.7 per triglyceride) and has therefore been employed extensively in polyurethane manufacturing.[17-20]

In this paper, castor oil-based fatty acid (COFA) was used to facilitate ring-opening of ESBO using a green, solvent-free/catalyst-free pathway. The polyol obtained had a higher crosslinking density than the polyols prepared from epoxide ring-opening using small molecules, resulting in better thermal and mechanical properties of the final polyurethane films. The effects of the molar ratio of the carboxyl to the epoxy groups, reaction time, and reaction temperature on the final

polyols' structure and functionalities were investigated. Proton nuclear magnetic resonance (^{1}H NMR), Fourier transform infrared spectroscopy (FTIR), gel permeation chromatography (GPC), and rheometry were used to characterize the polyols. In addition, the thermal/mechanical properties of PUs prepared from the newly developed polyols, castor oil, and methoxylated soybean oil polyol (MSOL) were compared.

2.3 Materials and Methods

2.3.1 Materials

Completely epoxidized soybean oil with approximately 4.5 oxirane rings per triglyceride was purchased from Scientific Polymer Inc., New York, NY. Magnesium sulfate ($MgSO_4$) and methyl ethyl ketone (MEK) were purchased from Fisher Scientific Company (Fair Lawn, NJ). Castor oil, hydrochloric acid, sodium hydroxide, isophorone diisocyanate (IPDI), and dibutyltin dilaurate (DBTDL) were obtained from Sigma-Aldrich (Milwaukee, WI). All materials were used as received without further purification.

2.3.2 Saponification of Castor Oil

Castor oil was saponified into fatty acid by heating with sodium hydroxide solution at 80 ^oC. Then, hydrochloric acid was added to neutralize the solution at 80 ^oC. Finally, the organic layer was purified by washing with water, drying over $MgSO_4$ and filtering, resulting in clear, light yellow castor oil fatty acids. While most of the fatty acid in castor oil is ricinoleic acid (87.7-90.4%),[20] there are some other acids such as linolenic, linoleic, oleic acid.

2.3.3 Preparation of Polyols Based on ESBO and COFA

The soy-castor oil based polyols (SCP) were prepared by ring opening reactions between ESBO and COFA. Initially, COFA and ESBO were mixed in a flask with a magnetic stirrer and maintained at 130~170 ^oC in dry nitrogen atmosphere. After several hours, a light

reddish/yellow, viscous liquid was obtained. Scheme 2-1 shows the preparation of representative green polyols.

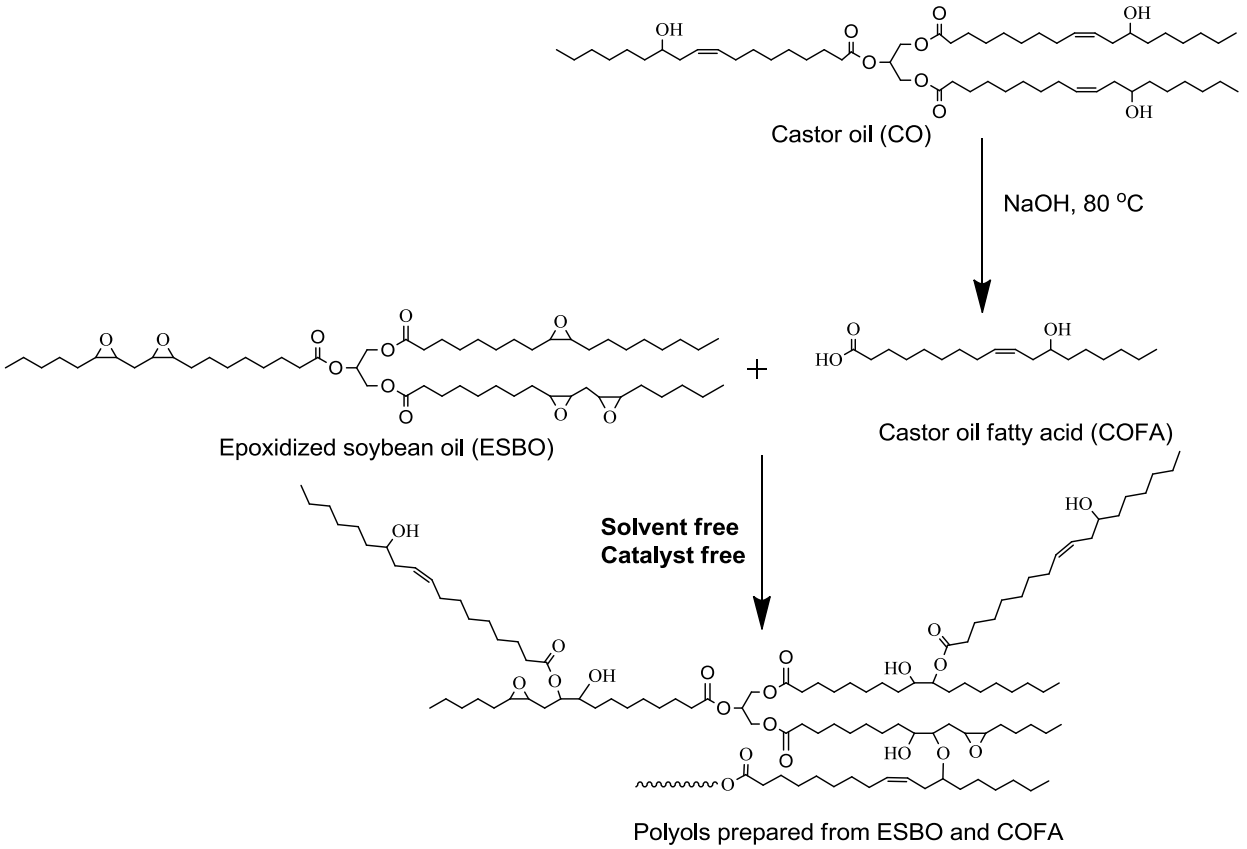

Scheme 2-1 Preparation of representative green polyols

2.3.4 Preparation of Polyurethanes Using Polyols

The polyurethanes were obtained through the reaction of polyol with a 5 % molar excess of IPDI using MEK as a solvent. The components were heated to 70 °C and mixed continuously for 3 hours. Then, the mixture was poured into a glass mold to produce 100 × 50 mm (length × width) sheets, which were dried overnight in an oven at 80 °C. Finally, the PU films were cut into specific dimensions for thermo-mechanical testing. Scheme 2-2 shows the preparation of representative polyurethanes from green polyols.

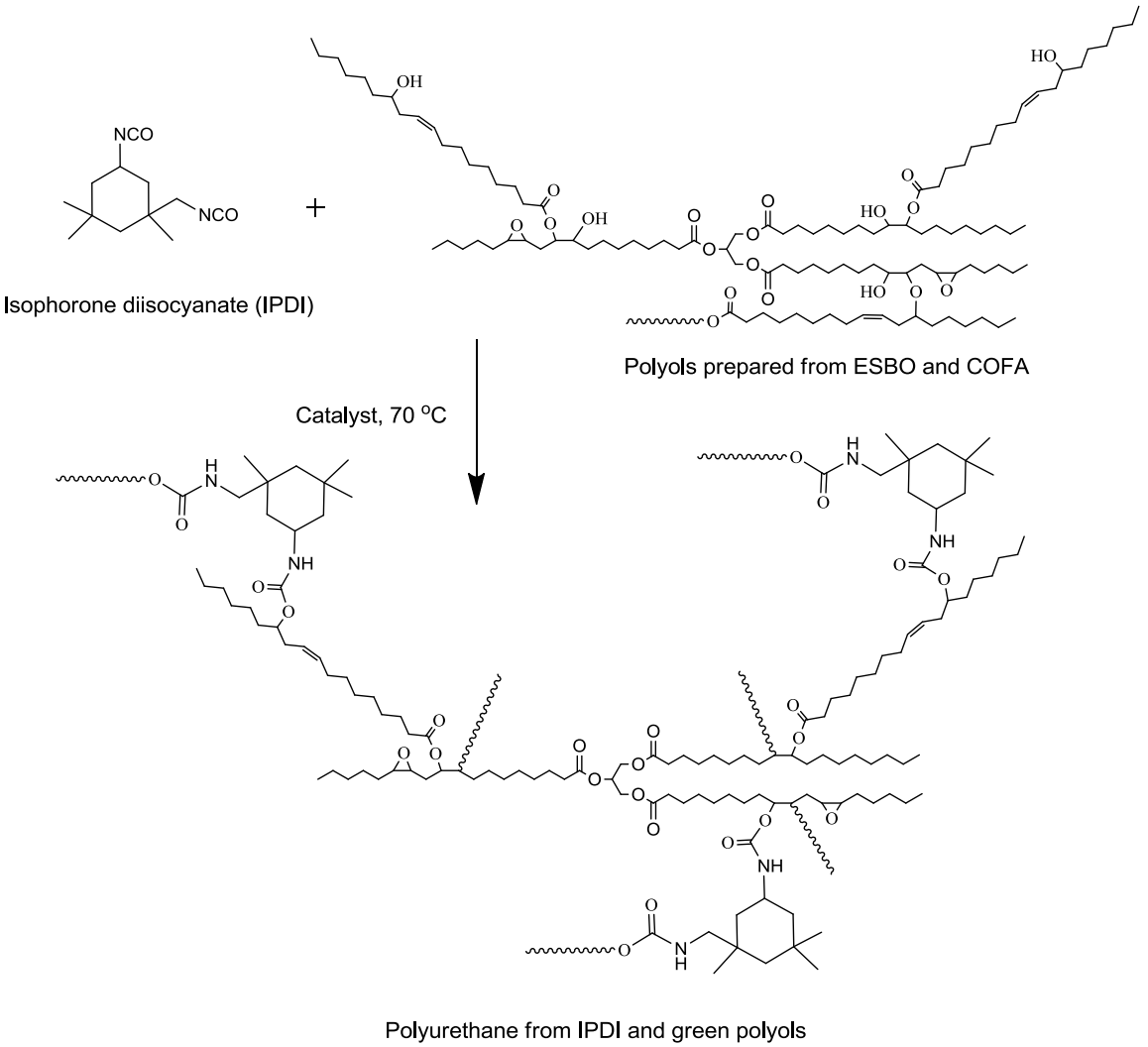

Scheme 2-2 Preparation of representative polyurethanes from green polyols

2.3.5 Characterization

A Varian spectrometer (Palo Alto, CA) at 300 MHz was used to record the ^{1}H NMR spectroscopic analysis of the monomers and final products. All measurements were made using $CDCl_3$ as the solvent. The FTIR spectra of monomers and polyols were recorded on a Nicolet 460 FTIR spectrometer (Madison, WI). Rheological experiments were conducted with an AR2000ex stress-controlled rheometer (TA Instruments) with parallel plate geometry at room temperature. The OH of the polyols were determined using the Unilever method.[21] The acid

number of the polyols were determined by AOCS Official Method Te 1a-64. The molecular weight was determined using a THF-eluted GPC equipped with a refractive index detector. The HPLC system used was a Thermo Scientific Dionex Ultimate 3000 (Sunnyvale, CA) equipped with a Shodex Refractive Index (RI). The eluent used was tetrahydrofuran with two Agilent PLgel 3µm 100Å 300 x 7.5mm (p/n PL1110-6320) and one Mesopore 300 x 7.5mm (p/n PL1113-6325). The column flow rate and temperature was 1.0 mL/min at 25°C.

Dynamic mechanical analysis (DMA) of the PU films was performed using a TA Instruments DMA Q800 dynamic mechanical analyzer with a film-tension mode of 1 Hz. Rectangular specimens of 0.6 mm × 10 mm (thickness × width) were used for the analysis. The samples were cooled and held isothermally for 3 min at –40 ^{o}C before the temperature was increased to 120 ^{o}C at a rate of 5 ^{o}C/min. The glass transition temperatures (T_gs) of the samples were obtained from the peaks of the tan δ curves.

Differential scanning calorimetry (DSC) was performed on a thermal analyzer (TA Instrument Q2000). The samples were heated from room temperature to 90 ^{o}C at a heating rate of 20 ^{o}C/min to erase their thermal history, equilibrated at –90 ^{o}C and then heated to 90 ^{o}C at a heating rate of 20 ^{o}C/min. T_gs of the samples were determined from the midpoint temperature in the heat capacity change of the second DSC scan. Samples of 5 mg were cut from the films and used for analysis.

Thermogravimetric analysis (TGA) of the films was carried out on a TA Instrument Q50 (New Castle, DE). The samples were heated from room temperature to 650 ^{o}C at a heating rate of 20 ^{o}C/min in nitrogen. Generally, 10 mg samples were used for the TGA.

The tensile properties of the PU films were determined using an Instron universal testing machine (model 4502) with a crosshead speed of 100 mm/min. Rectangular specimens of 50 mm

×10 mm (length × width) were used. Average values of at least four replicates of each sample were taken. The toughness of the polymer was obtained from the area under the corresponding tensile stress/strain curves.

2.4 Results and Discussion

2.4.1 Preparation and Properties of Soy-Castor-Based Polyol

To investigate the effects of reaction temperature, reaction time, and stoichiometry on the structures of the final polyols used in this research, four time variables (0 h, 2 h, 6 h, 8 h), four temperature variables (110 ^{o}C, 130 ^{o}C, 150 ^{o}C, 170 ^{o}C), and four ratio variables (mole ratios of carboxyl to epoxy group, 0.3:1, 0.5:1, 0.7:1, 0.9:1) were studied. For polyols prepared for different reaction times, a reaction temperature of 170 ^{o}C and mole ratios of carboxyl to epoxy group of 0.5:1 were used (these samples were identified as SCP_0h, SCP_2h, SCP_6h, SCP_8h). As shown in Figure 2-1(a), the epoxy groups in ESBO were totally ring opened in reaction time of 8 h. Therefore, a reaction time of 8 h and mole ratios of carboxyl to epoxy group of 0.5:1 were used (these samples were identified as SCP_110 ^{o}C, SCP_130 ^{o}C, SCP_150 ^{o}C, SCP_170 ^{o}C) to optimize the reaction temperature. Also, as shown in supporting information (Figure 2-1), the epoxy groups in ESBO were totally ring opened in reaction time of 8 h with a reaction temperature of 170 ^{o}C. Finally, for polyols prepared with different stoichiometries, a reaction time of 8 h and a reaction temperature of 170 ^{o}C were used (these samples were identified as SCP_0.3, SCP_0.5, SCP_0.7, SCP_0.9). More details are provided in the supporting information.

The ^{1}H-NMR spectra of polyols for different reaction times and with different ratios of carboxyl to epoxy groups are shown in Figure 2-1. With increasing reaction times as shown in Figure 2-1(a), the peaks between 2.8 and 3.2 ppm, corresponding to the epoxy groups,[22]

decreased. At the same time, new peaks were seen between 4.6 and 5.0 ppm, representing tertiary hydrogen atoms adjacent to the newly formed ester groups.[23, 24] The peaks corresponding to hydrogen bonded to carbons adjacent to the ester overlap with the peaks from the hydrogen attached to the carbon adjacent to OH (indicated as peak 3). With the exception of the sample with a ratio of 0.3:1 as shown in Figure 2-1(b), the spectra for all other samples indicated that the residual epoxy groups disappeared. Once the ratio of carboxyl group to epoxy group increased to 0.5:1 the epoxy groups underwent complete ring-opening.

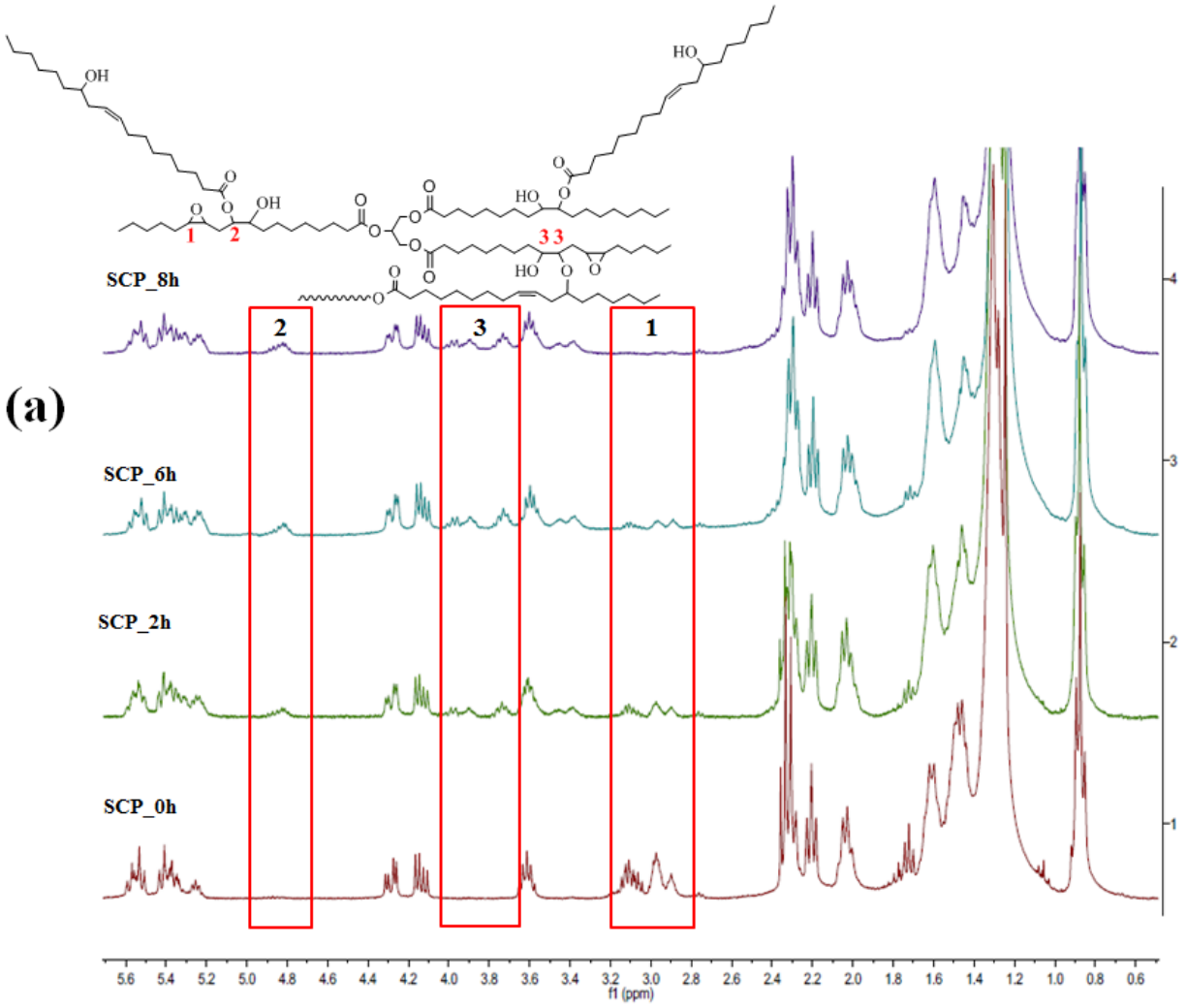

Figure 2-1 ^{1}H-NMR spectra of SCP for different reaction times (a)

Figure 2-1 continued

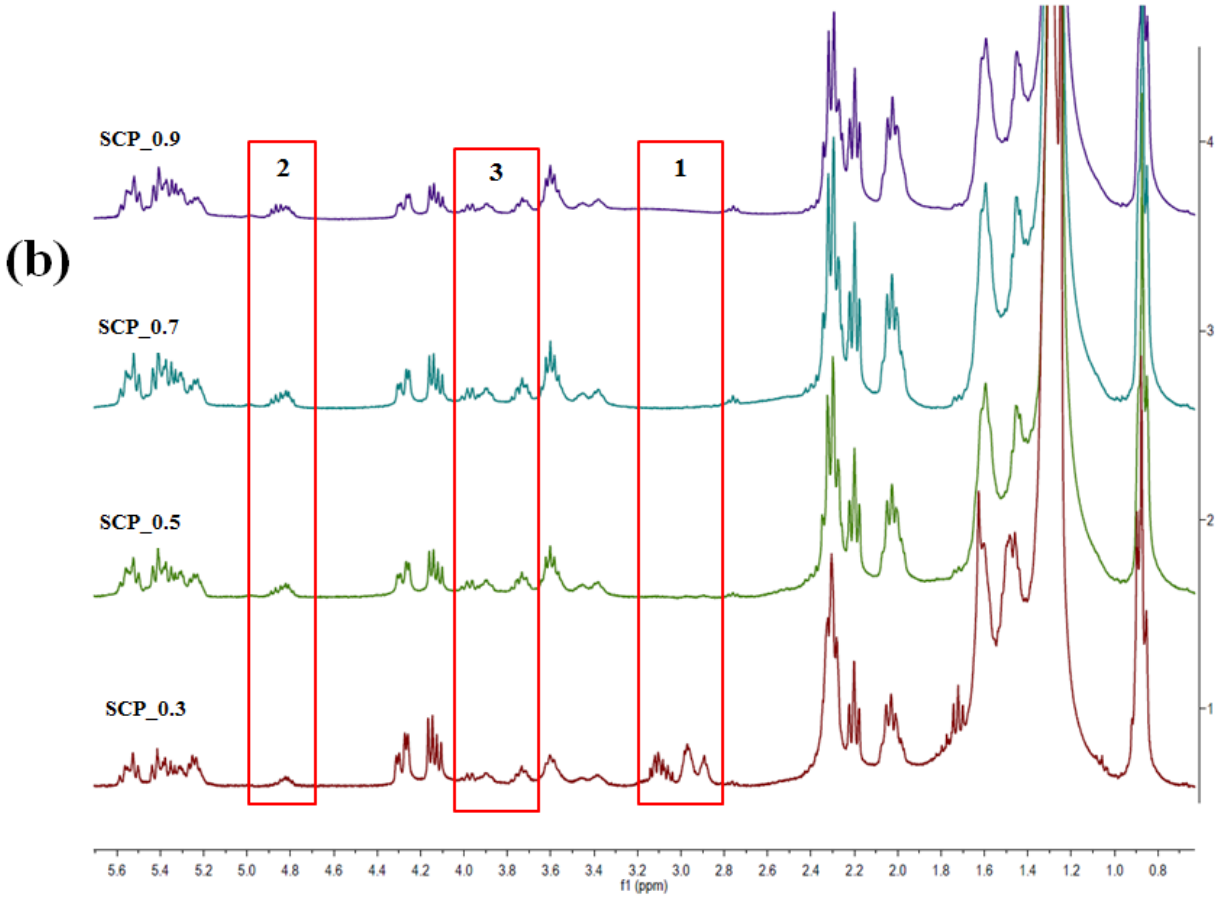

Figure 2-1 ^{1}H-NMR spectra of SCP with different ratios of carboxyl to epoxy groups (b)

GPC chromatograms of polyols with different ratios of carboxyl to epoxy groups are presented in Figure 2-2. Compared with the peaks for ESBO and COFA, which were the starting materials, the peaks of the polyols shifted to shorter retention times and became broadened, indicating increasing molecular weights. As the ratios of carboxyl to epoxy groups increased from 0.3:1 to 0.5:1, the left peak shifted to shorter retention time, indicating larger molecular weight caused by higher crosslinking levels. It indicates that at a ratio of 0.3:1, COFA did not provide sufficient functional groups to facilitate ring opening in ESBO while as the ratio of carboxyl to epoxy groups increased, more epoxy groups were ring opened by fatty acid, which also attached to ESBO. The ^{1}H-NMR results with different ratios of carboxyl to epoxy groups also confirmed this

conclusion. However, as the ratio continued to increase from 0.5:1 to 0.7:1 and 0.9:1, the GPC curves indicated unreacted COFA, because the combined number of carboxyl and hydroxyl groups was in excess of the epoxy groups for a complete reaction. It is notable that at a ratio of 0.5:1, the epoxy groups were totally ring opened and COFA were also completely consumed, which indicates the function groups reacted with an appropriate ratio. Considering there is another one OH group in COFA, which the number was almost identical with carboxyl. It is deduced that the OH groups in COFA, as well as newly formed OH in epoxides, were also involved in the ring opening reaction and possibly connected two ESBO molecules,[25, 26] leading to increasing molecular weight. During the reaction, the carboxyl groups also acted as acid catalysts. As ratio increased from 0.5:1 to 0.7:1 and 0.9:1, more carboxyl in COFA connected to ESBO, reducing the degree of connection of polyols caused by ring opening reaction by OH groups in COFA and newly formed OH in epoxides, which decreased the molecular weight. That is why the molecular weight of polyols with a ratio of 0.9:1 was lower than that with a ratio of 0.5:1 as shown in Figure 2-2.

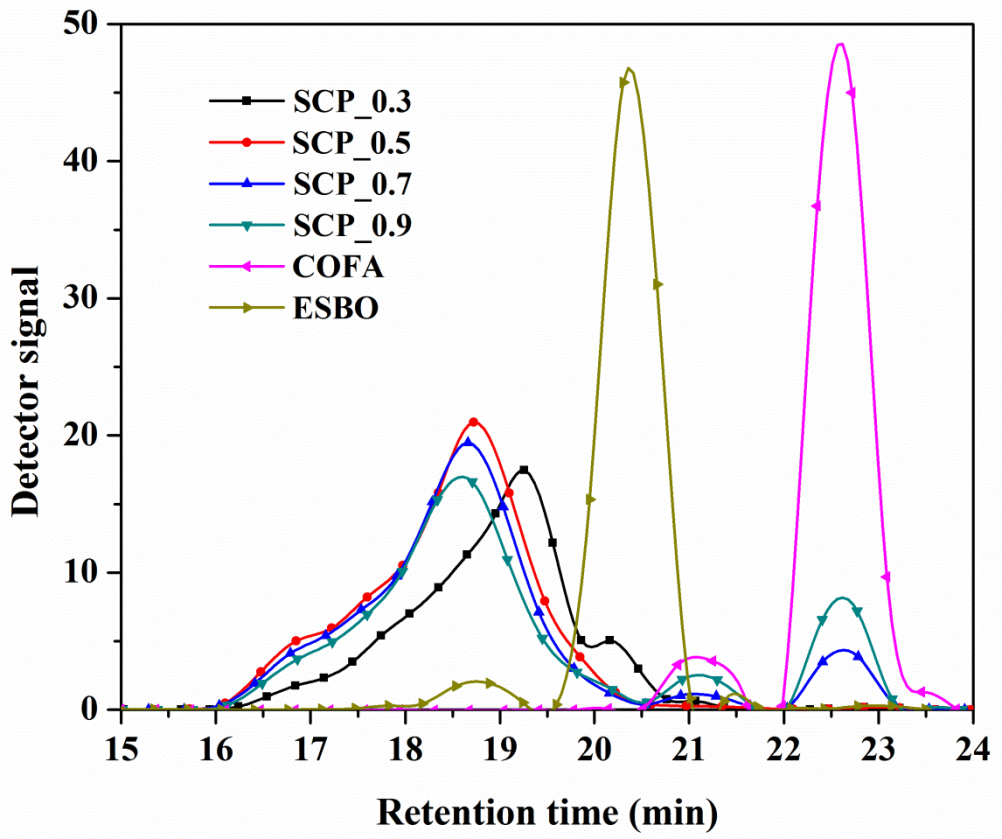

Figure 2-2 GPC curves of SCP with different ratios of carboxyl to epoxy groups

Therefore, a ratio of 0.5:1 was selected for the subsequent preparation of green, highly-crosslinked, and 100% bio-based polyols for further investigations. Other than SCP, two other polyols with similar OH numbers (castor oil and MSOL), were selected to prepare PUs for thermal/mechanical property comparisons. The MSOL was prepared following the procedure described by Guo and co-workers.[13] Table 2-1 summarizes the properties of all polyols studied. The acid numbers in Table 1 indicate that the carbonyl groups in COFA were totally consumed in SCP_0.5, which is consistent with the GPC results. Both viscosity and molecular weight values indicate that the fatty acid attached to the ESBO long chains and polyols exhibited a higher degree of cross-linking.

Table 2-1. Properties of polyols based on CO, MSOL, and SCP.

	Viscosity (Pa·s) at 30 °C with shear rate of 10/s	Number /weight average molecular weight	PDI	Acid number (mg KOH/g)	OH number (mg KOH/g)
SCP_0.3	2.4	2500/2840	1.13	-	-
SCP_0.5	9.9	2830/3260	1.15	0.8	159.7
SCP_0.7	6.9	2220/3160	1.43	-	-
SCP_0.9	5.0	1760/2850	1.64	-	-
SCP_110 °C	0.98	1110/1700	1.53	-	-
SCP_130 °C	2.5	1530/2220	1.45	-	-
SCP_150 °C	5.2	2110/2630	1.24	-	-
MSOL	-	1670/1910	1.14	0.3	164.5
Castor oil	-	-	-	0.3	162.8
ESBO	-	1420/1500	1.05	0.6	-
COFA	-	589/600	1.02	178.6	-

- Polydispersity index (PDI)

2.4.2 Polyurethane Properties

Figure 2-3 shows storage modulus and loss factor as functions of temperature for PU films in the temperature range of –35 to 120 °C. With increasing temperature, all films showed a similar trend. In detail, with temperature increasing from –35 °C, E' slightly decreased and once –10 °C was reached, a rapid decrease in E' was observed. A rubbery plateau for the storage modulus was observed in every curve in the higher temperature range of the tests and a peak maximum was observed in the tan δ versus temperature curves (α relaxation), which is taken as the glass transition temperature (T_g). All films show one tan δ peak, indicating the homogeneous nature of the polyurethane films. Moreover, the decreasing height of the tan δ peaks indicates increasing cross-linking densities for the films.[23, 27] As the cross-linking densities increases, molecular motions of polymer chains become more restricted and the amount of energy that can be dissipated throughout the polymers decreases dramatically, therefore, the tan δ peak shifts to a higher temperature and the $(\tan \delta)_{max}$ decreases.[27, 28] The higher T_g for PUs from SCP_0.5 shown

in Table 2-2 can be explained by higher cross linking densities restricting the polymer chain motion.

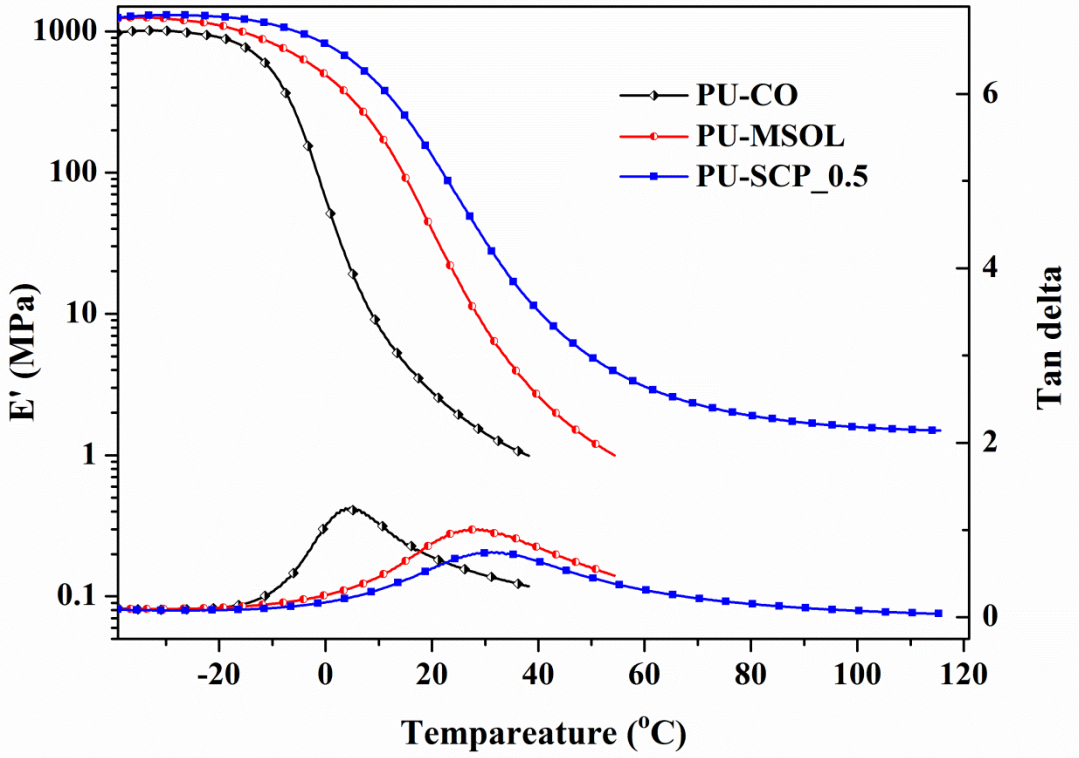

Figure 2-3 Storage modulus and loss factor as functions of temperature for PU films based on CO, MSOL, and SCP_0.5

Figure 2-4 shows DSC thermograms of three PU films and Table 2-2 summarizes their T_g data. Neither melting nor crystallization transitions were observed in the DSC curves, indicating the amorphous nature of these PUs. Each curve exhibits two T_gs, corresponding to the hard and soft segments of the obtained PUs, respectively. The three T_gs related to the hard segments were almost identical, which can be explained by a similar number of OH and urethane groups. However, PUs based on SCP_0.5 exhibited a higher T_g corresponding to their soft segment, while castor oil-based PUs exhibited the lowest T_g, due to higher cross linking of SCP_0.5, which was deduced in previous discussion. The difference between the T_g values obtained from DSC and DMA tests is caused by the nature of these two methods. DSC measures the change in

heat capacity from frozen to unfrozen chains, while DMA measures the change in the mechanical response of the polymer chains.

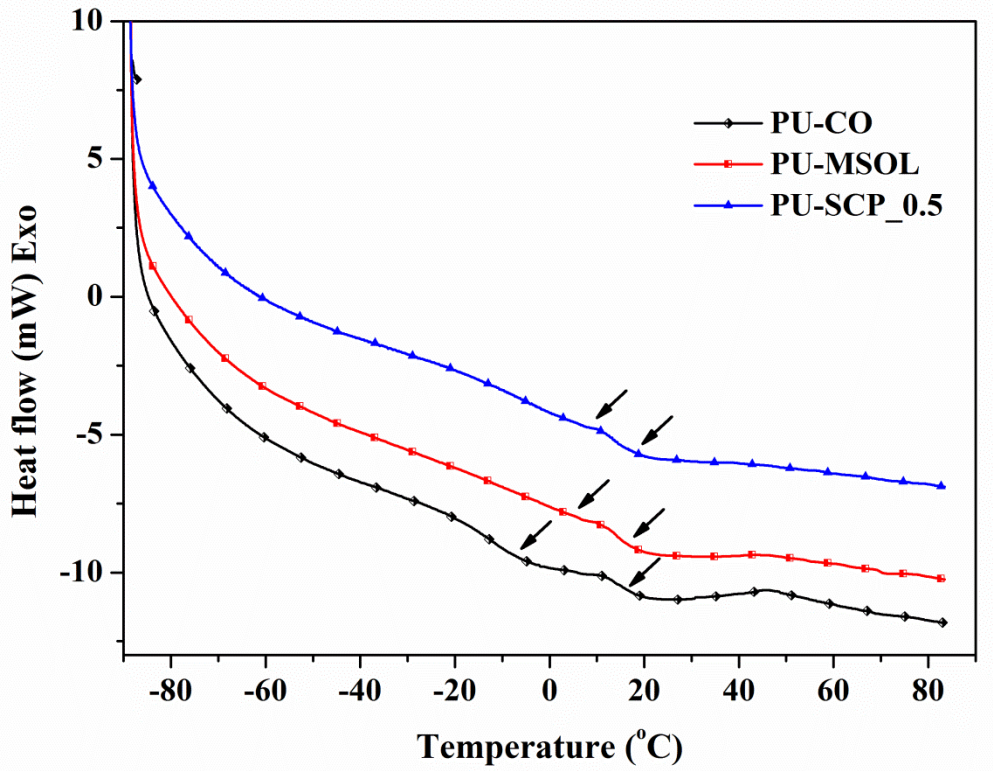

Figure 2-4 DSC scans of PU films based on CO, MSOL, and SCP_0.5

Figure 2-5 shows TGA weight loss and weight loss derivative curves in nitrogen for polyurethane films. The degradation of polyurethanes observed at temperatures between 200 ^{o}C and 300 ^{o}C can be attributed to the decomposition of labile urethane groups. Degradation observed in the temperature range from 300 ^{o}C to 450 ^{o}C resulted from chain scission in the soybean oil. Because these three polyols used to produce the three polyurethanes had similar OH numbers, which determines the amounts of urethane bonds, the weight losses observed in the temperature range from 200 ^{o}C to 300 ^{o}C, which were caused by dissociation of urethane bonds, did not differ significantly. In the second decomposition stage (temperature range from 300 ^{o}C to 450 ^{o}C), the PUs based on SCP_0.5 exhibited higher thermal resistance than those based on MSOL because they had higher levels of ester cross-linking between the polyols. Also, the

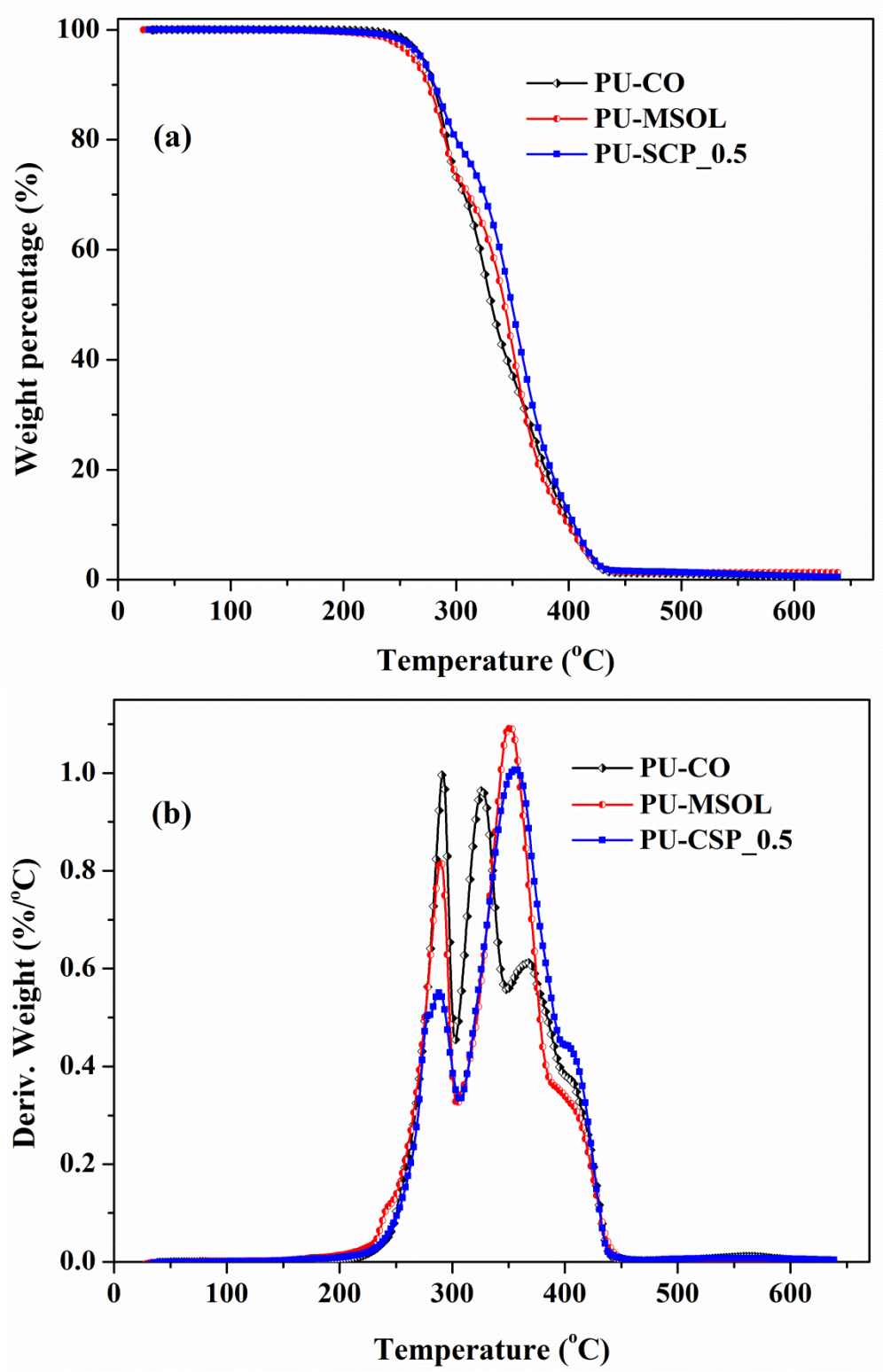

Figure 2-5 TGA curves (a) and their derivative curves (b) for PU films based on CO, MSOL, and SCP_0.5

higher molecular weight of PUs based on MSOL resulted in higher thermal resistance than in PUs based on CO. Table 2-2 shows that 50% degradation (T_{50}) occurred at 349 ^{o}C, 343 ^{o}C, and 331 ^{o}C, respectively for the three PUs investigated; at 357^{o}C, 351 ^{o}C, and 326 ^{o}C, respectively a second T_{max} was detected. TGA curves of PUs in nitrogen indicated that all PUs decomposed above 450 ^{o}C, because no further reactions in nitrogen were observed at higher temperatures.[22, 26]

The tensile stress-strain curves for PUs based on CO, MSOL, and SCP_0.5 are shown in Figure 2-6. Table 2-2 summarizes Young's moduli, tensile strength, elongation at break, and toughness of the polyurethane films investigated. PUs based on SCP_0.5 exhibited higher tensile strength (11.6 MPa) and a higher Young's modulus (5.8 MPa) than the PUs based on MSOL and CO. However, polyurethanes based on SCP_0.5 showed a lower value for elongation at break (232.7 %) than the films based on MSOL and CO because of the higher crosslinking density of their starting polyols.

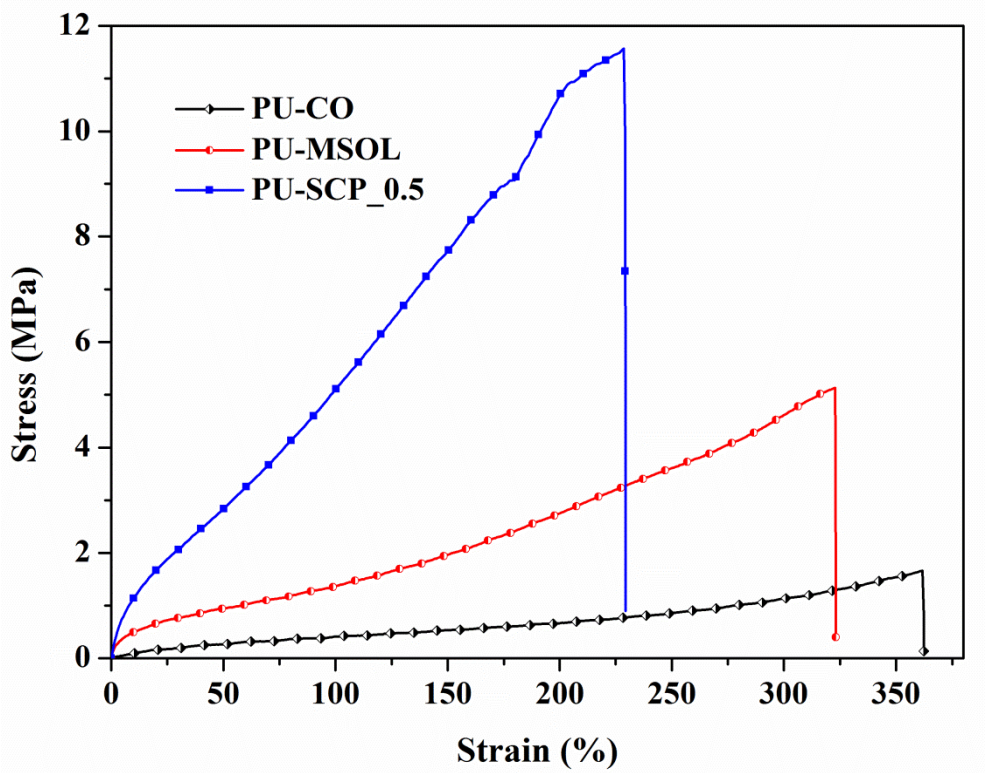

Figure 2-6 Stress/strain curves of PU films based on CO, MSOL, and SCP_0.5

Table 2-2 shows that the toughness of the polyurethane films based on SCP_0.5 is much higher than the toughness of PU films based on MSOL and CO. Generally, higher crosslinking density imparts higher tensile strength; however, it also causes lower elongation at break values. Therefore, flexible fatty acid chains together with high crosslinking density in the PU films based on SCP_0.5 yielded the highest toughness values.[29]

Table 2-2. Thermal and mechanical properties of PUs based on CO, MSOL, and SCP_0.5.

	DMA T_g (^oC)	DSC T_g (^oC)	TGA in nitrogen (^oC)			Tensile strength (MPa)	Young's modulus (MPa)	Elongation at break values (%)	Toughness (MPa)
			T_{10}	T_{50}	T_{max} (first/second)				
PU-SCP_0.5	31.3	6.6/ 14.4	281	349	288/357	11.6±0.4	5.8±0.5	232.7±18.0	13.85
PU-MSOL	27.8	6.5/ 14.2	275	343	290/351	4.9±0.4	2.3±0.3	314.3±17.0	7.67
PU-CO	4.6	9.43/ 14.2	279	331	292/326	1.6±0.1	0.9±0.1	356.2±8.1	2.51

2.5 Conclusions

A solvent-free/catalyst-free method for preparing soy-castor oil based polyols for PU production was developed. When the ratio of carboxyl to epoxy groups exceeded 0.5:1, the epoxy groups in ESBO and the carboxyl groups in COFA were totally consumed. The carboxyl groups also acted as catalysts, resulting in ring opening of the epoxies by OH groups in COFA and newly formed OH groups. The properties of PU films based on this novel polyol were compared to the properties of PU films based on two other established pathways using CO and MSOL, respectively. The comparison showed that PU films based on this novel polyol exhibited higher thermal and mechanical properties, including higher T_gs, tensile strength, and Young's modulus and better thermal stability because of the higher crosslinking density of this novel polyol. The technique reported here offers a number of advantages, including low cost, easy

performance, solvent-free/catalyst-free, and 100% bio-based content, opening any number of opportunities for this environmentally-friendly, green polyol in the polyurethane industries.

2.6 Acknowledgement

This work was sponsored by Kumho Petrochemical Co.

2.7 Notes and references

1. C. K. Williams and M. A. Hillmyer, *Polym Rev*, 2008, **48**, 1-10.

2. Y. Xia and R. C. Larock, *Green Chem*, 2010, **12**, 1893-1909.

3. Z. S. Petrovic, *Polym Rev*, 2008, **48**, 109-155.

4. D. P. Pfister, Y. Xia and R. C. Larock, *Chemsuschem*, 2011, **4**, 703-717.

5. A. Campanella, L. M. Bonnaillie and R. P. Wool, *J Appl Polym Sci*, 2009, **112**, 2567-2578.

6. X. Kong and S. S. Narine, *Biomacromolecules*, 2007, **8**, 2203-2209.

7. X. H. Kong, J. Yue and S. S. Narine, *Biomacromolecules*, 2007, **8**, 3584-3589.

8. K. S. Chian and L. H. Gan, *J Appl Polym Sci*, 1998, **68**, 509-515.

9. R. Tanaka, S. Hirose and H. Hatakeyama, *Bioresource Technol*, 2008, **99**, 3810-3816.

10. A. Zlatanic, C. Lava, W. Zhang and Z. S. Petrovic, *J Polym Sci Pol Phys*, 2004, **42**, 809-819.

11. V. Sharma, J. S. Banait and P. P. Kundu, *J Appl Polym Sci*, 2009, **111**, 1816-1827.

12. V. H. R. de Souza, S. A. Silva, L. P. Ramos and S. F. Zawadzki, *J Am Oil Chem Soc*, 2012, **89**, 1723-1731.

13. A. Guo, Y. J. Cho and Z. S. Petrovic, *J Polym Sci Pol Chem*, 2000, **38**, 3900-3910.

14. Z. S. Petrovic, A. Guo and W. Zhang, *J Polym Sci Pol Chem*, 2000, **38**, 4062-4069.

15. C. S. Wang, L. T. Yang, B. L. Ni and G. Shi, *J Appl Polym Sci*, 2009, **114**, 125-131.

16. X. Pan and D. C. Webster, *Chemsuschem*, 2012, **5**, 419-429.

17. M. Pavlova, M. Draganova and V. Kabaivanov, *Plaste Kautsch*, 1986, **33**, 233-234.

18. V. D. Athawale and K. R. Joshi, *J Polym Mater*, 2004, **21**, 165-173.

19. D. S. Ogunniyi, *Bioresource Technol*, 2006, **97**, 1086-1091.

20. H. Mutlu and M. A. R. Meier, *Eur J Lipid Sci Tech*, 2010, **112**, 10-30.

21. M. D. Phaneuf, M. J. Bide, M. Szycher, M. B. Gale, H. X. Huang, C. Q. Yang, F. W. LoGerfo and W. C. Quist, *Asaio J*, 2001, **47**, 634-640.

22. Y. S. Lu and R. C. Larock, *Biomacromolecules*, 2007, **8**, 3108-3114.

23. Y. Xia and R. C. Larock, *Polymer*, 2010, **51**, 2508-2514.

24. S. Caillol, M. Desroches, G. Boutevin, C. Loubat, R. Auvergne and B. Boutevin, *Eur J Lipid Sci Tech*, 2012, **114**, 1447-1459.

25. S. B. Wu and M. D. Soucek, *Polymer*, 1998, **39**, 3583-3586.

26. S. B. Wu and M. D. Soucek, *Abstr Pap Am Chem S*, 1996, **212**, 108-POLY.

27. Y. Xia and R. C. Larock, *Macromol Mater Eng*, 2011, **296**, 703-709.

28. Z. S. Petrovic, W. Zhang, A. Zlatanic and C. C. Lava, *Abstr Pap Am Chem S*, 2002, **223**, D95-D95.

29. F. K. Li and R. C. Larock, *J Polym Sci Pol Phys*, 2001, **39**, 60-77.

2.8 Supporting information

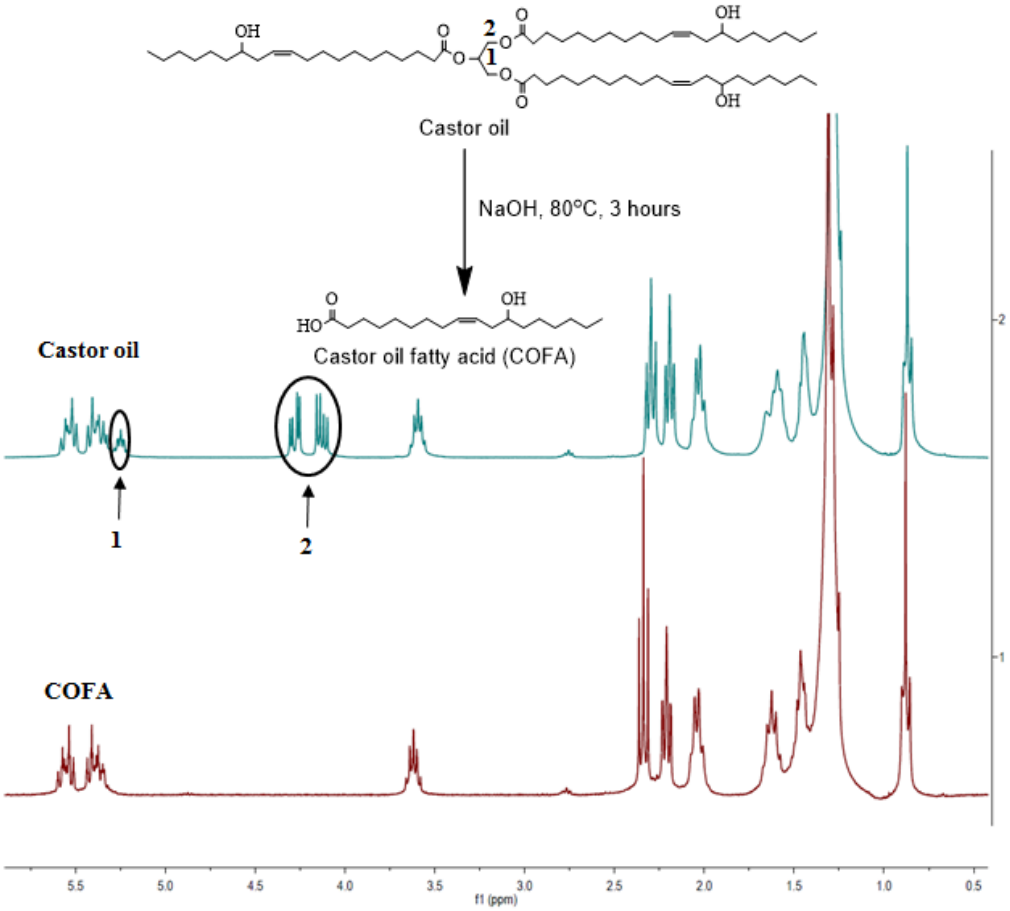

Figure 2-7 ^{1}H-NMR spectra of CO and COFA

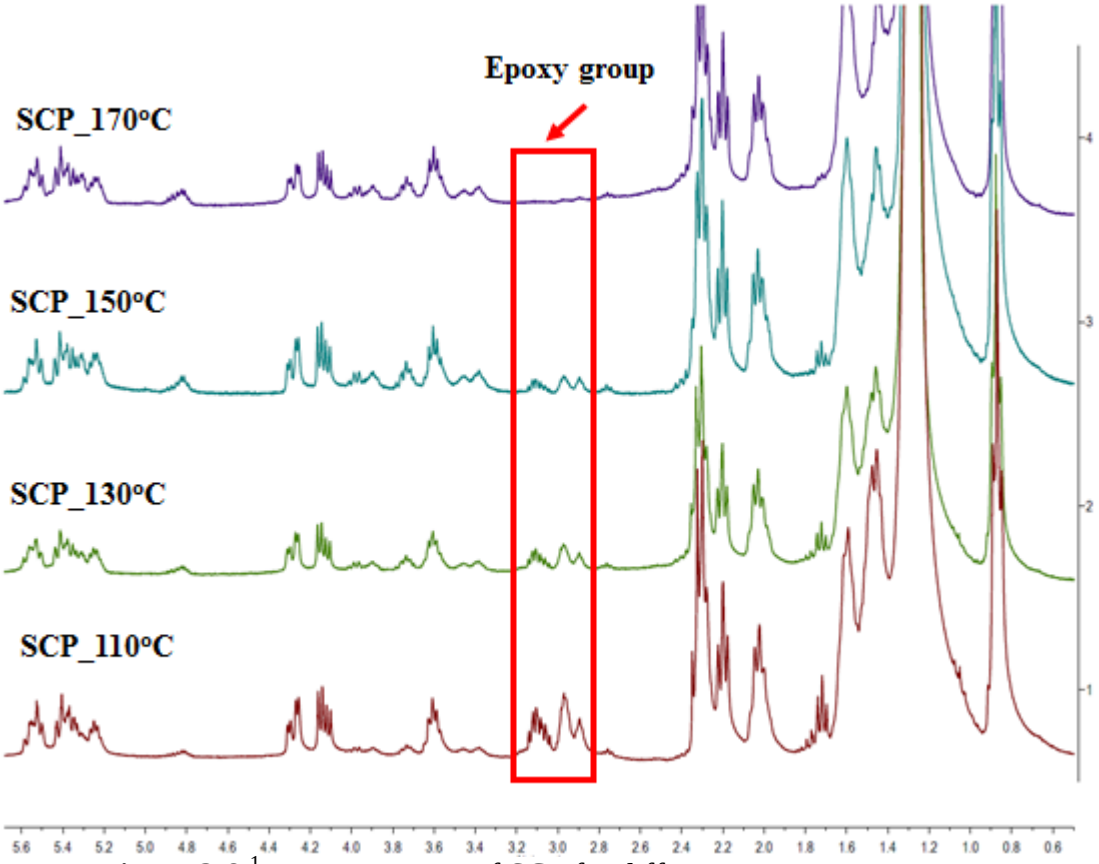

Figure 2-8 ^{1}H-NMR spectra of SCP for different reaction temperatures

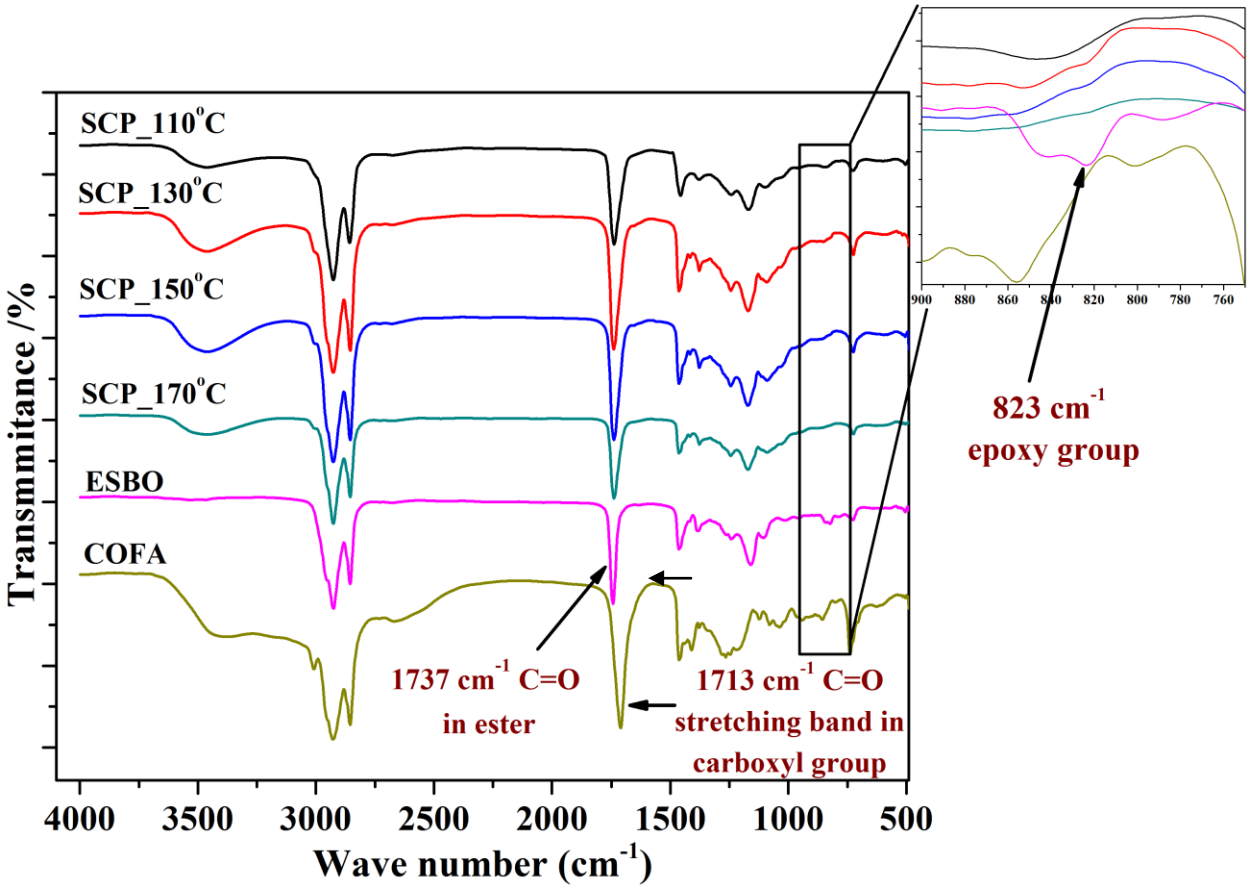

Figure 2-9 FTIR spectra of SCP for different reaction temperatures

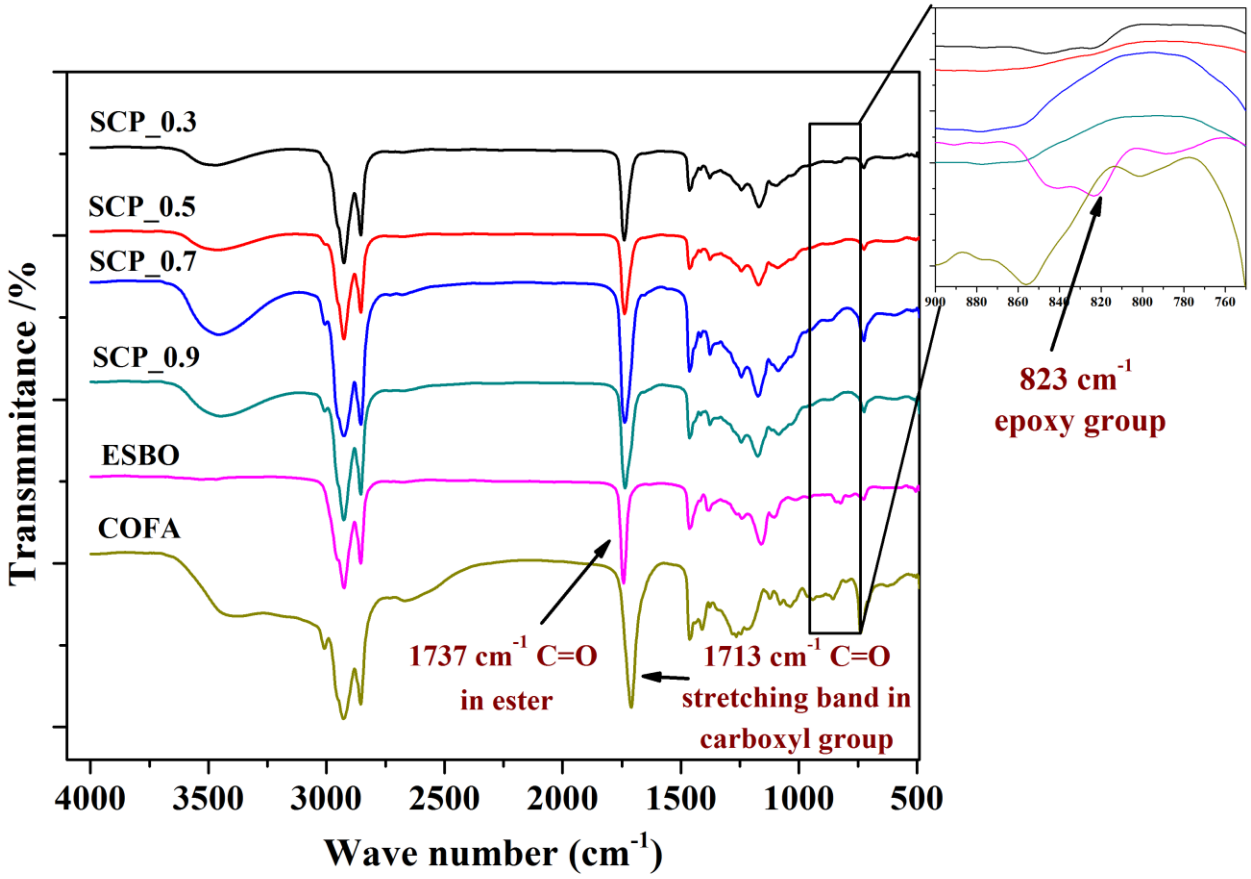

Figure 2-10 FTIR spectra of SCP for different reaction ratios of carboxyl to epoxy groups

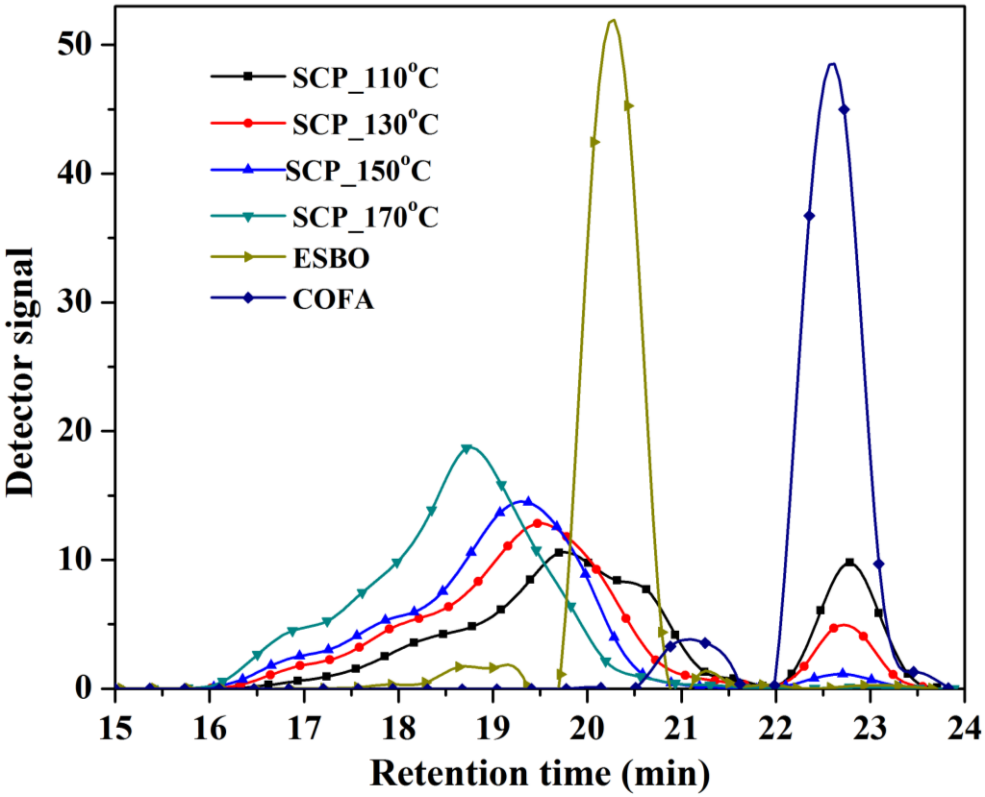

Figure 2-11 GPC curves of SCP for different reaction temperatures

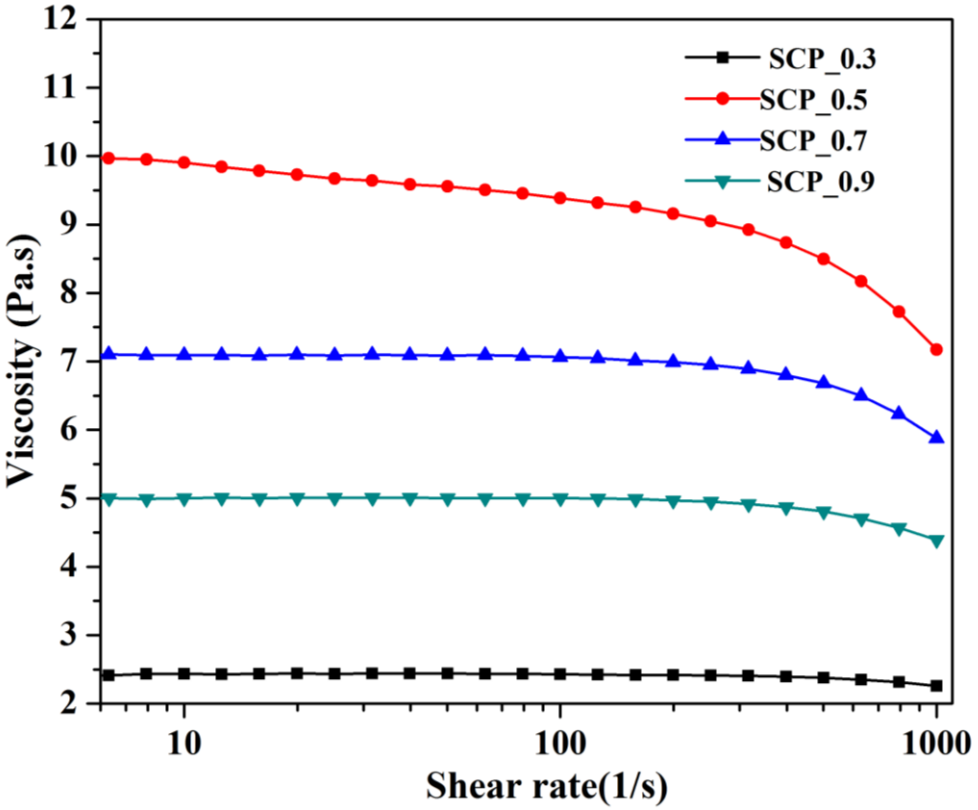

Figure 2-12 Rheological behavior of polyols prepared with different ratios of carboxyl to epoxy groups

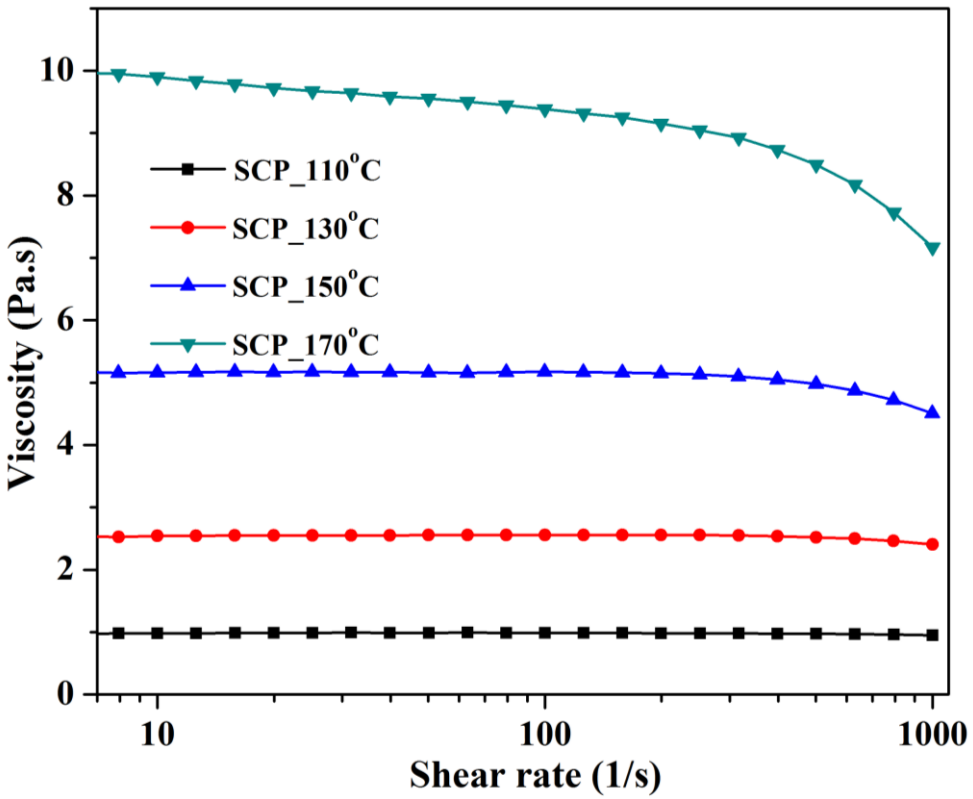

Figure 2-13 Rheological behavior of polyols prepared at different reaction temperatures

CHAPTER 3: POLYURETHANES PREPARED FROM DIFFERENT VEGETABLE OILS USING A SOLVENT/CATALYST-FREE METHOD

A paper to be submitted to Bioresource Technology

Chaoqun Zhang[a], Samy A. Madbouly[a,c], Michael R. Kessler[a,b*]

[a] Department of Materials Science and Engineering, Iowa State University, Ames, IA, USA

[b] School of Mechanical and Materials Engineering, Washington State University, Pullman, WA, USA

[c] Department of Chemistry, Faculty of Science, Cairo University, Orman-Giza, Egypt

[*] Author for correspondence

3.1 Abstract

In this study, a series of bio-based polyols were prepared from olive, canola, grape seed, linseed, and castor oil using a novel, solvent/catalyst-free synthetic method: The bio-based triglyceride oils were first oxidized into epoxidized vegetable oils with formic acid and hydrogen peroxide, followed by ring opening reaction with castor oil fatty acid. The molecular structures of the polyols were characterized by proton nuclear magnetic resonance, Fourier transform infrared spectroscopy, gel permeation chromatography, and rheometer. In addition, polyurethanes were successfully synthesized from those polyols with isophorone diisocyanate. The properties of polyurethanes were characterized by dynamic mechanical analysis, differential scanning calorimetry, thermogravimetric analysis, and tensile tests. The effects of cross-linking density and the structures of polyols on the thermal, mechanical, and shape memory properties of the polyurethanes were also investigated.

Keywords: Vegetable oil; Polyol; Polyurethane; Shape memory

3.2 Introduction

Polyurethanes (PUs), prepared via a polyaddition reaction between a diisocyanate and a polyol, are widely used in applications such as coatings, adhesives, sealants, and foams because of their excellent abrasion resistance, high toughness, chemical resistance, and low film-forming temperatures [1-3]. The global market for PUs was estimated at 14 million tons in 2010, and is expected to increase by 28% by 2016 [4]. Over the past decades, most of the starting materials for the production of PUs are derived from petroleum-based resources, which are widely regarded as unsustainable. Recently, environmental concerns, the depletion of the world crude oil stock and the increasing price of crude oil have triggered increasing interest to utilize bio-based resources for the production of PUs [5, 6].

Several bio-based materials, including cellulose, starch, natural oil, and sugar, have been utilized as starting materials for PUs [7-9]. Vegetable oils are among the most promising, because they are an inexpensive, readily available, and renewable resource. Vegetable oils are triglyceride of saturated and unsaturated fatty acids. The six most common fatty acids are palmitc (C16:0), stearic (C 18:0), oleic (C 18:1), linoleic (C 18:2), linolenic (C 18:3), and ricinoleic (C18:1 OH) acids (in this notation, the first number represents the number of carbon atoms, the second number represents the number of carbon-carbon double bonds, and OH represents hydroxyl groups in the fatty acid). In order to utilize vegetable oils for PU applications, a variety of techniques are used to introduce hydroxyl groups into the fatty acid chains at the position of carbon-carbon double bonds, thus creating polyols.

Epoxidation of vegetable oils, followed by oxirane ring opening is one of the most important reactions to provide various polyols. Different ring opening chemical agents, such as H_2 [10], hydrohalic acids [10], organic acids [11], and amines [12] are typically used to initiate the ring opening reaction; they create polyols with different functionalities for PUs that exhibit a broad range of properties, from soft and rubbery to hard and glassy. However, almost all ring opening agents used to prepare polyols by ring-opening of epoxidized vegetable oils are petroleum-based, small molecules. Currently, several research groups dedicate considerable effort to the development of 100% bio-polyols for the production of PUs. Kiatsimkul [13] initiated ring opening reactions of epoxidized soybean oil with linoleic acid, ricinoleic acid, and ricinoleic acid estolide to prepare high hydroxyl equivalent weight polyols. Recently, polyols were developed by ring opening reaction between epoxidized soybean oil and castor oil fatty acid (COFA) using a solvent method without catalyst [14].

The mechanical and physical properties of PUs strongly depend on the types of polyol used (the number and distribution of hydroxyl groups), the diisocyanate, and the diisocyanate index. Lu et al. investigated the effect of different OH functionalities of soy-methanol polyols on the thermophysical and mechanical properties of waterborne PU films [15]. Petrovic et al. reported the effect of OH/NCO molar ratios on the physical, thermal and mechanical properties of soy-methanol-PU [16]. Peruzzo et al. studied the effect of different diisocynates structures on the morphology and properties of waterborne PU-acrylates [17]. It was reported that soy-castor oil based polyol prepared using a solvent/catalyst-free method resulted in PUs with better thermophysical and mechanical properties than those from soy-methanol polyols and castor oil based polyols because of the pre-crosslinking structures of soy-castor oil based polyol [14].

Shape memory is an important property for many polymers, that are stimuli-responsive (temperature, light, solvent), *i.e.*, have the ability to return from a deformed (temporary) state to their original, primary shape when an external trigger is applied. Numerous PUs exhibit shape memory properties [18]. The shape memory properties of PUs from those 100% bio-based polyols using a solvent/catalyst-free method have not been determined.

In this study, a solvent/catalyst-free method was applied to prepare a series of vegetable oil-based polyols from olive, canola, grape seed, linseed, and castor oils. The properties of these polyols were characterized by proton nuclear magnetic resonance (^{1}H NMR), Fourier transform infrared spectroscopy (FTIR), gel permeation chromatography (GPC), and rheometer. In addition, PUs were prepared from these polyols and IPDI. The properties of the PUs were characterized by dynamic mechanical analysis (DMA), differential scanning calorimetry (DSC), thermogravimetric analysis (TGA), and tensile strength tests. The effect of cross-link density and structure of the polyols on the thermal, mechanical, and shape memory properties of the PUs were discussed. A key objective of this work was to evaluate the effect of structure of polyols from different oils on the thermo-mechanical, thermal resistance, and shape memory properties of PUs.

3.3 Materials and Methods

3.3.1 Materials

Epoxidized linseed oil (approximately 6 oxirane rings per triglyceride) was purchased from Scientific Polymer Inc., New York, NY. Magnesium sulfate ($MgSO_4$), hydrogen peroxide, methyl ethyl ketone (MEK), and ethyl ether were purchased from Fisher Scientific Company (Fair Lawn, NJ). Olive oil, canola oil, castor oil, grape seed oil, hydrochloric acid, sodium hydroxide, sodium bicarbonate, formic acid, isophorone diisocyanate (IPDI), and dibutyltin

dilaurate (DBTDL) were obtained from Sigma-Aldrich (Milwaukee, WI). All materials were used as received without further purification.

3.3.2 Synthesis of the Epoxidized Vegetable Oils

Epoxidized vegetable oils with different epoxy groups were prepared according to a method previously reported [19]. Briefly, vegetable oils and formic acid (the molar ratio of these two is 1 : 4.12) were charged into a 500 mL flask at 50 °C under vigorous stirring. Then, hydrogen peroxide (50%, the molar ratio of hydrogen peroxide to double bonds in triglyceride is 1.8 : 1.) was added slowly using syringe over a 4 h period. The reaction was continued at 50 °C for another 4 h. Then, sodium bicarbonate was added to neutralize the solution and ethyl ether was added, resulting in two layers. The organic layer was washed with distilled water until the solution became neutral. Epoxidizied vegetable oils were obtained after drying with $MgSO_4$ and filtering, removal of organic solvent by rotary evaporation, and drying in vacuum oven overnight.

3.3.3. Synthesis of Castor Oil Fatty Acid

Castor oil was saponified into fatty acid with a sodium hydroxide solution at 80 ^oC, followed by neutralization with hydrochloric acid [14]. Finally, castor oil fatty acids (COFA, which consist of 87.7-90.4% ricinoleic acid, the rest are linolenic, linoleic, oleic acid [20, 21]) were obtained after the organic layer was purified by washing with water, drying over $MgSO_4$, and filtering.

3.3.4. Synthesis of Vegetable Oils Based-Polyols

The polyols were prepared by ring opening reactions between epoxidized vegetable oils and COFA. The polyols were identified as olive-castor oil based polyols (OCP), canola-castor oil based polyols (CaCP), castor-castor oil based polyols (CCP), grape seed-castor oil based polyols (GCP), and linseed-castor oil based polyols (LCP). Initially, COFA and epoxidized vegetable oil

were mixed in a flask with a magnetic stirrer and maintained at 170 ^{o}C in dry nitrogen atmosphere. The molar ratio of the carboxyl to the epoxy groups was 0.5. After 8 h, a viscous liquid was obtained.

3.3.5. Polyurethane Preparation

The PUs were synthesized through the reaction of polyol with a 5 % molar excess of IPDI in the presence of DBTDL. The viscosity of the mixture was reduced by the use of MEK. The solution was heated to 70 °C and mixed continuously for 3 h. Then, the mixture was poured into a Teflon mold to produce 50 mm × 50 mm (length × width) sheets, which were dried overnight in an oven at 80 °C. Finally, the PU films were cut into specific dimensions for thermo-mechanical tests.

3.3.6. Characterization

A Varian spectrometer (Palo Alto, CA) at 300 MHz was used to record the ^{1}H-NMR spectroscopic analyses of the monomers and final products. All measurements were carried out using $CDCl_3$ as solvent. The FTIR spectra of the polyols were recorded on a Nicolet 460 FTIR spectrometer (Madison, WI). The OH number of polyols were determined using the Unilever method [10]. The acid numbers of the polyols were determined by AOCS Official Method Te 1a-64. The molecular weight was determined using a THF-eluted GPC equipped with a refractive index detector. Thermal and mechanical properties of the resulting PU films were characterized using a TA Instruments Q800 dynamic mechanical analyzer with a film-tension mode of 1 Hz. Rectangular specimens of 0.6 × 10 mm (thickness × width) were used for the analysis. The samples were cooled and held isothermally for 2 min at -80 ^{o}C before the temperature was increased to 150 ^{o}C at a heating rate of 3 ^{o}C/min. A TA Instrument Q2000 differential scanning calorimeter was used to examine the glass transition temperature (T_g). Approximately 6 mg of

different PU samples was heated in a first cycle from room temperature to 120 ^{o}C at a rate of 20 ^{o}C/min to erase their thermal history. Then the samples were equilibrated at -60 ^{o}C and heated for a second cycle to 120 ^{o}C at a heating rate of 20 ^{o}C/min. TGA was carried out using a TA Instrument Q50 to evaluate the thermal stability of the PU films. Samples with a weight of approx. 10 mg were heated from room temperature to 700 ^{o}C at a heating rate of 20 ^{o}C/min in air. An Instron universal testing machine (model 4502) with a crosshead speed of 100 mm/min was used to determine the tensile properties of the PU films Rectangular specimens of 50 mm ×10 mm (length × width) were used. Average values of at least four replicates of each sample were taken. The toughness of the PU samples was determined from the area under the corresponding tensile stress/strain curves.

Shape memory properties of the PUs were investigated using a TA Instruments Q800 dynamic mechanical analyzer. The samples were equilibrated at T_{prog} and held for 2 min, then stretched to the maximum strain (ε_m) at a rate of 10% /min. While maintaining the stress applied, the samples were cooled down to T_{low} at 10 ^{o}C/min and hold at this temperature for 10 min. Then the stress released and the sample was held for another 2 min to reach a predetermined strain (ε_u). Finally, the temperature was increased to T_{high} at a rate of 3 ^{o}C/min and held at this temperature for 30 min to recover a fixed strain (ε_p). The values of T_{prog}, T_{low}, T_{high} based on the different T_gs of samples will be discussed later. The PU-GCP samples underwent four consecutive cycles.

3.4 Results and Discussion

3.4.1 Structures and Properties of Polyols

Figure 3-1 (a) shows the pathway for the preparation of green polyols. ^{1}H-NMR spectra of castor oil, epoxidized castor oil, and the castor-castor oil based polyol are shown in Figure 3-1 (b). The area under the peaks at 4.1-4.2 ppm (-C**H$_2$**-CHCH$_2$-) was used as a constant of 2 for

normalization to obtain the number of carbon-carbon double bonds and epoxy groups in the structure of the vegetable oils and epoxidized vegetable oils, see Table 3-1. Figure 3-1 (b) shows that after epoxidation, the carbon-carbon double bonds (peaks between 5.3 and 5.6 ppm) in castor oil disappeared and epoxy groups (peaks between 2.8 and 3.2 ppm in spectra of epoxidized castor oil) were formed. As seen in Table 3-1, the conversion ratios of double bonds to epoxy groups (number of epoxy groups in epoxidized vegetable oils/number difference of

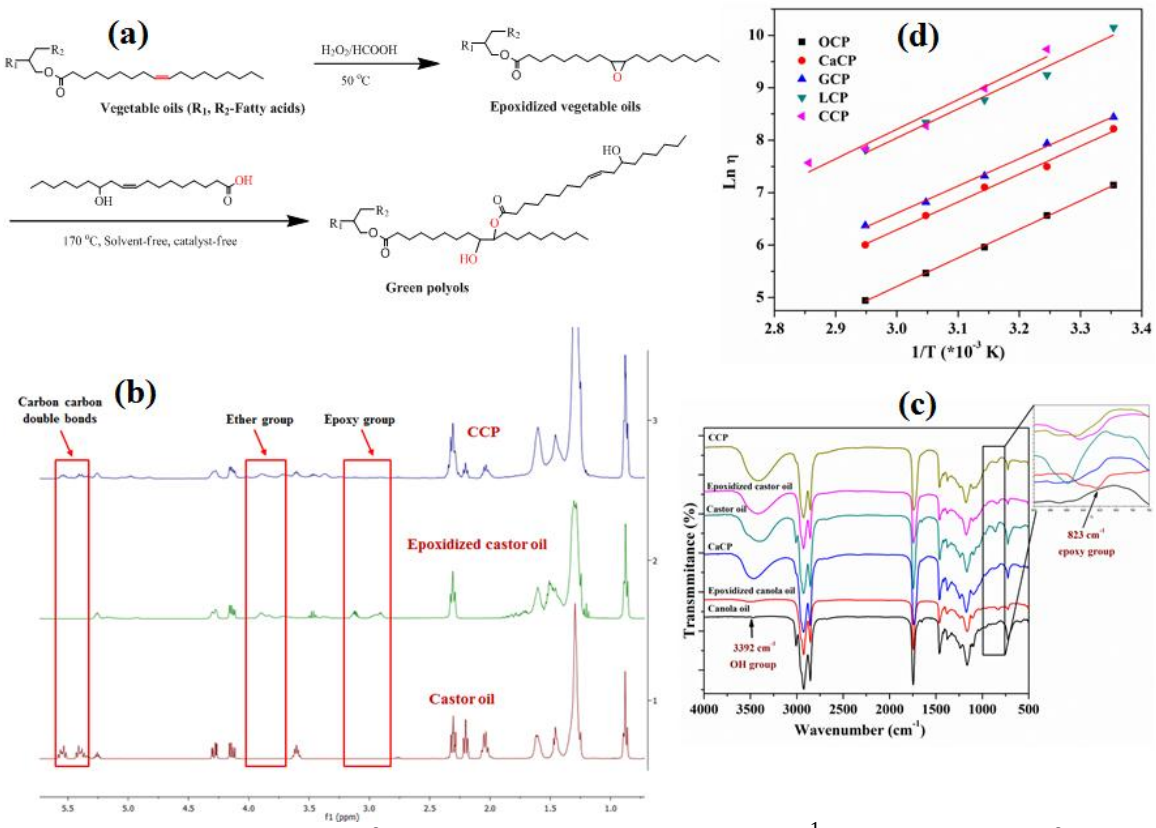

Figure 3-1 (a) Preparation of vegetable oils-based polyols, (b) ^{1}H-NMR spectra of castor oil, epoxidized castor oil, and CCP, (c) FTIR spectra of CCP, epoxidized castor oil, castor oil, CaCP, epoxidized canola oil, and canola oil, (d) viscosity-temperature relationship for OCP, CaCP, GCP, LCP, and CCP.

carbon-carbon double bonds between epoxidized vegetable oils and vegetable oil) are only 70 % while other vegetable oils are approximately 90%. This was attributed to the fact that the newly

formed epoxy groups were ring opened by hydroxyl groups that originally existed in castor oil with formic acid as catalyst, seen in the decrease of peaks at 3.5-3.6 ppm corresponding the hydrogen attached to the carbon adjacent to OH in the spectra of castor oil and in the appearance of new peaks between 3.6 and 4.0 ppm that represent tertiary hydrogen atoms adjacent to the newly formed ether in the spectra of epoxidized castor oil. Subsequent to the ring opening reaction between epoxidized castor oil and COFA, the number of epoxy groups decreased. In addition, the presence of new peaks between 4.6 and 5.0 ppm, representing tertiary hydrogen atoms adjacent to the newly formed ester groups, indicated that COFA (contains carbon-carbon double bonds) was attached to the long carbon chain of epoxidized oils. The re-appearance of carbon-carbon double bond peaks in the spectra of CCP also confirmed this result. Similar results were found for other vegetable oil systems shown in Figure 3-1 in the supplementary information.

The successful preparation of polyols was also confirmed by FTIR. Figure 3-1 (c) shows the FTIR spectra of CCP, epoxidized castor oil, castor oil, CaCP, epoxidized canola oil, and canola oil. After epoxidation from castor oil and canola oil, oxirane absorption at 823 cm^{-1}, corresponding to epoxy groups appeared and carbon-carbon double bonds at 3000-3010 cm^{-1} [22] almost disappeared. After the ring opening reaction was initiated by COFA, the epoxy groups in epoxidized castor oil and epoxidized canola oil decreased, while a broad peak at 3392 cm^{-1} appears in CaCP, which suggests that the epoxy groups in epoxidized castor and canola oil were ring-opened and hydroxyl groups were formed. Because castor oil originally contained OH groups, it exhibited a broad peak at 3392 cm^{-1} while canola oil did not exhibit this peak.

Table 3-1 Properties of the OCP, CaCP, GCP, LCP and CCP**.

		C=C bonds	Epoxy	OH number (mg KOH/g)	Number/ average molecular weight	PDI	State at room temperature
# 1	OO	2.48	0	-	1295/1327	1.03	Liquid
	E- OO	0	2.47	-	1333/1366	1.02	Liquid
	OCP	-	-	109.1±0.1	2118/2675	1.26	Liquid
# 2	CaO	3.54	0	-	1305/1358	1.04	Liquid
	E- CaO	0	3.29	-	1371/1425	1.04	Liquid
	CaCP	-	-	132.7±0.4	2419/3380	1.4	Liquid
# 3	CO	2.94	0	-	1391/1461	1.05	Liquid
	E-CO	0.24	1.9	-	1862/2217	1.19	Wax
	CCP	-	-	227.9±0.5	2553/3581	1.4	Wax
# 4	GO	4.17	0	-	1392/1435	1.03	Liquid
	E-GO	0	4.17	-	1530/1620	1.06	Liquid
	GCP	-	-	140.1±0.9	2624/3546	1.35	Liquid
# 5	E-LO	0	6.00	-	1337/1590	1.19	Liquid
	LCP	-	-	173.2±3	2842/4827	1.7	Liquid

**OO-Olive oil, CaO-Canola oil, CO-Castor oil, GO-Grape seed oil, LO-Linseed oil, E-Epoxidized, PDI-Polydispersity index

Table 3-1 shows that OCP, CaCP, GCP, and LCP were liquid state at room temperature, while CCP was a waxy state. Figure 1 (d) shows the viscosity of OCP, CaCP, GCP, LCP, and CCP as a function of temperature. At 66 ^{o}C and a shear rate of 25 s^{-1}, the viscosity of polyols increased from OCP<CaCP<GCP<LCP<CCP, see Table 3-2, because of the effect of hydrogen bonding. The number of carbon carbon double bonds for vegetable oils increased from olive oil<castor oil<canola oil<grape seed oil, while the number of epoxy groups for epoxidized vegetable oils increased from epoxidized castor oil<epoxidized olive oil<epoxidized canola oil<epoxidized grape seed oil<epoxidized linseed oil. Among these five epoxidized vegetable oils, only epoxidized castor oil originally contained OH groups. Also, the ring opening of one epoxy group generated one OH group in all systems. Therefore, the OH numbers of the polyols increased from OCP<CaCP<GCP<LCP<CCP, see Table 3-1. The highest OH number in CCP generates

greatest hydrogen bonding, resulting in CCP a waxy state at room temperature. When plotted against the reciprocal temperature (Figure 1 (d)), the viscosities obeyed the Andrade dependence [23].

$$\eta = 3\eta_0 e^{E_{ac}/RT} \quad (3\text{-}1)$$

where η_0 is a reference viscosity, E_{ac} is the viscous-flow activation energy, R is the universal gas constant and T is the temperature. The activation energies were calculated from the slopes of the lines in Figure 3-1 (d) and are summarized in Table 3-2. The activation energy of different polyols did not change significantly. However, the activation energies of the polyols were higher than those of ESBO and castor oil because of the effect of hydrogen bonding.

Table 3-2 Viscosity at 66 ^{o}C and the activation energy of the viscous-flow for polyols.

	Viscosity (Pa·s) at 66 ^{o}C at a shear rate of 25 s^{-1}	E_{ac} (kJ/mol)
OCP	0.14	45.3
CaCP	0.40	44.1
GCP	0.59	43.2
LCP	2.47	46.0
CCP	2.52	46.9
ESBO [10]	0.06 (70 ^{o}C)	35
Castor oil [10]	0.09 (70 ^{o}C)	33

3.4.2 Properties of PUs

Figure 3-2 (a) shows the DSC curves of the PUs from different polyols, and their T_gs are summarized in Table 3-3, which were determined from the midpoint temperature in the heat capacity change of the DSC scan. All PUs exhibited only one T_g and neither melting nor crystallization transitions were observed in the DSC curves, indicating the amorphous nature of these PUs. As the OH numbers increased from OCP, CaCP, GCP, LCP to CCP, the T_gs increased from -22.9 to 54.55 ^{o}C, respectively, which was explained by the fact that urethane linking increased with increasing OH numbers, leading to higher crosslinking densities, that restricted

the mobility of the polymer chains. Kong [24] and Javni [25] reported that as the OH numbers of vegetable oil-based polyols increased, the increasing amount of isocyanate necessary during PU preparation contained more rigid aliphatic rings, and resulted in higher T_gs.

Table 3-3 Thermal properties of PUs based on polyols from different vegetable oils.

	DMA T_g (°C)	DSC T_g (°C)	v_e (mol/m^3)	E' at 25 °C (MPa)	TGA in air (°C)	
					T_{10} [a]	T_{50} [b]
PU-OCP	-1.58	-22.9	48.8	0.5	310.3	378.3
PU-CaCP	20.11	-6.3	339.1	9.1	312.6	386.2
PU-GCP	27.2	-4.5	412.1	32.5	308.0	380.0
PU-LCP	53.46	30.5	841.8	713.4	311.6	377.7
PU-CCP	82.3	54.55	948.6	798.6	302.4	368.4

[a] 10% weight loss temperature. [b] 50% weight loss temperature.

The thermal and mechanical properties of the polymer phase were investigated by DMA. Figures 3-2 (b) and (c) show the storage modulus and tan δ as functions of temperature ranging from –80 to 150 °C for PUs from different vegetable oils. The temperature corresponding to tan δ_{max} is taken as the glass transition temperature (T_g, α relaxation). At low temperatures, all PU samples were in the glassy state with E' values on the order of 1000 MPa. As temperature increased, E' gradually decreased until a rapid decrease was observed. At higher temperatures, the storage moduli of all PUs reached a rubbery plateau. All samples show only one tan δ peak, indicating the homogeneous nature of the PU films. As the OH numbers of the polyols increased from OCP, CaCP, GCP, LCP to CCP, the tan δ peak of the respective PUs shifted to higher temperatures and their maxima decreased. This was contributed to the fact that increasing OH numbers caused higher crosslinking densities (v_e) and thus less energy was dissipated throughout the polymers, see Table 3-3. The cross-linking densities of all films were determined from the rubbery moduli using the kinetic theory of rubber elasticity [26]

$$E' = 3v_eRT' \quad (3\text{-}2)$$

where T' is the absolute temperature at T_g +40 ^oC, and E' is the storage modulus at T'. R is the gas constant.

Figure 3-2 (d) shows that the T_gs exhibited linear behavior as functions of the polyols' OH number, which matches reports by Lu [27] and Petrovic et al [28]. The T_gs determined by DMA were approx. 20–30 °C higher than those determined by DSC because of the different principles underlying these two methods. Also, T_g values from DMA are frequency dependent and the temperature control is not as good as in DSC while the determination of T_g in DSC is not accurate as the reading the position of maxima in DMA [29].

TGA weight loss and weight loss derivative curves in air for PU films from different oils are shown in Figure 3-3 (a) and (b), respectively. The weight loss derivative curves of the PUs revealed that all films underwent three main degradation processes: The degradation between 200 and 340 ^oC was initiated by the decomposition of unstable urethane bonds, leading to primary or second amines, olefin, and dioxide [30, 31]. As OH numbers of the polyols increased, the thermal stability of the corresponding PUs decreased because of the increasing urethane bonds. The weight loss in the temperature range

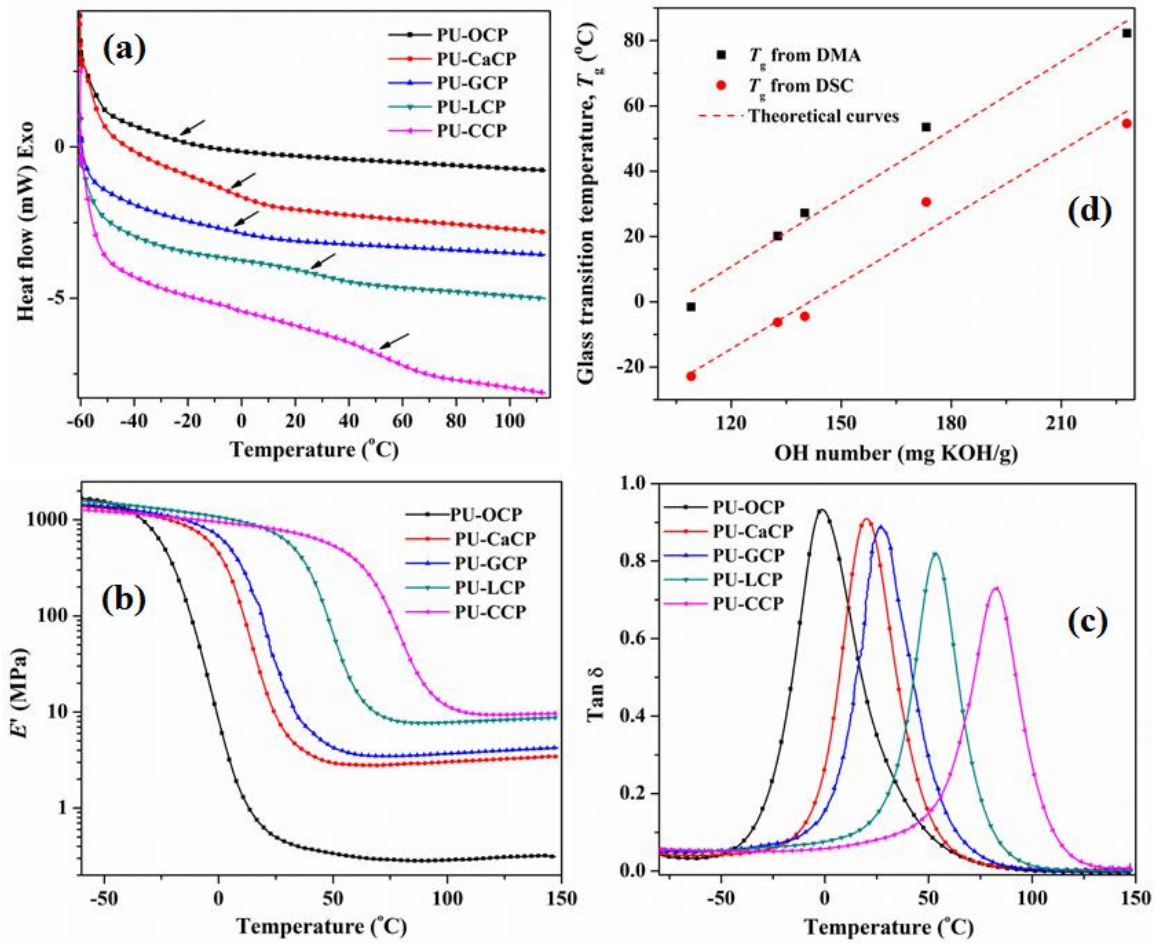

Figure 3-2 (a) DSC traces (20 ^{o}C/min), (b) temperature dependence of E' , and (c) temperature dependence of tan δ of PUs from OCP, CaCP, GCP, LCP and CCP, (d) the dependence of T_g of PU films on the OH number of corresponding polyols.

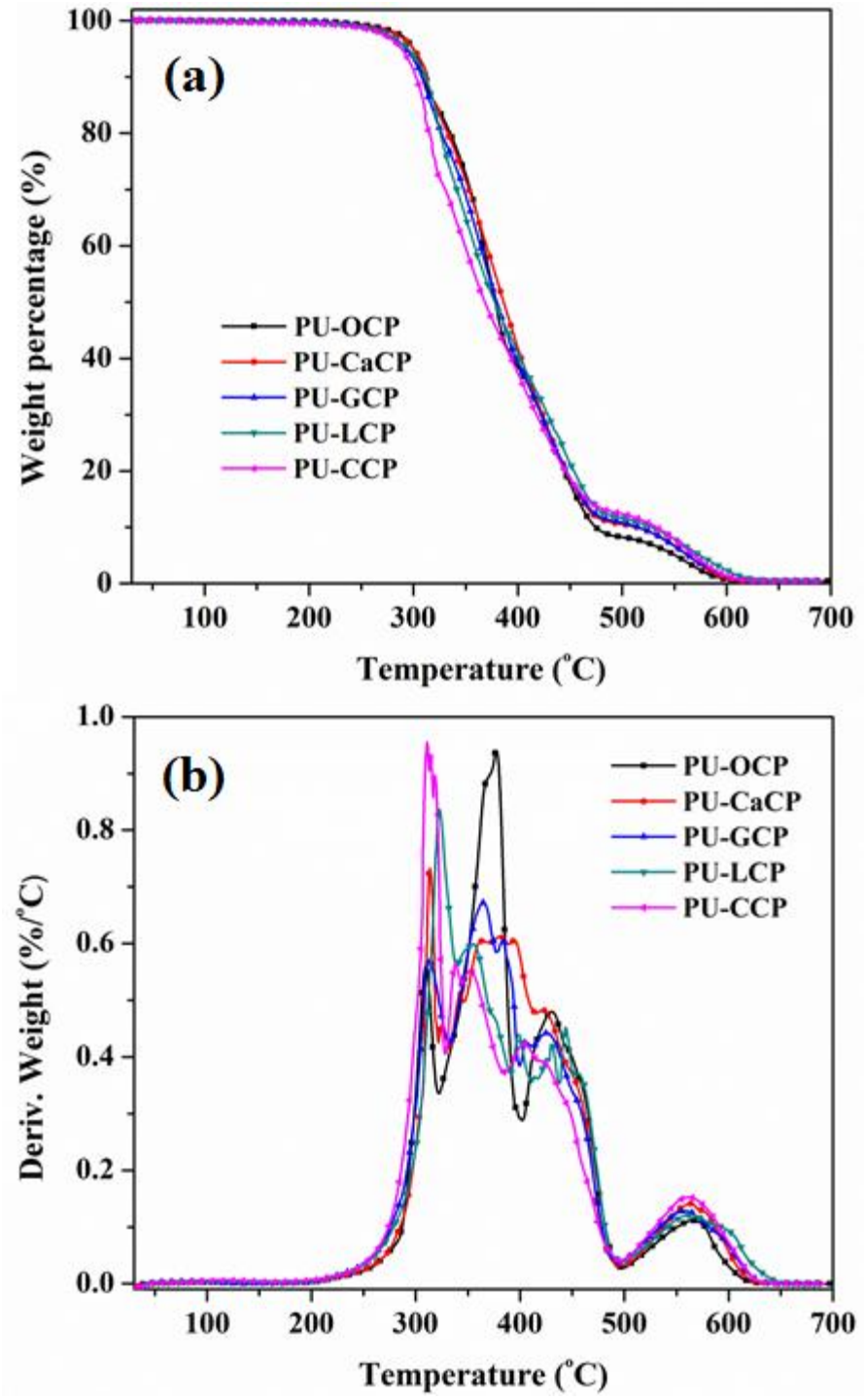

Figure 3-3 (a) TGA curves, and (b) TGA derivative curves of PUs from OCP, CaCP, GCP, LCP and CCP.

from 340 ^{o}C to 500 ^{o}C corresponded to chain scission of the oils. At this stage, there was no obvious trend, because with increasing OH numbers, the positive effect of the ester group (pre-crosslinking) on the weight loss to some extent compensated for the negative effect of the urethane groups on the thermal stability of the PUs. The decomposition of PUs above 500 ^{o}C contributed to further thermo-oxidation of the PU films.

Figure 3-4 shows the representative stress-strain curves of PUs from different vegetable oils. Young's modulus, tensile strength, elongation at break, and toughness of PU films are summarized in Table 3-4. The PUs derived from OCP, CaCP, and GCP exhibited the elastic region and yield point of typical elastomeric polymers while PUs from linseed oil and castor oil exhibited the stress-strain behavior of hard plastics with followed by strain softening and strain hardening before breaking. As the OH number of the polyols increased, the tensile strength of the PUs increased. Except for PU-CCP, the elongation at break of all PUs ranged from 80% to 120%, which was attributed to the fact that the functional groups were located in the middle of the fatty acid chains, leading to high number of dangling chains in the respective polyols.

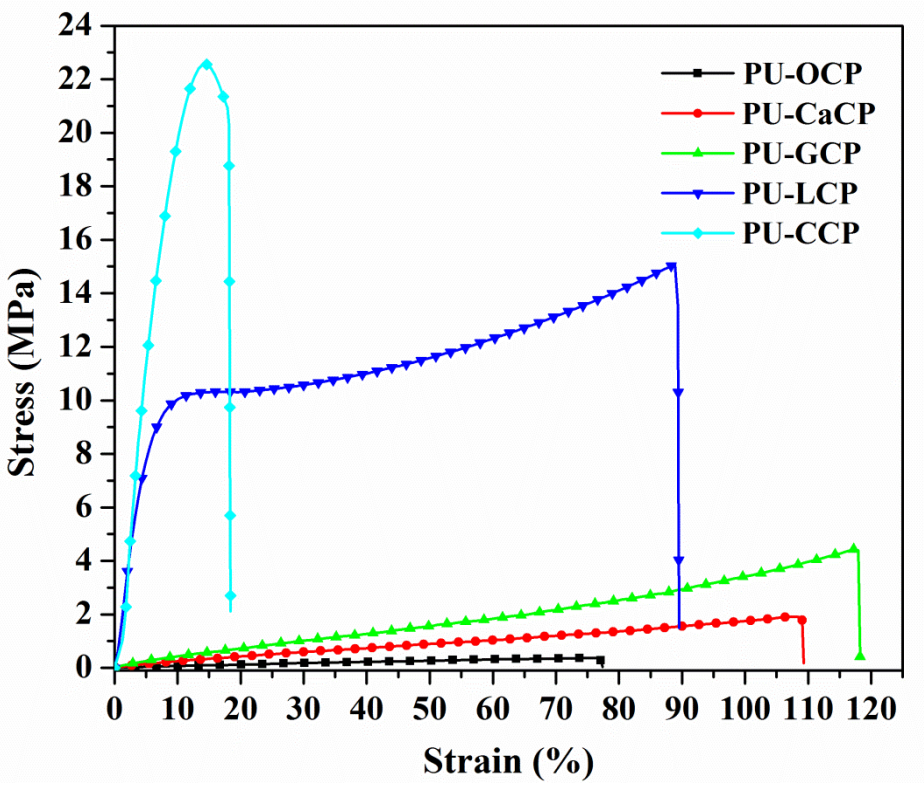

Figure 3-4 Stress-strain curves of PUs from OCP, CaCP, GCP, LCP and CCP.

Table 3-4 Mechanical properties of PUs based on polyols from different vegetable oils.

	Tensile strength (MPa)	Young's modulus[+] (MPa)	Elongation at break (%)	Toughness (MPa)
PU-OCP	0.4±0.1	0.8±0.1	79.2±7.1	0.16
PU-CaCP	1.7±0.4	2.2±0.2	96.7±15.6	1.06
PU-GCP	3.7±0.6	5.5±0.7	96.8±17.7	2.33
PU-LCP	17.3±3	197.3±6.2	98.0±12.9	10.15
PU-CCP	29.1±4	495.3±41.9	11.0±0.2	2.84

[+] Modulus calculated from the initial slope of the stress-strain curve

Cyclic thermomechanical tensile tests were used to study the thermally induced shape memory effect (SME) for different vegetable oil-based PUs. Before the cyclic tests, the samples were stretched to ε_m = 100% at $T_{prog} = T_g + 10$ °C and rapidly cooled down to T_{low} (T_{low} was at least 20 °C lower than the T_g of each sample) under an applied stress to induce the temporary shape. Vegetable oil-based PU films are thermosets and their chemical crosslinks act as permanent netpoints, determining the permanent shape. The shape recovery was recorded as a function of

temperature by heating the samples at a rate of 3 °C/min to $T_{high} = T_{prog} + 10$ °C. The cyclic thermomechanical tests were investigated under stress controlled conditions (σ = 0 MPa). So that the SME could be quantified by determination of rate of recovery, R_r, and rate of fixity, R_f, from the ε versus time recovery curve.

Figure 3-5 (a) shows a typical thermomechanical tensile test for GCP-based PUs under stress-controlled conditions for the first cycle. The thermomechanical tensile test was repeated four times (N = 4) under identical conditions. The value of R_f and R_r can be calculated from the deformation in the temporary shape ε_u (N) and the extension at the stress free state after recovery ε_p (N) according to the following equation[32]:

$$R_f = \varepsilon_u(\mathrm{N})/\varepsilon_m \tag{3-3}$$

$$R_r = \left[\varepsilon_u(\mathrm{N}) - \varepsilon_p(\mathrm{N})\right]/\varepsilon_p(\mathrm{N}) \tag{3-4}$$

Table 3-5 shows that R_f remains at approximately 98.5 % independent of the number of thermomechanical test cycles. However, the value of R_r decreased from 83 % for the first cycle to 79.8 % for the fourth cycle.

Table 3-5 Shape memory properties of GCP-based PUs

	1st cycle		2st cycle		3st cycle		4st cycle	
	R_f (%)	R_r (%)	R_f (%)	R_r (%)	R_f (%)	R_r (%)	R_f (%)	R_r (%)
PU-GCP	98.46%	83.00%	98.49%	81.70%	98.47%	80.13%	98.45%	79.76%
T_{prg} = 6 °C, T_{low} = -20 °C, T_{high} = 16 °C, ε_m= 100%								

Table 3-6 Shape memory properties of different vegetable oil-based PUs

	$T_{prog} = T_{g\text{-}DSC}$+10 (°C)	T_{low} (°C)	$T_{high} = T_{g\text{-}DSC}$ +20 (°C)	R_f (%)	R_r (%)
PU-OCP	-13	-30	-3	92.76	98.19
PU-CaCP	4	-20	14	98.74	87.22
PU-GCP	6	-20	16	98.47	84.39
PU-LCP	41	-10	51	98.59	80.10
PU-CCP	65	0	75	97.92	78.97
ε_m = 70%					

Figure 3-5 (b) shows the time dependence of strain under stress-controlled conditions for different vegetable oil-based PUs. The rate of fixity for all vegetable oil-based PU samples was approximately 98 %, with the exception of PU-OCP, for which R_f was approx. 93 %. This experimental result was attributed to the fact that PU-OCP's T_{low} (-30 ^{o}C) was only 20 ^{o}C lower than its T_{prog} (see Table 3-6). The value of R_r decreased systematically from OCP-based PU (98.19 %) to CCP-based PU (78.97 %) because of the difference in crosslinking density, as already mentioned.

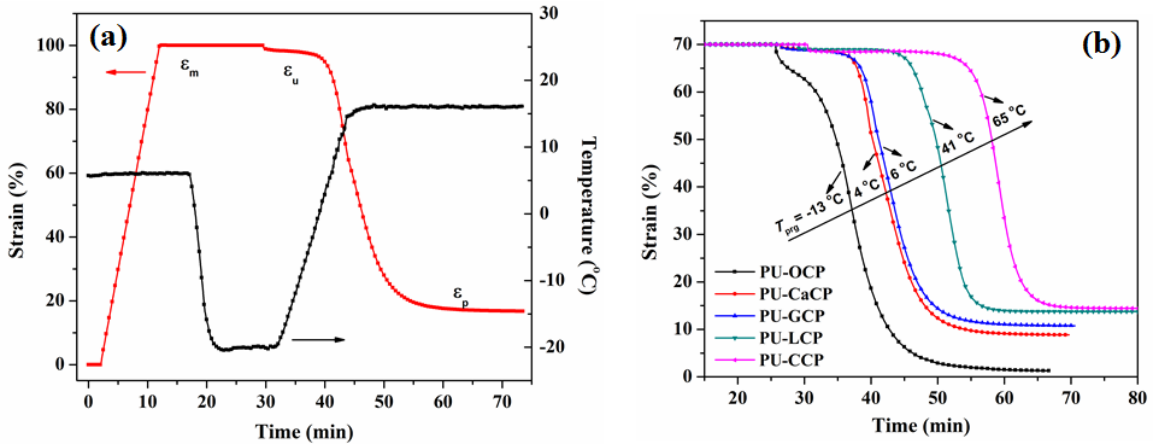

Figure 3-5 (a) Strain curves of GCP-based PUs as a function of time under stress-controlled condition for the first cycle, (b) time dependence of strain under stress-controlled condition for different vegetable-oil-based PUs.

3.5 Conclusions

Bio-polyols with different functionalities were prepared from olive, canola, grape seed, linseed, and castor oil using a solvent/catalyst-free method. Polyurethanes from these polyols were successfully prepared and characterized. The polyols from castor oil had the highest OH numbers while polyols from olive oil had the lowest minimum OH number. Increasing OH numbers of the polyols resulted in an increase in crosslinking densities of the resulting PUs, leading to increasing T_gs, Young's modulus, and tensile strength. The value of R_r decreased systematically

from OCP-based PUs (98.19 %) to CCP-based PUs (78.97 %) because of the difference in their crosslinking densities.

3.6 Acknowledgements

This work was sponsored by Kumho Petrochemical Co. All authors would like to give special thanks to Mengguo Yan from Department of Chemical and Biological Engineering at Iowa State University for her valuable discussions and suggestions.

3.7 References

1. Z. S. Petrovic, *Polym Rev*, 2008, **48**, 109-155.

2. Y. Kurimoto, M. Takeda, S. Doi, Y. Tamura and H. Ono, *Bioresource Technol*, 2001, **77**, 33-40.

3. Y. Xia and R. C. Larock, *Green Chem*, 2010, **12**, 1893-1909.

4. B. Nohra, L. Candy, J. F. Blanco, C. Guerin, Y. Raoul and Z. Mouloungui, *Macromolecules*, 2013, **46**, 3771-3792.

5. D. P. Pfister, Y. Xia and R. C. Larock, *Chemsuschem*, 2011, **4**, 703-717.

6. M. Ionescu, *Chemistry and technology of polyols for polyurethanes*, Rapra Technology, Shawbury, Shrewsbury, Shropshire, U.K., 2005.

7. A. Gandini, *Macromolecules*, 2008, **41**, 9491-9504.

8. R. Tanaka, S. Hirose and H. Hatakeyama, *Bioresource Technol*, 2008, **99**, 3810-3816.

9. X. L. Luo, S. J. Hu, X. Zhang and Y. B. Li, *Bioresource Technol*, 2013, **139**, 323-329.

10. A. Guo, Y. J. Cho and Z. S. Petrovic, *J Polym Sci Pol Chem*, 2000, **38**, 3900-3910.

11. X. Pan and D. C. Webster, *Chemsuschem*, 2012, **5**, 419-429.

12. S. D. Miao, S. P. Zhang, Z. G. Su and P. Wang, *J Appl Polym Sci*, 2013, **127**, 1929-1936.

13. P. P. Kiatsimkul, G. J. Suppes, F. H. Hsieh, Z. Lozada and Y. C. Tu, *Ind Crop Prod*, 2008, **27**, 257-264.

14. C. Q. Zhang, Y. Xia, R. Q. Chen, S. Huh, P. A. Johnston and M. R. Kessler, *Green Chem*, 2013, **15**, 1477-1484.

15. Y. S. Lu and R. C. Larock, *Biomacromolecules*, 2008, **9**, 3332-3340.

16. Z. S. Petrovic, W. Zhang, A. Zlatanic, C. C. Lava and M. Ilavsky, *J Polym Environ*, 2002, **10**, 5-12.

17. P. J. Peruzzo, P. S. Anbinder, O. R. Pardini, J. R. Vega and J. I. Amalvy, *Polym J*, 2012, **44**, 232-239.

18. E. del Rio, G. Lligadas, J. C. Ronda, M. Galia, M. A. R. Meier and V. Cadiz, *J Polym Sci Pol Chem*, 2011, **49**, 518-525.

19. S. N. Khot, J. J. Lascala, E. Can, S. S. Morye, G. I. Williams, G. R. Palmese, S. H. Kusefoglu and R. P. Wool, *J Appl Polym Sci*, 2001, **82**, 703-723.

20. H. Mutlu and M. A. R. Meier, *Eur J Lipid Sci Tech*, 2010, **112**, 10-30.

21. D. S. Ogunniyi, *Bioresource Technol*, 2006, **97**, 1086-1091.

22. S. Dworakowska, D. Bogdal and A. Prociak, *Polymers-Basel*, 2012, **4**, 1462-1477.

23. H. H. Dai, L. T. Yang, B. Lin, C. S. Wang and G. Shi, *J Am Oil Chem Soc*, 2009, **86**, 261-267.

24. X. H. Kong, G. G. Liu, H. Qi and J. M. Curtis, *Prog Org Coat*, 2013, **76**, 1151-1160.

25. I. Javni, D. P. Hong and Z. S. Petrovic, *J Appl Polym Sci*, 2013, **128**, 566-571.

26. D. D. Andjelkovic, M. Valverde, P. Henna, F. K. Li and R. C. Larock, *Polymer*, 2005, **46**, 9674-9685.

27. Y. S. Lu and R. C. Larock, *Prog Org Coat*, 2010, **69**, 31-37.

28. Z. S. Petrovic, L. T. Yang, A. Zlatanic, W. Zhang and I. Javni, *J Appl Polym Sci*, 2007, **105**, 2717-2727.

29. A. Zlatanic, C. Lava, W. Zhang and Z. S. Petrovic, *J Polym Sci Pol Phys*, 2004, **42**, 809-819.

30. I. Javni, Z. S. Petrovic, A. Guo and R. Fuller, *J Appl Polym Sci*, 2000, **77**, 1723-1734.

31. F. Gaboriaud and J. P. Vantelon, *J Polym Sci Pol Chem*, 1982, **20**, 2063-2071.

32. S. D. Miao, N. Callow, P. Wang, Y. Y. Liu, Z. G. Su and S. P. Zhang, *J Am Oil Chem Soc*, 2013, **90**, 1415-1421.

3.8 Supplementary information

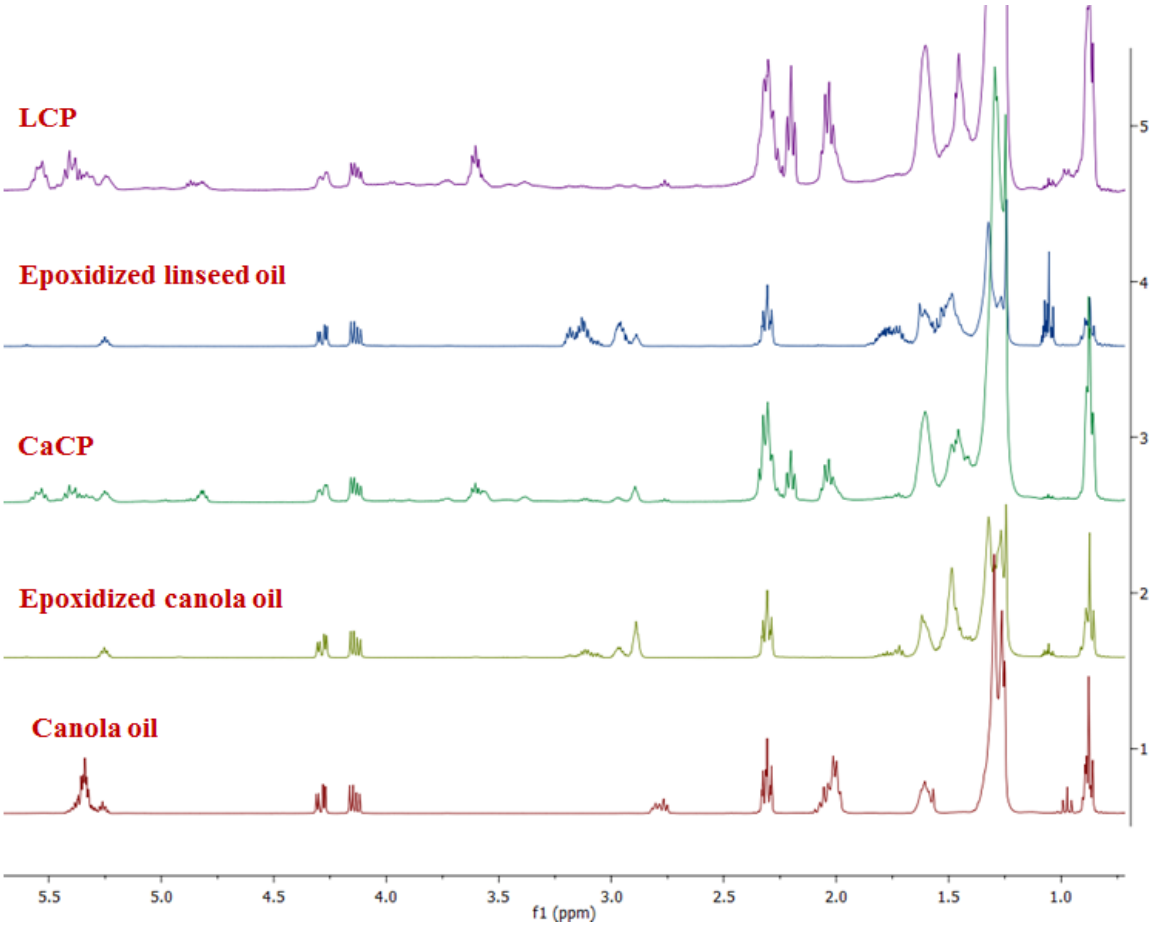

Figure 3-6 ^{1}H-NMR spectra of canola oil, epoxidizied canola oil, CaCP, epoxidized linseed oil, and LCP

CHAPTER 4: POLYURETHANES FROM SOLVENT-FREE VEGETABLE OIL BASED POLYOLS

A paper to be submitted to ACS Sustainable Chemistry & Engineering

Chaoqun Zhang[a], Yuzhan Li[a], Ruqi Chen[a] Ying Xia[a], Seungmoo Huh[e], Patrick A. Johnston[c], Michael R. Kessler[a,b,d,*]

[a] Dept. of Materials Science and Engineering, Iowa State University, Ames, IA, USA

[b] Dept. of Mechanical Engineering, Iowa State University, Ames, IA, USA

[c] Center for Sustainable Environmental Technologies, Iowa State University, Ames, IA, USA

[d] Ames Laboratory, US Dept. of Energy, Ames, IA, United States

[e] Kumho Petrochemical R&BD Center, Daejeon, South Korea

[*] Author for correspondence

4.1 Abstract

The catalytic effects of 1,8-diazabicyclo[5.4.0]undec-7-ene (DBU) and pyridine on the ring opening reaction between epoxidized soybean oil (ESBO) and castor oil-based fatty acids (COFA) were studied using differential scanning calorimetry (DSC). The kinetics of the ring opening reaction between ESBO and COFA with DBU as catalyst was investigated in detail using dynamic DSC and both a model-free method and a model-fitting method. In addition, bio-polyols were prepared from ESBO and epoxidized linseed oil (ELO) using a solvent-free method with DBU as catalyst under mild reaction conditions. The properties of the polyols were characterized by proton nuclear magnetic resonance (^{1}H NMR), Fourier transform infrared spectroscopy (FTIR), and gel permeation chromatography (GPC). The effect of the ratio of carboxylic groups to epoxy groups on the final polyols' structures was discussed. Also, polyurethanes were prepared from isophorone diisocyanate (IPDI) and bio-polyols and characterized by dynamic mechanical analysis (DMA), thermogravimetric analysis (TGA), and

tensile tests. The mechanical and thermal properties of polyurethanes were compared with those of polyurethanes from bio-polyols manufactured using a catalyst-free method. The comparison showed that polyurethanes from LCP-D_0.7 exhibited higher glass transition temperatures, tensile strength, and Young's modulus because of their higher crosslinking density. Polyurethanes from polyols manufactured with DBU as catalyst exhibited good thermo-mechanical properties compared to polyurethanes from polyols manufactured using a catalyst-free method, which was attributed to the homogeneous structure of their crosslinking network.

4.2 Introduction

Polyurethanes (PUs), formed by step-growth polymerization of isocyanate with polyol, are an important class of polymers with an exceptionally versatile range of properties and applications[1, 2]. In order to meet specific requirements, their structure and properties can be tailored by the appropriate selection of polyol and polyisocyanate monomers. In industry, only a limited number of polyisocyanates are commonly used, while a variety of polyols is available[3]. Therefore, the choice of polyol typically determines the properties of the created polyurethane. Although recently much progress has been made in the development of new polyols for polyurethanes, most of the starting materials are petroleum-based, which causes environmental concerns and subjects the polyurethanes to the large price fluctuations of crude oil[4].

Vegetable oils are among the most promising options as feedstock for green polyols to produce polyurethane because they are readily available in large quantities, inherently sustainable, and available at relatively low cost[2, 5]. Vegetable oils are triglycerides consisting of glycerol and three fatty acids. The most common fatty acids are:

- Saturated: palmitic (C16:0)[2] and stearic (C18:0)[a],

[a)] In this notation, the first number represents the number of carbon atoms in the fatty acid chain and the second number represents the number of carbon-carbon double bonds in the fatty acid.

- Unsaturated: oleic (C18:1), linoleic (C18:2), and linolenic (C18:3).

Some fatty acids have specific functional groups, such as hydroxyl-containing ricinoleic acid (C18:1–OH). Different vegetable oils have different compositions of fatty acids, depending on the plant type and climatic conditions at harvest[6]. Generally, the reactive sites within vegetable oils are esters and carbon-carbon double bonds, which can be utilized to introduce functional groups for variety of monomers.

Epoxidation and subsequent oxirane ring opening is a common method to prepare polyols from vegetable oil using ring opening agents, such as alcohols, inorganic acids, and hydrogenation for ring opening[7-11]. However, most of ring opening agents in the past were derived from petroleum, and as a result, the polyols were only partially composed of bio-renewable materails. Currently, several research groups dedicate considerable effort to the development of 100% bio-polyols for PUs. For example, Kiatsimkul[12] prepared high hydroxyl equivalent weight polyols from epoxidized soybean oils that were ring opened by linoleic acid (LA), ricinoleic acid (RC), or ricinoleic acid estolide without catalysts. Our group developed polyols by ring-addition of epoxidized soybean oil and castor oil fatty acid using a solvent/catalyst free method[13]. However, the reactions were conducted at high temperatures (approx. 170 ^{o}C) and with long cycle times (approx. 8 hours), which not only increased the cost of preparation, but also promoted side reactions. One approach to overcome these issues is the use of amine catalysts for the ring opening reaction. Pan[9] reported the use of DBU as catalyst in polyols preparation from epoxidized sucrose esters of soybean oil ring-opened by several organic acids. Matharu[14] synthesized thermosetting resins from epoxidized linseed oil and bio-derived diacid crosslinker with different amine catalysts and reported that 4-demethylaminopydine aided crosslinking between the epoxy and the carboxylic groups, followed by etherification. But few

researchers systematically investigated the reaction kinetics of the ring opening reaction between epoxidized vegetable oils and the ring-opening agents, and the effects of amine catalysts on the preparation of polyols for polyurethanes are still not fully understood.

In this paper, the effects of DBU and pyridine on the ring opening reaction between ESBO and COFA were studied using DSC. Furthermore, bio-polyols were prepared from ESBO and ELO using a solvent-free method with DBU as catalyst under mild reaction condition. Moreover, polyurethanes were prepared from IPDI and bio-polyols. The mechanical and thermal properties of polyurethanes were compared with those of polyurethanes from bio-polyols manufactured using a catalyst-free method.

4.3 Materials and Methods

4.3.1 Materials

ESBO (approximately 4.3 oxirane rings per triglyceride) and ELO (approximately 6 oxirane rings per triglyceride) were purchased from Scientific Polymer Inc., New York, NY. Magnesium sulfate ($MgSO_4$) and methyl ethyl ketone (MEK) were purchased from Fisher Scientific Company (Fair Lawn, NJ). Castor oil, hydrochloric acid, sodium hydroxide, isophorone diisocyanate (IPDI), and 1,8-diazabicyclo[5.4.0]undec-7-ene (DBU) were obtained from Sigma-Aldrich (Milwaukee, WI). All materials were used as received without further purification.

4.3.2 Saponification of Castor Oil

COFA have been prepared by saponification of castor oil[13]. Briefly castor oil saponification was conducted at 80 °C by heating with sodium hydroxide solution for 3 hoursThen, the solution was neutralized by hydrochloric acid Finally, COFA was obtained by purification of solution through washing with water, drying over $MgSO_4$ and filtering COFA is consist of ricinoleic acid (87.7–90.4%) and some other acids, such as linolenic, linoleic, oleic acid.

4.3.3 Preparation of Polyols Based on ESBO, ELO and COFA with DBU as Catalyst

Two series polyols **(**Soy-castor oil based polyols, SCP-D and linseed-castor oil based polyols, LCP-D**)** were prepared from ESBO and ELO ring opened by COFA. Briefly, COFA and ESBO were weighted and mixed in a flask with a magnetic stirrer. Then, DBU (1 wt.% amount of COFA and ESBO) was added in the mixture. Finally, the mixture was stirred homogenous and maintained at 130 °C in the protective atmosphere of nitrogen. The procedure was monitored with interval of 0.5 hour by ^{1}H NMR, which was stopped when the residual epoxy groups were stable in following one hour. Scheme 4-1 shows the preparation of representative green polyols. According to the ratios of carboxylic group to epoxy group and the vegetable oils used, these polyols were identified as SCP-D_0.3, SCP-D_0.5, SCP-D_0.7, SCP-D_0.9, LCP-D_0.5 and LCP-D_0.7 (where S = epoxy soybean oil, C = COFA, L = epoxy linseed oil, P = polylol, D = DBU).

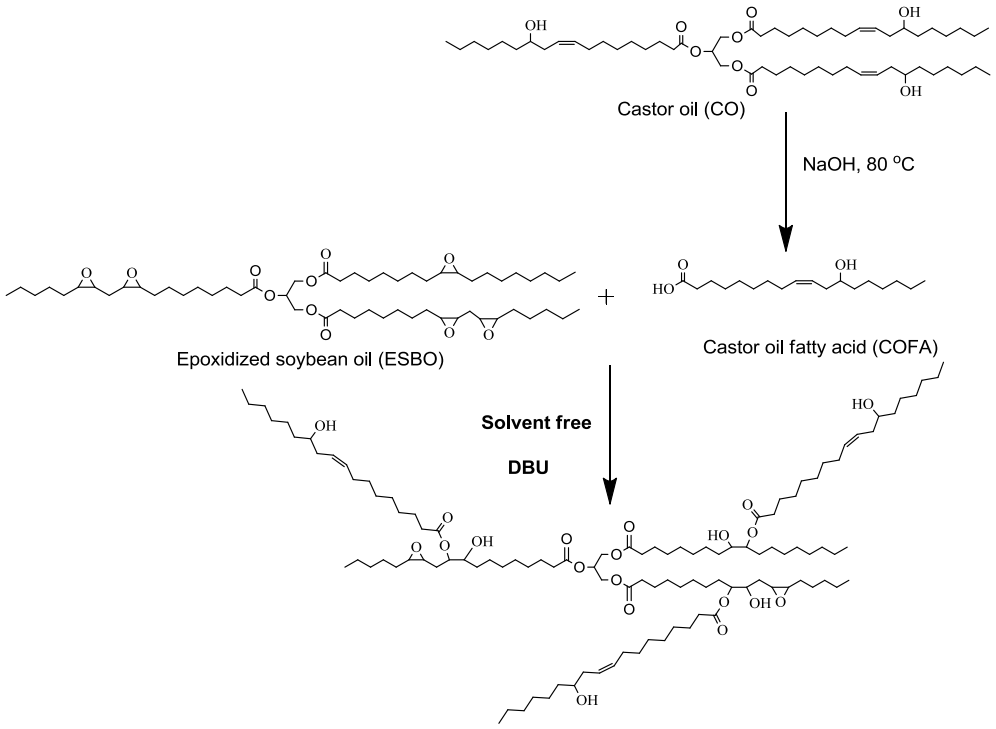

Scheme 4-1 Preparation of representative polyols

4.3.4 Preparation of Polyurethanes Using Polyols

The polyurethanes were prepared as following procedure: First, polyols, IPDI (5% molar excess) and MEK were mixed continuously and maintained at 70 °C for 3 hours. Additional catalyst was not necessary, because DBU used in ring opening reaction could also act as catalyst for PU curing. Then, the solutions were poured into a glass mold (length × width: 100 × 50 mm) and keep in oven at 80 °C overnight. Finally, the PUs films were removed from the mold and cut into specific dimensions for thermo-mechanical testing.

4.3.5 Characterization

^{1}H NMR spectroscopic analysis of the monomers and final products were conducted with a Varian spectrometer (Palo Alto, CA) at 300 MHz All measurements were made using $CDCl_3$ as the solvent. Nicolet 460 FTIR spectrometer (Madison, WI) was used to record the FTIR spectra of monomers and polyols The OH numbers of the polyols were determined using the Unilever method.[15] The acid numbers of the polyols were determined according to AOCS Official Method Te 1a-64. The molecular weight was determined using a THF-eluted GPC equipped with a refractive index detector. The HPLC system used was a Thermo Scientific Dionex Ultimate 3000 (Sunnyvale, CA) equipped with a Shodex Refractive Index (RI). The eluent used was tetrahydrofuran with two Agilent PLgel 3 μm 100 Å 300 × 7.5mm (p/n PL1110-6320) and one Mesopore 300 × 7.5 mm (p/n PL1113-6325). The column flow rate and temperature was 1.0 ml/min at 25 °C.

The following formulation was used to calculate the bio-content of polyols. During calculation, the weight of catalyst are neglected.

Bio-content = Weight of polyols/(Weight of polyols + Weight of isocyanates)

TA Instruments DMA Q800 dynamic mechanical analyzer with a film-tension mode of 1 Hz was used to conduct dynamic mechanical analysis (DMA) of the PU films Rectangular specimens of 0.6 mm × 10 mm (thickness × width) were used for the analysis. The samples were first cooled and held isothermally for 3 min at –40 ^{o}C and then heated to 150 ^{o}C at a rate of 5 ^{o}C/min. The glass transition temperatures (T_gs) of the samples were obtained from the peaks of the tan δ curves.

Thermogravimetric analysis (TGA) of the films was carried out on a TA Instrument Q50 (New Castle, DE). The samples were heated from room temperature to 800 °C at a heating rate of 20 °C min^{-1} in air. Generally, 10 mg samples were used for the TGA.

Instron universal testing machine (model 4502) with a crosshead speed of 100 mm/min was used to determine the tensile properties of the PU films Rectangular specimens of 50 mm ×10 mm (length × width) were used. Average values of at least four replicates of each sample were taken.

4.4 Results and Discussion

4.4.1 The Effect of DBU Catalysts on Ring Opening Reactions

The DSC thermograms of the reactions between ESBO and COFA (with 1 wt.% DBU/pyridine and without catalyst) are shown in Figure 4-1. For the formulations without catalyst, the thermograms showed two separate exothermic peaks at approx. 155 ^{o}C and above 170 ^{o}C (a broad peak), respectively. When pyridine was used as catalyst, both peaks shifted to a lower temperature region and the magnitude of the second peak reduced significantly. For the formulations catalyzed with DBU, the first peak continued to shift to lower temperatures and the second peak almost disappeared (the two thermal events may still have been present but were beyond the resolution of the instrument). The peak temperatures of formulations with pyridine

and DBU are shown in Table 4-1. Matharu *et al*. studied the ring opening reaction between epoxidized linseed oil and carboxyl groups and reported that the first exothermic peak was related to the ring opening reaction by the carboxyl groups, while the second thermal event corresponded to subsequent ring opening by the hydroxyl groups and cross-linking reactions[14]. Our investigation showed that use of DBU and pyridine reduced the reaction barrier and accelerated the reactions while hindering ring opening reactions by the hydroxyl groups. In particular DBU almost prevented ring opening reactions by the hydroxyl groups, resulting in no obvious secondary exothermic peak, as seen in Figure 4-1. As reported earlier, both hydroxyl groups and carboxylic group involved ring opening reaction, connecting two polyols together and leading to pre-crosslinking of polyols in the formulations of ESBO and COFA without catalyst [13]. From above discussion, it was seen that DBU and

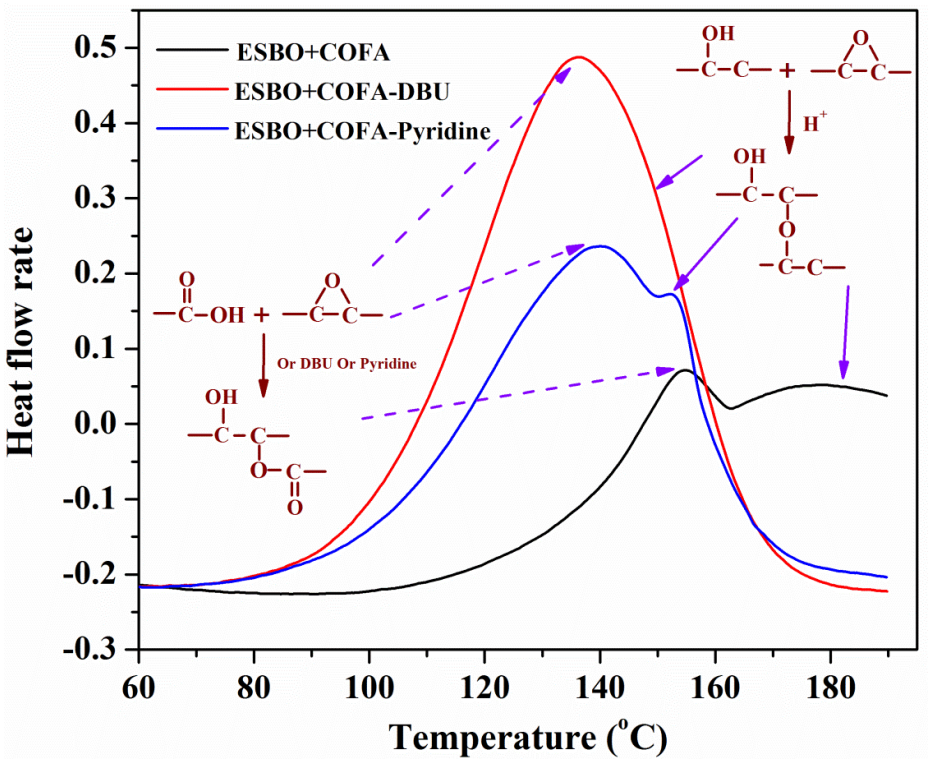

Figure 4-1 Thermograms of mixtures of ESBO and COFA, with catalyst and without catalyst

pyridine reduced crosslinking by hindering ring opening reactions by the hydroxyl groups, leading to less oligomerization and a more homogenous structure of the polyols. Wu[16, 17] offered the following explanation for a possible hydroxyl group ring-opening mechanism: The catalyst protonates the oxygen atom in the oxirane group. An oxygen atom from a hydroxyl group then attacks one of the oxirane carbon atoms and one hydroxyl atom attacks the oxirane oxygen atom. Finally, deprotonation regenerates the acid catalyst as shown in Scheme 4-2. In the formulations without DBU and pyridine, the carboxyl groups acted as acid catalysts and a hydroxyl group came from OH in COFA and the newly generated OHs from the ring-opened epoxies. When DBU and pyridine were used in the formulation, the amine group attracted the protons released by the carboxyl groups and prevented the protonation of the oxygen atom in the oxirane group. Therefore, ring opening reactions by the hydroxyl group was prevented without protons as catalysts, as reported by Petrovic[18], who observed that ring opening reactions only occur in the presence of protonic acids or Lewis acids. Because of the obvious catalyzing effect of DBU on reducing reaction barrier and depression of oligomerization, reaction kinetics of ring opening reaction between ESBO and COFA catalyzed by DBU continued to be systematically studied by dynamic DSC in the following investigation. It is notable to mention that DBU also can act as a catalyst, functionalized as dibutyltin dilaurate used in the literatures[8, 13], in the preparation of polyurethanes.

Table 4-1. DSC analysis

Catalyst	Peak 1 temperature (^{o}C)	Peak 2 temperature (^{o}C)
None	154.7	>170
Pyridine	140.1	152.2
DBU	136.5	-

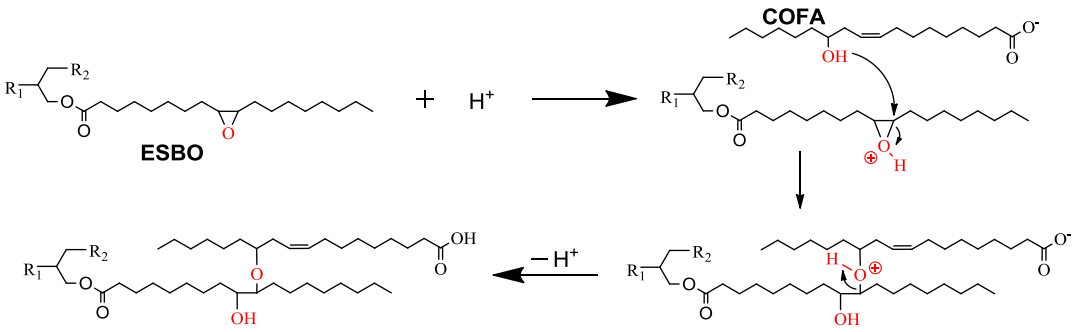

Scheme 4-2 Mechanism of ring-opening reactions between epoxy and hydroxyl group with acid as catalyst

4.4.2 Reaction Kinetics of Ring Opening Reactions with DBU as Catalyst

The effect of DBU on the reaction kinetics of the system was studied using dynamic DSC. The DSC measurements were performed at heating rates of 0.6, 0.8, 1.0, and 1.2 ^{o}C/min under a constant flow of helium at 25ml/min. Data obtained were analyzed using Netzsch Thermokinetics program (version 3.1). Both the model-free isoconversional method and the model-fitting method were used to extract the kinetic parameters.

In kinetic analysis, the rate of reaction can be described by Eq. 1

$$\frac{d\alpha}{dt} = k(T)f(\alpha) = A\exp(-\frac{E}{RT})f(\alpha) \quad (4\text{-}1)$$

Where k(T) is the temperature-dependent rate constant, and f(α) is the reaction model. k(T) is commonly described by the Arrhenius equation, in which R is the universal gas constant, E is the activation energy, and A is the pre-exponential factor. The heat flow dH/dt measured by DSC is directly related to the reaction rate by the following equation[19].

$$\frac{d\alpha}{dt} = \frac{dH/dt}{\Delta H} \quad (4\text{-}2)$$

For experiments carried out at a constant heating rate, Eq. 1 can be rearranged so that

$$\frac{d\alpha}{dT} = \frac{A}{\beta}\exp\left(-\frac{E}{RT}\right)f(\alpha) \quad (4\text{-}3)$$

where β = dT/dt is the heating rate.

Model-Free Isoconversional Method. The model-free isoconversional method is well suited to describe the kinetics of complex reactions. It does not assume any definite form of a reaction model, which allows for the variation of activation energy as the degree of cure[20]. The Friedman differential method is a commonly used isoconversional analysis method and can be derived by taking the logarithms of Eq. 1.

$$\ln\left(\frac{d\alpha}{dt}\right)_{\alpha,i} = \ln\left(A_\alpha f(\alpha)\right) - \frac{E_\alpha}{RT_{\alpha,i}} \tag{4-4}$$

For a specific α at several heating rates β_i, the values of $(d\alpha/dt)_{\alpha,i}$ and $T_{\alpha,i}$ were determined from the DSC thermograms. The activation energy dependence of the degree of cure was then estimated from the plots of $\ln(d\alpha/dt)_{\alpha,i}$ vs. $1/T_{\alpha,}$ (Friedman plots). Kinetic information obtained through this isoconversional approach can then be used in the model-fitting method.

Model-Fitting Method. A multivariate version of the Borchardt and Daniels method is frequently used in the evaluation of dynamic DSC data[19]. In this method, the kinetic parameters (A and E) can be obtained by a linearizing transformation of Eq. 3 so that

$$\ln\frac{d\alpha/dT}{f(\alpha)} = \ln\left(\frac{A}{\beta}\right) - \left(\frac{E}{RT}\right) \tag{4-5}$$

Different kinetic models can then be used to obtain the optimal fit of the kinetic parameters by multiple linear regressions. In addition, the Netzsch Thermokinetics program allows fitting of a multiple-step reaction, providing better simulation of the experimental results.

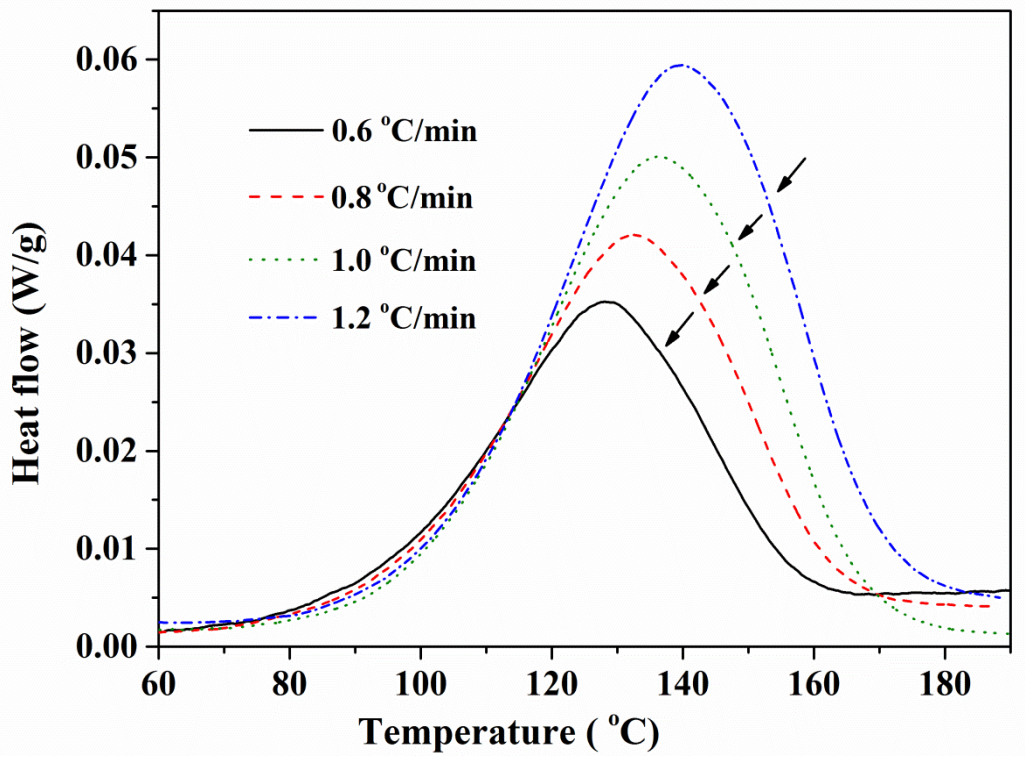

Figure 4-2 DSC dynamic scans at heating rates of 0.6, 0.8, 1, 1.2 °C/min.

Figure 4-2 shows the dynamic DSC scans of the reacting system at different heating rates and the total enthalpy of reaction is summarized in Table 4-2. The main peaks shifted to higher temperature regions with increasing heating rate. A shoulder was observed after the major exothermic peak (see arrows), indicating the presence of a multiple-step reaction.

Table 4-2 Total enthalpy of reaction at different heating rates

Heating Rate (°C/min)	Total Enthalpy of Reaction (J/g)
0.6	119.2
0.8	124.9
1	123.2
1.2	123.8

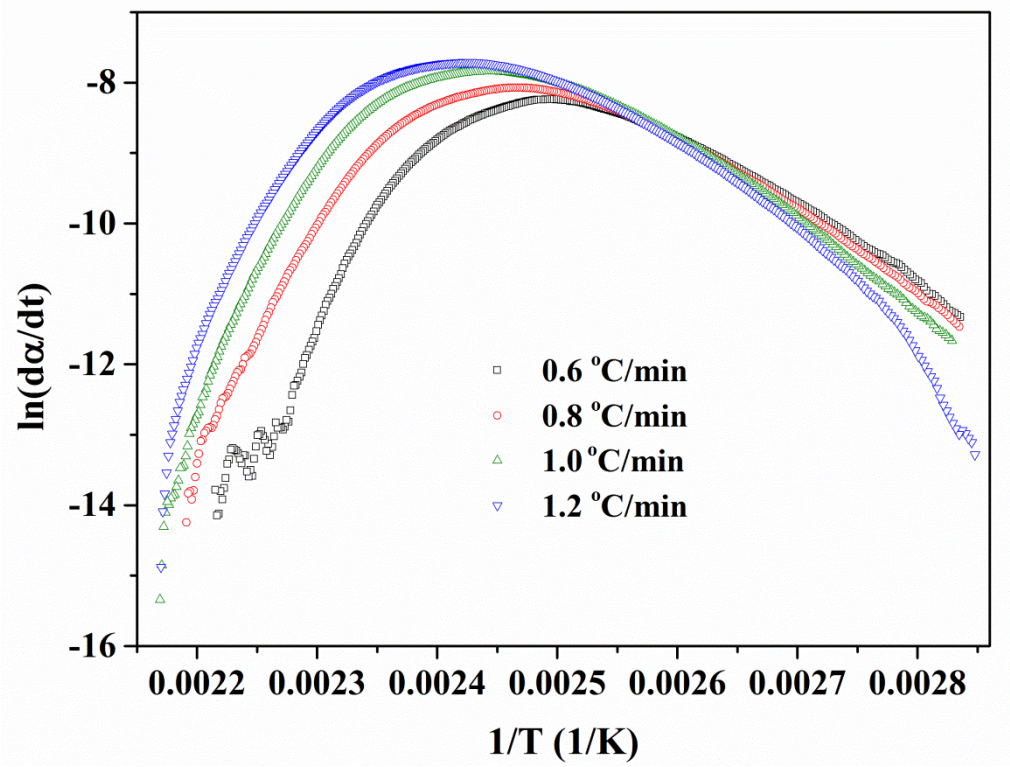

Figure 4-3 Friedman plot

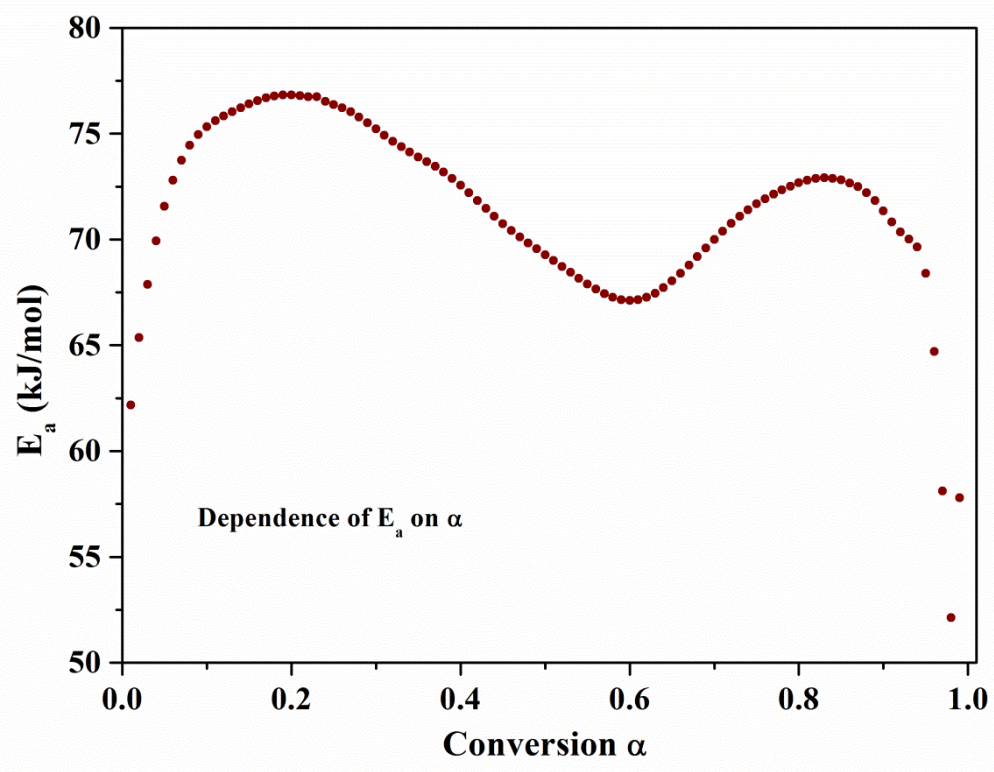

Figure 4-4 Activation energy dependence of conversion determined by Friedman analysis.

To estimate the activation energy for each step involved in the overall reaction, a Friedman plot was created, shown in Figure 4-3. The conversion dependence of the activation energy was then determined from the Friedman plot. As shown in Figure 4-4, two processes with different activation energies were observed, possibly attributed to the reaction between epoxy group and carboxylic group and hydroxyl group, respectively. The two reactions were considered independent and were simulated using an expanded Prout-Tompkins model[21] shown in Eq. 5. Fitting results are shown in Figure 4-5 and kinetic parameters extracted from the modeling are summarized in Table 4-3.

$$f(\alpha)=(1-\alpha)^n\alpha^m \tag{4-6}$$

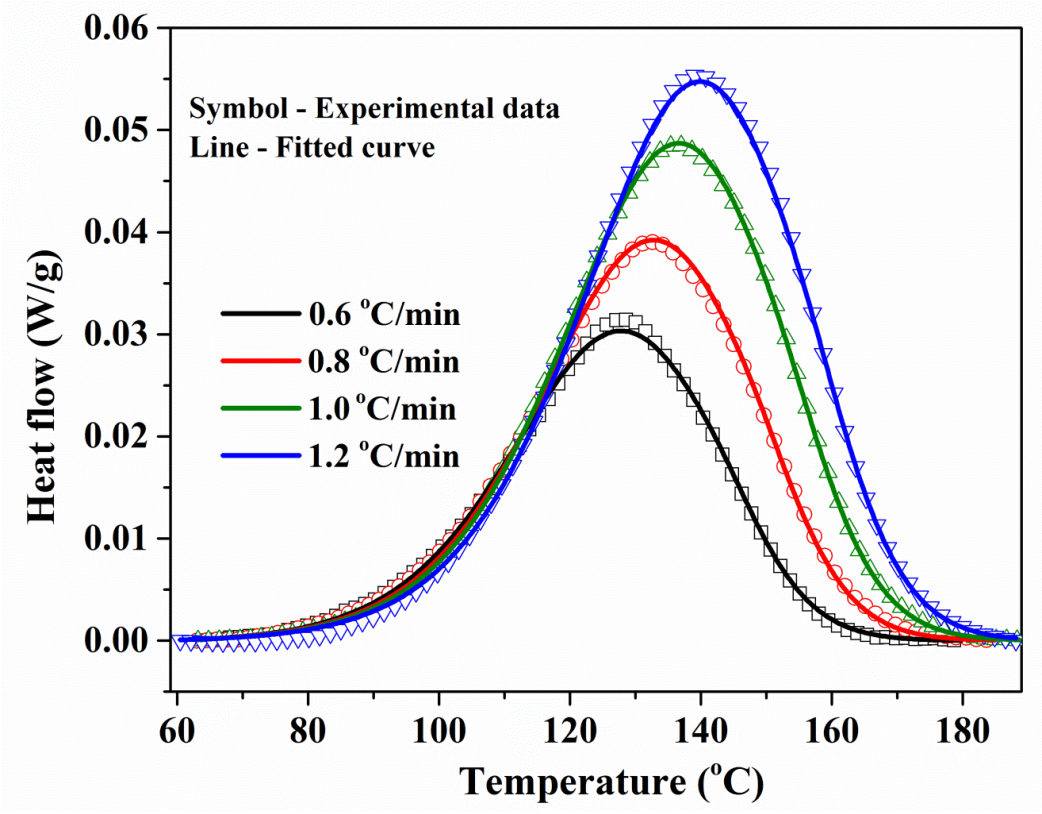

Figure 4-5 Model fits of DSC data

Table 4-3 Results of multiple linear regression analysis

	Process 1	Process 2
Model designation	$f(\alpha)=(1-\alpha)^n\alpha^m$	$f(\alpha)=(1-\alpha)^n\alpha^m$
log [A] (s^{-1})	6.333	6.634
E (kJ/mol)	72.218	75.083
n	1.166	1.139
m	0.267	0.651
Correlation coefficient	0.999777	

The model curves fit the experimental data reasonably well over the entire temperature range. Table 4-3 shows that the activation energy for the ring opening reaction between carboxylic acid and epoxy groups was 72.2 kJ/mol, while for the ring opening reaction between hydroxyl group and epoxy groups it was 75.1 kJ/mol. Erhan[22] reported that the Arrhenius activation energy between propionic acid and epoxidation of methyl oleate under pseudo-first order conditions was 66.7 kJ/mol. Activation energy by *ab initio* calculation was 60.7 kJ/mol for the ring opening of an epoxide through an inversion transition state[23]. The activation energy values obtained by our study were higher than those reported; however, this was attributed to the fact that the molecules in our system had longer carbon chains than those used in the literature. The activation energy of ring opening reaction between hydroxyl group and epoxy groups with weak acid catalyst were 75.08 kJ/mol, a little higher than that between carboxylic acid and epoxy groups.

4.4.3 The Preparation and Characterization of Polyols with DBU as Catalyst

Polyols were prepared from epoxidized soybean oils, ring opened by COFA. To confirm the catalyzing effect of DBU in the ring opening reaction, polyols from epoxidized linseed oils were also prepared. As shown in Table 1, the peak temperature corresponding to the ring opening reaction by carboxylic groups for formulations with DBU as catalyst was measured at 136.5 ^oC. Therefore, a temperature of 130 ^oC was chosen to prepare polyols with different ratios of

carboxylic to epoxy groups. Scheme 4-1 showed the preparation of representative green polyols. The properties of the polyols were characterized by proton nuclear magnetic resonance (^{1}H NMR), Fourier transform infrared spectroscopy (FTIR), and gel permeation chromatography (GPC).

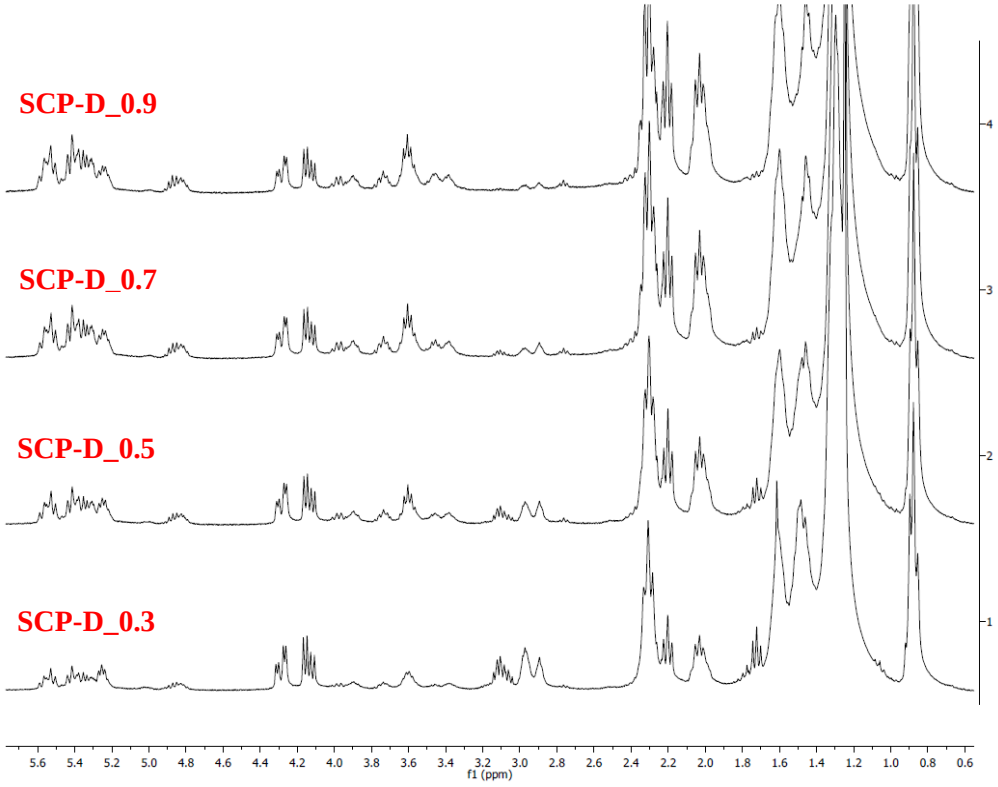

Figure 4-6 ^{1}H-NMR spectra of SCP-D with different ratios of carboxyl to epoxy groups

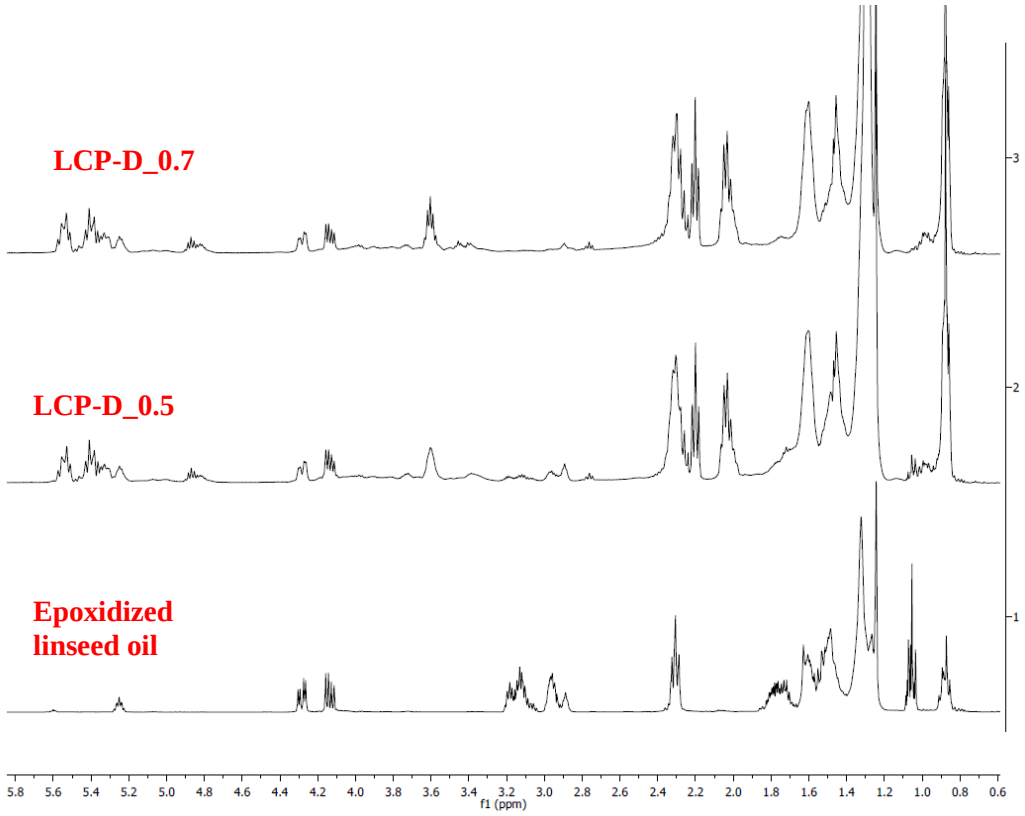

Figure 4-7 ^{1}H-NMR spectra of LCP-D with different ratios of carboxyl to epoxy groups

Figure 4-6 and Figure 4-7 show the NMR spectra of polyols prepared from epoxidzied soybean oil and epoxidized linseed oil, ring opened by COFA using DBU as catalyst. It can be seen that, as the content of COFA increased, the residual epoxy group (the peaks between 2.8 and 3.2 ppm) in SCP-D and LCP-D both decreased. The presence of new peaks between 4.6 and 5.0 ppm, representing tertiary hydrogen atoms adjacent to the newly formed ester groups, indicated that COFA was attached to the long carbon chain of the epoxidized oils. As the content of COFA increased, the peak at 5.3–5.6 ppm (corresponding to carbon-carbon double bonds in COFA) increased, indicating that more COFAs were attached to the long carbon chain of the epoxidized oils. The time needed to complete the reaction is shown in Table 4. It can be seen that, as the content of COFA increased, longer time was needed to complete the reaction because of the increasing steric effect of the long chains in the polyols' structures, which may hinder the

accessibility of the acid groups as more COFA was attached to the long chains. However, the time needed to complete the reaction with DBU as catalyst was shorter than the time needed without catalyst, indicating that DBU reduced the reaction time. Furthermore, the value of the integrated area for the peaks at 4.1–4.2 ppm (-C**H$_2$**-CHCH$_2$-) was used as a constant of 2 for normalization. The residual epoxy groups and carbon-carbon double bonds for different polyols are listed in Table 4.

Table 4-4 Properties of SCP-D and LCP-D.

	Reaction time	C=C bonds	Epoxy	Number /Average Mw	PDI*	Acid number (mg KOH/g)	Titrated OH number(mg KOH/g)
SCP-D_0.3	5 h	1.632	2.929	2033/2358	1.16	0.5	124.1
SCP-D_0.5	5 h	2.756	1.624	2411/2780	1.15	3.3	140.9
SCP-D_0.7	6.5 h	3.473	0.988	2255/2944	1.31	10.2	150.9
SCP-D_0.9	6.5 h	4.672	0.029	1960/2879	1.47	22.0	157.61
LCP-D_0.5	6.5 h	3.0835	1.545	2799/3358	1.2	0.8	176.72
LCP-D_0.7	6.5 h	4.4425	1.292	2679/3615	1.35	9.2	183.84

*PDI = Polydispersity index

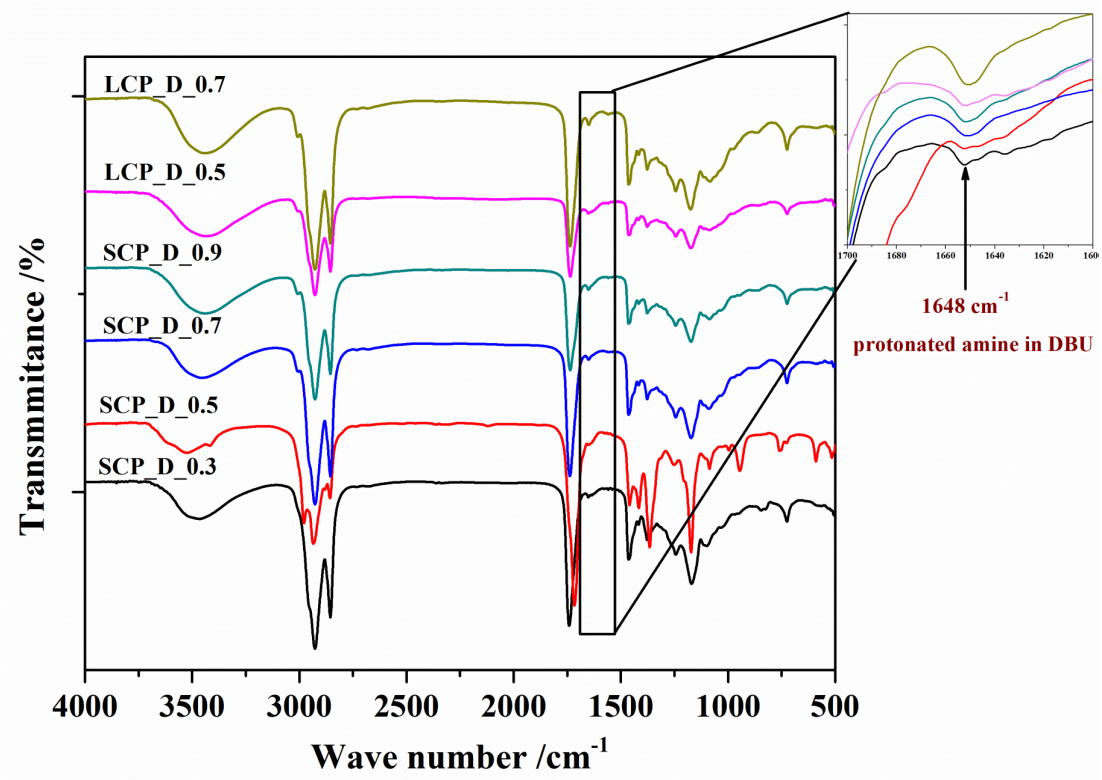

Figure 4-8 FT-IR spectra of SCP-D and LCP-D with different ratios of carboxyl to epoxy groups

Figure 4-8 shows the FT-IR spectra of polyols prepared by COFA oxirane ring opening of ESBO and ELO. Oxirane absorption at 823 cm^{-1} corresponded to epoxy groups, while a broad peak at 3392 cm^{-1} appeared in polyol [24], suggesting that the epoxy groups in ESBO were ring-opened and hydroxyl groups had been formed. A band at 1648 cm^{-1} was observed in the DBU system, corresponding to protonated amine[25, 26], which confirmed the earlier conclusion that the amine group attracted the protons released by the carboxyl groups.

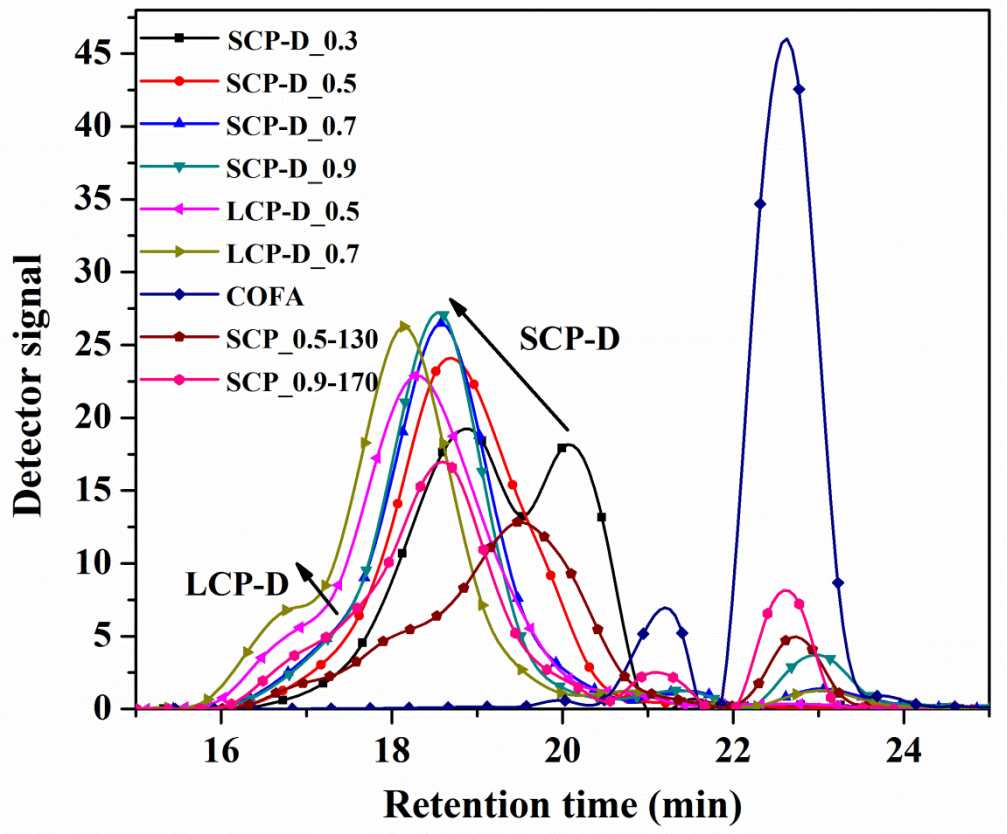

Figure 4-9 GPC curves of SCP-D and LCP-D with different ratios of carboxyl to epoxy groups

The GPC curves of SCP-D and LCP-D with different ratios of carboxyl to epoxy groups are shown in Figure 4-9. It can be seen that, as reaction ratios of carboxylic to epoxy groups increased in polyols prepared from ESBO, the main peak of the polyols shifted to lower retention times, indicating increased molecular weight. The same trend was observed for polyols prepared from ELO. Compared to SCP_0.5-130 and SCP_0.9-170 , which were prepared without catalyst, SCP-D_0.5 and SCP-D_0.9 contained less residual COFA, as shown in the peak at a retention time of 23 min, indicating that more COFA was attached to the long chains of epoxidized oils in the presence of a DBU catalyst. The GPC curve of SCP-D_0.9 indicated a narrow molecular weight distribution without the oligomerization peak (at a retention time of 16–17 min) seen for SCP_0.9-170. This can be explained by the fact that DBU hinders ring opening by hydroxyl

groups, leading to less connection of polyols and less oligomerization. The molecular weights of the polyols is listed in Table 4-4.

4.4.4 Polyurethane from SCP-D and LCP-D

SCP-D_0.3, SCP-D_0.5, SCP-D_0.7, and LCP-D_0.7 were chosen to prepare PUs, and their properties were characterized by DMA, TGA, and tensile strength tests. Because the PU from SCP-D_0.3 was too soft, it was difficult to collect mechanical data.

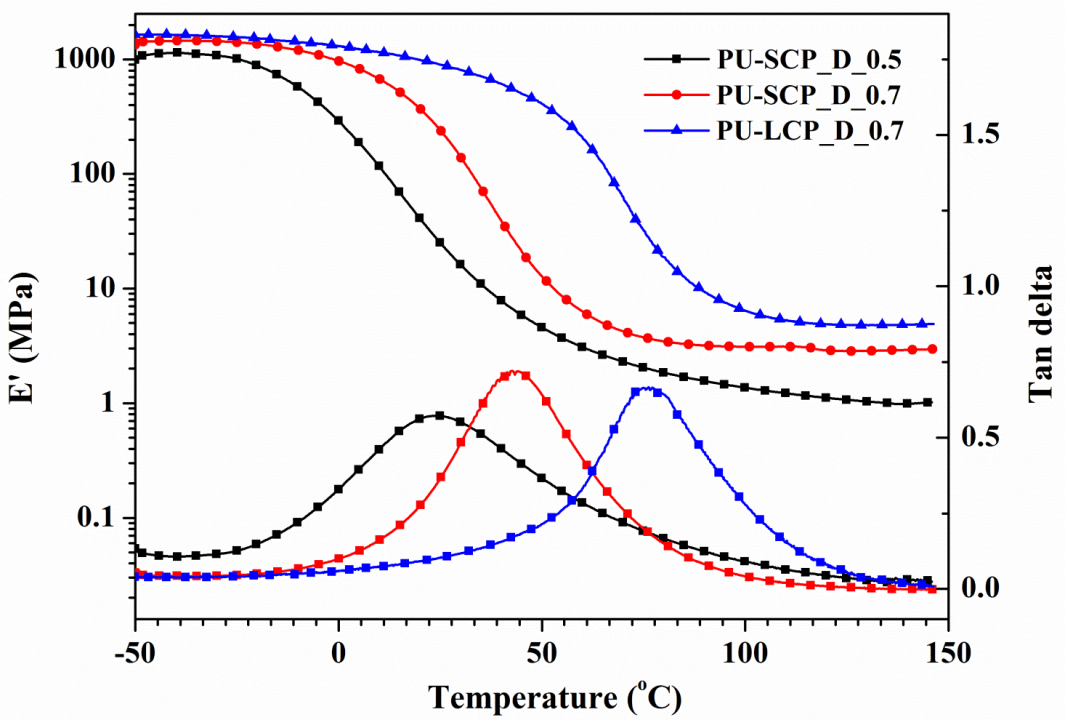

Figure 4-10 Storage modulus and loss factor as functions of temperature for PU films based on SCP-D and LCP-D

Figure 4-10 shows storage modulus and loss factor as functions of temperature for PU films in the temperature range from –50 to 150 °C. With increasing temperature, all films showed a similar trend. In detail, with temperature increasing from –35 °C, E' slightly decreased and once –10 °C was reached, a rapid decrease in E' was observed. A rubbery plateau for the storage modulus was observed in every curve in the higher temperature range of the tests and a peak

maximum was observed in the tan δ versus temperature curves (α relaxation), which was taken as the glass transition temperature (T_g). All films show one tan δ peak, indicating the homogeneous nature of the polyurethane films. As the crosslinking densities increased, the molecular motion of the polymer chains became more restricted and the amount of energy dissipated throughout the polymer decreased dramatically; therefore, the tan δ peak shifted to higher temperatures.[8, 27] As the OH number increased, crosslinking density increased, leading to a higher T_g and higher storage modulus. Compared with PUs from SCP_0.5, PUs from SCP-D_0.5 had a higher bio-content, but a lower T_g as shown in Table 5. However, PUs from SCP-D_0.7 had a higher bio-content and a higher T_g.

Figure 4-11 shows TGA weight loss and weight loss derivative curves in air for polyurethane films. The degradation of polyurethanes observed at temperatures between 200 and 350 ^oC was attributed to the decomposition of labile urethane groups. The degradation observed in the temperature range from 350 to 500 ^oC resulted from chain scission in the soybean oil. The last degradation step above 500 ^oC corresponded to further thermo-oxidation of the PU films in air. In the first decomposition stage, as the COFA content increased, leading to higher OH numbers, the thermal stability of the PU films from SCP-D and LCP-D decreased as a result of the higher number of urethane bonds. PUs from SCP_0.5 had more urethane bonds and therefore exhibited lower thermal stability than PU from SCP-D. In the second and third degradation stage, as the COFA content increased, the thermal stability of PU from SCP-D and LCP-D decreased because the thermal resistance of COFA is lower compared to that of ESBO. PUs from SCP_0.5

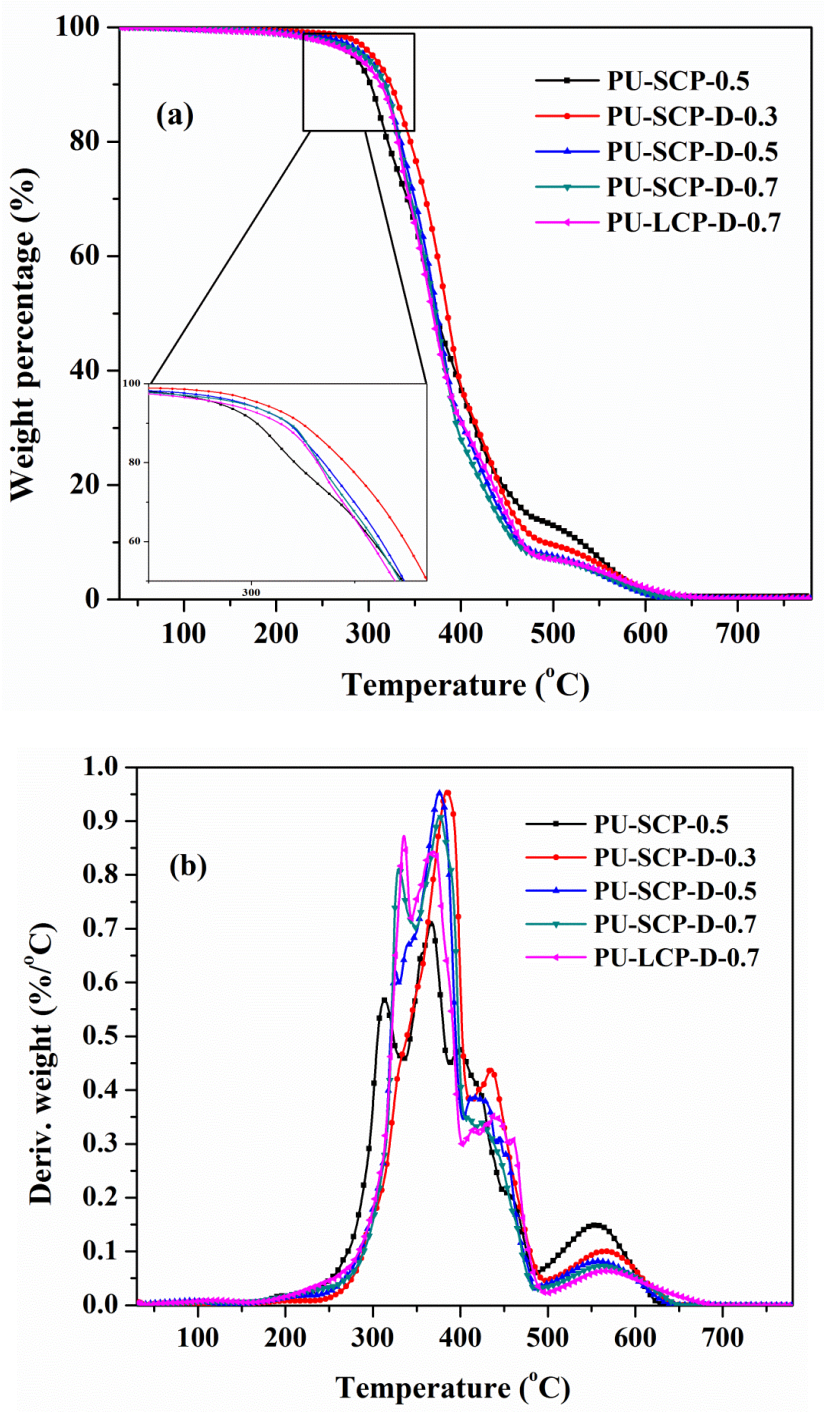

Figure 4-11 TGA curves (a) and their derivative curves (b) for PU films based on SCP, SCP-D, LCP-D

exhibited higher thermal resistance than PUs from SCP-D and LCP-D because of the crosslinking of the polyols. Table 4-5 shows that 10% degradation (T_{10}) occurred at 302 °C, 324

^{o}C, 318 ^{o}C, 318 ^{o}C, and 314 ^{o}C, respectively for the five PUs investigated; 50% degradation (T_{50}) was detected at 373^{o}C, 385 ^{o}C, 374 ^{o}C, 372 ^{o}C and 370 ^{o}C, respectively.

Table 4-5 Thermal and mechanical properties of PUs based on SCP-D_0.3, SCP-D_0.5, SCP-D_0.7 and LCP-D_0.7

	DMA T_g (^{o}C)	TGA in air (^{o}C)		Tensile strength (MPa)	Young's modulus (MPa)	Elongation at break (%)	Bio-content
		T_{10}	T_{50}				
PU-SCP-D_0.3	-	324	385	-	-	-	80%
PU-SCP-D_0.5	24.0	318	374	3.5 ± 1.1	5.6±1.1	107%±4.1	76%
PU-SCP-D_0.7	42.5	318	372	12.4 ±0.5	36.9±5.6	157.3%±13.6	75%
PU-LCP-D_0.7	69.0	314	370	20.1±2.1	303.7±45.7	104.0%±5.0	71%
PU-SCP_0.5[13]	31.3	302	373	11.6±0.4	5.8±0.5	232.7±18.0	72%

Table 4-5 summarizes Young's moduli, tensile strength, elongation at break, and bio-content of the polyurethane films investigated. PUs based on LCP-D_0.7 exhibited the highest tensile strength (20.1 MPa) and a higher Young's modulus (303.7 MPa) compared to other PU films because of their higher crosslinking density. Although PUs from SCP-D_0.5 exhibited lower tensile strength and Young's moduli than PUs from SCP_0.5 because of their lower crosslinking density, they had a higher bio-content. PUs from SCP-D_0.7 exhibited higher tensile strength and Young's moduli, and bio-content than PUs from SCP_0.5. This fact was attributed to the fact that the homogeneous structure of SCP-D caused the good mechanical properties of the corresponding polyurethanes. The oligomerization structure of SCP compromised the polyurethanes' tensile strength. However, polyurethanes based on SCP-D and LCP-D exhibited a lower value for elongation at break compared to PUs based on SCP

4.5 Conclusions

DBU not only reduced the barrier for ring opening reactions between epoxidized vegetable oils and COFA, resulting in a decrease in reaction temperature and reaction time, but also hindered the epoxy ring opening reaction by the hydroxyl group, leading to less oligomerization and a homogeneous structure of the polyols. The activation energy of the ring opening reaction between epoxy and carboxylic group with DBU as catalyst was 72.2 kJ/mol, while the activation energy of the ring opening reaction between epoxy and hydroxyl group with protons as catalysts was 75.1 kJ/mol. The kinetic model developed suggested that the ring opening reactions between epoxy group and carboxylic group, hydroxyl group follows nth order about 1.1 and have a total reaction order (n+m) of 1.4, 1.8 respectively. The homogenous structure of the polyols had a positive effect on the properties of the final polyurethanes, such as higher T_g and higher Young's modulus. It is worth noting that ring-opening reaction and the subsequent polymerization reaction shared the same catalyst, namely DBU. Thus, it is not necessary to remove the catalyst between the two steps, making this approach both time- and cost-effective.

4.6 Acknowledgement

This work was sponsored by Kumho Petrochemical Co.

4.7 Reference

1. G. Lligadas, J. C. Ronda, M. Galia and V. Cadiz, *Biomacromolecules*, 2007, **8**, 686-692.
2. Y. Xia and R. C. Larock, *Green Chem*, 2010, **12**, 1893-1909.
3. D. P. Pfister, Y. Xia and R. C. Larock, *Chemsuschem*, 2011, **4**, 703-717.
4. Z. S. Petrovic, *Polym Rev*, 2008, **48**, 109-155.
5. C. K. Williams and M. A. Hillmyer, *Polym Rev*, 2008, **48**, 1-10.
6. M. A. R. Meier, J. O. Metzger and U. S. Schubert, *Chem Soc Rev*, 2007, **36**, 1788-1802.

7. A. Guo, Y. J. Cho and Z. S. Petrovic, *J Polym Sci Pol Chem*, 2000, **38**, 3900-3910.

8. Z. S. Petrovic, W. Zhang, A. Zlatanic and C. C. Lava, *Abstr Pap Am Chem S*, 2002, **223**, D95-D95.

9. X. Pan and D. C. Webster, *Chemsuschem*, 2012, **5**, 419-429.

10. C. S. Wang, L. T. Yang, B. L. Ni and G. Shi, *J Appl Polym Sci*, 2009, **114**, 125-131.

11. Z. S. Petrovic, A. Guo and W. Zhang, *J Polym Sci Pol Chem*, 2000, **38**, 4062-4069.

12. P. P. Kiatsimkul, G. J. Suppes, F. H. Hsieh, Z. Lozada and Y. C. Tu, *Ind Crop Prod*, 2008, **27**, 257-264.

13. C. Q. Zhang, Y. Xia, R. Q. Chen, S. Huh, P. A. Johnston and M. R. Kessler, *Green Chem*, 2013, **15**, 1477-1484.

14. N. Supanchaiyamat, P. S. Shuttleworth, A. J. Hunt, J. H. Clark and A. S. Matharu, *Green Chem*, 2012, **14**, 1759-1765.

15. M. D. Phaneuf, M. J. Bide, M. Szycher, M. B. Gale, H. X. Huang, C. Q. Yang, F. W. LoGerfo and W. C. Quist, *Asaio J*, 2001, **47**, 634-640.

16. S. B. Wu and M. D. Soucek, *Abstr Pap Am Chem S*, 1996, **212**, 108-POLY.

17. S. B. Wu and M. D. Soucek, *Polymer*, 1998, **39**, 3583-3586.

18. Y. J. Xu and Z. S. Petrovic, *J Am Oil Chem Soc*, 2008, **85**, 1185-1186.

19. M. R. Kessler and S. R. White, *Journal of Polymer Science Part a-Polymer Chemistry*, 2002, **40**, 2373-2383.

20. S. Vyazovkin and N. Sbirrazzuoli, *Macromolecular Rapid Communications*, 2006, **27**, 1515-1532.

21. J. R. Opfermann, E. Kaisersberger and H. J. Flammersheim, *Thermochimica Acta*, 2002, **391**, 119-127.

22. K. M. Doll, B. K. Sharma and S. Z. Erhan, *Ind Eng Chem Res*, 2007, **46**, 3513-3519.

23. S. Harder, J. H. Vanlenthe, N. J. R. V. Hommes and P. V. Schleyer, *J Am Chem Soc*, 1994, **116**, 2508-2514.

24. A. Adhvaryu and S. Z. Erhan, *Ind Crop Prod*, 2002, **15**, 247-254.

25. D. J. Heldebrant, P. G. Jessop, C. A. Thomas, C. A. Eckert and C. L. Liotta, *J Org Chem*, 2005, **70**, 5335-5338.

26. A. Huczynski, M. Ratajczak-Sitarz, A. Katrusiak and B. Brzezinski, *J Mol Struct*, 2008, **888**, 84-91.

27. Y. Xia and R. C. Larock, *Macromol Mater Eng*, 2011, **296**, 703-709.

CHAPTER 5: BIO-POLYURETHANE FOAM MADE FROM COMPATIBLE BLENDS OF VEGETABLE OIL-BASED POLYOL AND PETROLEUM-BASED POLYOL

A paper to be submitted to Bioresource Technology.

Chaoqun Zhang[a], Michael R. Kessler[a,b*]

[a] Department of Materials Science and Engineering, Iowa State University, Ames, IA, USA

[b] School of Mechanical and Materials Engineering, Washington State University, Pullman, WA, USA

[*] Author for correspondence

5.1 Abstract

This study determined the Hansen solubility parameters of a soy-castor oil-based polyol (SCP) and a petroleum-based polyol (P-450) as well as compatibility between these two polyols using theoretical predictions and dissolution tests confirmation. It was confirmed that SCP was compatible with P-450 at different ratios in a temperature range between 25 ^{o}C and 90 ^{o}C. The blends with different ratios of these two polyols were used to prepare polyurethane (PU) foams. With increasing levels of SCP content, the number of open foam cells increased and their size became smaller; also, the thermal stability of the PU foams improved, and their thermal conductivity increased. The foam's compression strength decreased because SCP exhibited lower activity, lower hydroxyl numbers, and higher viscosity than P-450. This study provided a method to evaluate the blend compatibility of a bio-component and petroleum based component for the preparation of polymeric materials that balances economic and environmental considerations.

Keywords: Polyurethane foam, Blends, Hansen solubility parameter, Thermal conductivity

5.2 Introduction

Rigid and flexible polyurethane (PU) foams are widely used in building construction and in the automotive, packaging, and medical device industries because they offer many numerous advantages, including light weight, excellent strength, low thermal conductivity and high weight-carrying capacity [1, 2]. In general, PU foam is the result of a reaction between polyisocyanate and polyol in the presence of a catalyst, which produce the PU matrix and of the reaction between isocyanate and water, which produce urea and carbon dioxide that acts as a blowing agent to create the foam cells. Historically, petroleum has been the feedstock for polyols and isocyanates for the production of PU foams. Over the past decade, depleting fossil reserves, increasing petroleum prices, and environmental concerns have triggered growing interest in the development of biorenewable feedstocks to substitute petrochemically derived counterparts in the production of some polymeric materials, including PU.

Currently, some of the most widely studied renewable resources for the polymer industry include plant oils, starch, woods, and cellulose [3, 4]. Vegetable oils are one potential sustainable resource for polyols in the PU foam industry because they are inexpensive, readily available, and renewable [5, 6].

Several vegetable oil-based polyols were developed for the manufacture of PU foams, ranging from flexible to rigid, with a broad range of properties. Guo prepared bio-polyols from epoxidized soybean oil ring-opened by methanol and the resulting rigid PU foam exhibited comparable mechanical, and insulating properties, and better thermal resistance properties than foams from petrochemical feedstocks [7]. Dworakowska developed polyols from rapeseed oil

through microwave-assisted synthesis for flexible PU foams. The effects of the renewable content on the cell structure, tensile strength, and resilience values of foam were investigated [8]. Veronese synthesized polyols with high functionalities from castor oil by transesterification with triethanolamine and glycerin. The corresponding rigid PU foam exhibited slightly lower mechanical properties than rigid foams from petroleum based polyols [9]. Lee prepared epoxidized diethanolamides as polyols by reacting epoxidized palm oil with diethanolamine, and produced PU foam with acceptable dimensional stability [10]. Moreover, Tu reported that epoxidized soybean oil can directly react with isocyanate and that the blends of epoxidized soybean oil and petroleum-based polyether polyols can be used for preparation of rigid and flexible PU foams [11]. However, the preparation methods of vegetable oil-based polyols often caused high viscosity, secondary functional groups (relative low reactivity), and low hydroxyl numbers, resulting in PU foams with inferior properties, such as heterogeneous cell structure [12] and difficulty in density control [13]. Also, the controversy over food-grade feedstocks being used for the production of polymeric materials impedes their wide application on an industrial scale. Therefore, a partial replacement of petroleum-based polyols with bio-based polyols is a widely accepted approach to the preparation of PU foam. Another motivation for the partial substitution of petroleum-based polyols is the opportunity to tailor mechanical, thermal and physical properties of PU foams by blending vegetable oil-based polyols and petroleum-based polyols [11, 14].

This approach is feasible only as long as the two polyols are compatible given their differences in molecular weight, density, and molecular structure. Incompatibility of the blend partners may not only cause phase separation during prolonged storage and/or shipment, but it also strongly influences the performance of the corresponding PU foams, such as physical instabilities, heterogeneous structure, and poor properties [15, 16]. Tu indicated that the incompatibility between

epoxidized soybean oil and petroleum polyol caused phase separation, leading to large bubbles in rigid PU foam [11]. However, this issue has not received further attention. It is necessary to develop a method to evaluate the compatibility between blends of polyols in order to design novel polyols and to determine appropriate formulations for the manufacture of PU foams.

Traditionally, Hansen solubility parameters are used to estimate the compatibility of two materials [17, 18]. The idea is based on the assumption that two materials that have matched solubility parameters will have balanced forces, and therefore are miscible, which can be used to predict the compatibility of two materials. The solubility parameter is a cohesion parameters describing interaction between molecules [17, 19] and can be calculated from the cohesive energy per unit volume (cohesive energy density) [20]. The cohesive energy is the sum of internal energy that hold the materials intact, consisting of dispersion cohesion energy (E_D), polar cohesion energy (E_P), and hydrogen bonding cohesion energy (E_H).

$$\delta_T = \sqrt{\frac{E_T}{V}} \tag{1}$$

$$E_T = E_D + E_P + E_H \tag{2}$$

Therefore, Hansen defined three parameters affecting a solvent's solubility: the dispersion parameter (δ_D), meant to quantify the London dispersion forces of the solvent; the polar parameter (δ_P), which is attributed to a molecule's fixed dipole moment; and the hydrogen bonding parameter (δ_H), which accounts for a molecule's hydrogen bonding forces [21].

$$\delta_T^2 = \delta_D^2 + \delta_P^2 + \delta_H^2 \tag{3}$$

Upon calculating all three solubility parameters, any solvent can be plotted on a three-dimensional plot called a solvent map. Each solvent has a fixed radius on the map. Any species whose parameters reside within the resulting sphere (the solubility region) should be soluble in the solvent, while those whose parameters exclude in the resulting sphere should be non-soluble

in the solvent. The most common method for the prediction of Hansen solubility parameter values of materials was proposed by Krevelen and Hoftyzer based on the contributions of functional groups [22]. However, this method is not suitable for vegetable oil-based polyols that contain a complex combination of multiple fatty acid structures.

In this research, the Hansen solubility parameters of bio-polyol (SCP) and petroleum based polyol (P-450) were determined using dissolution tests. Compatibility between these two polyols was evaluated by theoretical prediction and experimental confirmation in the temperature range between 25 ^{o}C and 90 ^{o}C, relevant for PU foaming. Finally, PU foams were prepared from blends with various ratios of vegetable oil and petroleum based polyols. The morphologies of the PU foams were characterized by scanning electron microscope (SEM). In addition, the thermal, physical, and mechanical properties of the PU foams were characterized using thermal conductivity tests, thermogravimetric analyses, and compression tests. The effects of bio-polyol content on the thermal-mechanical properties of the resulting PU foams were discussed.

5.3 Materials and Methods

5.3.1 Materials

Polyol 450 (P-450), a reaction product of propylene oxide and glycerin, and polymeric diphenylmethane-4, 4'-diisocyanate (PMDI, NCO content: 31 wt. %) were provided by Kumho Petrochemical Co. The catalysts (POLYCAT® 5 and POLYCAT® 7) and surfactant (Dabco® DC 5357) were kindly provided by Air Products (Vandalia, IL). Distilled water was used as a blowing agent. SCP was prepared by ring opening reaction of epoxidized soybean oil by castor oil fatty acid using a procedure previously reported [23]. All solvents used to determine the Hansen solubility parameters of the polyols were common laboratory solvents of high purity obtained

from commercial chemical suppliers (Sigma-Aldrich, Milwaukee, WI) and were used as received.

Table 5-1 Properties of SCP and P-450

	OH number (mg KOH/g)	Acid number (mg KOH/g)	Number average molecular weight	Polydispersity index	Viscosity (Pa·s) at 25 ^{o}C, shear rate of 30/s
SCP	148	3.7	2611	1.32	8.24
P-450	355	-	702	1.05	0.29

5.3.2 Determination of solubility parameters for SCP and P-450

The Hansen solubility parameters for both polyols (SCP, and P-450) were determined by qualitatively measuring the dissolution of the polyols in various common organic solvents (28 types) with well-known parameters. A predetermined amount of 0.4 g polyol was added to a 20 ml vial containing 4 ml of the respective solvent. The mixture was sealed and mixed vigorously for 7 h, and subsequently kept at room temperature for 3 days. After visual inspection, the dissolution test results were classified into two categories: soluble and non-soluble. With the dissolution information for SCP and P-450 in various solvents, the Hansen solubility parameters and the interaction radii were calculated using HSPiP software. Finally, the compatibility between SCP and P-450 was predicted by determining whether the Hansen solubility parameters of SCP and P-450 were in the each other's solubility sphere.

Also, the compatibility of SCP and P-450 was confirmed by experimental dissolution tests. The blends with different weight percentages of SCP (0 %, 20 %, 40 %, 60 %, 80 %) were mixed vigorously for 7 h. The mixtures were put in oven at different temperatures (25 ^{o}C, 50 ^{o}C, 75 ^{o}C,

90 ^{o}C) for 1 day, after which the miscibility of the blend partners was determined by visual inspection.

5.3.3 Preparation of PU Foam

Polyurethane foams were prepared according to a reported foam formulation [24] as shown in Table 5-2. The polyols were pre-mixed in specific weight percentages. The polyol blends, catalysts (Polycat ® 5 and Polycat ® 8), surfactant (Dabco ® DC5357), and blowing agent (distilled water) were mixed in a plastic cup for 30s using a high speed mixer. The PMDI was added quickly into the mixture using a syringe and the mixture was mixed for another 12 s. Subsequently, the mixture was allowed to foam and settle for 8 days prior to analysis.

Table 5-2 Formulations for PU foam

Polyol blends	Polycat ® 5	Polycat ® 8	Dabco ® DC5357	Water	PMDI
100	1.26	0.84	2.5	3.0	Index ×1.1

5.3.4 Characterization of Polyols and PU Foam

The OH values of the polyols were titrated according to the Unilever method [25]. The acid numbers of the polyols were determined by AOCS Official Method Te 1a-64. Rheological tests of polyols were conducted using an AR2000ex stress-controlled rheometer (TA Instruments) with parallel plate geometry at room temperature.

The apparent density of the PU foam was measured according to ASTM D 1622-08. Four samples per foam formulation were measured and the average result was reported. The compressive properties of the PU foams were evaluated on an Instron universal testing machine with a crosshead speed of 4 mm/min according to ASTM D 1621-10. At least three samples were tested to obtain average values. The test specimens were cylinders with a diameter of 60mm and a thickness of 40mm.

Solvent extraction tests were conducted using the following procedure: 0.1 g samples cut from middle of the middle of the PU foam samples were immersed in 15 ml dimethyl formamide for 4 days at room temperature followed by oven drying at 70 ^{o}C for 2 days. The weight loss after solvent extraction was recorded based on an average of 4 samples per foam formulation. Transient plane source technique (ASTM C518-91) was employed to measure the thermal conductivity of the PU samples , using a hot disk TPS 1500 system (ThermTest Inc) with 80 s measure time and 15 mW heating power. The experiments were carried out at room temperature by placing the sensor between two cylindrical samples with a diameter of 60 mm and a thickness of 20 mm. The cellular structure of the samples was investigated using a FEI Quanta 250 field emission scanning electron microscope (FE-SEM) operated at 8 kV. The foams were frozen in liquid nitrogen and cut with a razor blade into rectangular samples with the dimension of 10 mm $\times$ 5 mm $\times$ 3 mm. The top surface of each sample was sputter coated with 5 nm iridium to avoid electrostatic charging during examination. Thermogravimetric analyses were carried out using a TA Instrument Q50 (New Castle, DE). Samples with a weight of approx. 4 mg were heated from room temperature to 800 ^{o}C at a rate of 20 ^{o}C/min in air.

5.4 Results and Discussion

5.4.1 Hansen solubility parameters of SCP and P 450

The outcomes of the dissolution tests with SCP and P-450 in different solvents are shown in Table 5-3. The dissolution tests were conducted in 28 solvents, 20 of which were good solvents and 8 bad solvents for SCP, while 24 were good and 4 were bad for P-450. For example, SCP dissolved in acetic acid, forming a uniform solution while SCP was not miscible with ethylene glycol, demonstrating a clearly visible phased separation as shown in Figure 5-1. It is noteworthy that SCP did not dissolve in water because of the hydrophobic nature of its triglycerides and the

lower polarity of oil-based polyols. Therefore, pure SCP was not used to prepare PU foams in this study. The solubility parameters of SCP and P-450 were calculated using HSPiP software, based on the dissolution test results. Water was excluded from the determination of the solubility parameters because of its very high δ_h and its tendency to form a special structure with other substances [19, 26]. The software automatically calculated Hansen solubility parameters and the interaction radius for polyols by including the dissolving solvents inside the solubility sphere and excluding the non-dissolving solvents outside the solubility sphere as many as possible by trial and error method.

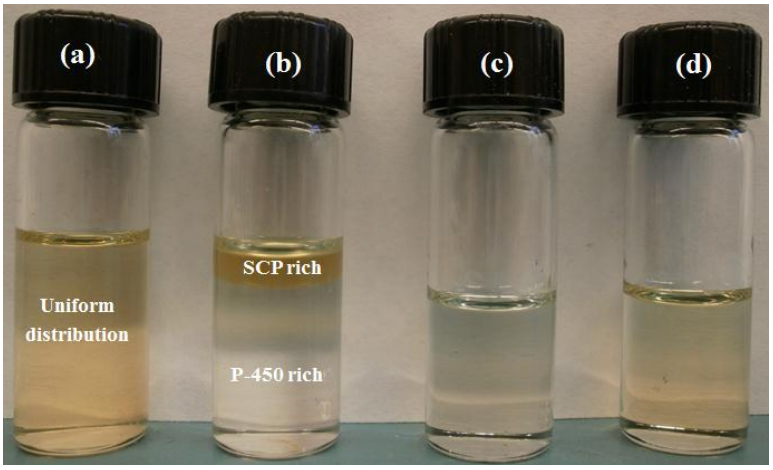

Figure 5-1 SCP in acetic acid (a), SCP in ethylene glycol (b), blends of 20 % SCP with P-450 (c), and 40 % SCP with P-450 (d).

Table 5-3 Solubility test results for SCP and P-450: soluble (+), and non-soluble (-)

Solvent name	Solubility parameters[1]			P-450	SCP	Relative polarity[2]
	δ_d $(MPa)^{1/2}$	δ_p $(MPa)^{1/2}$	δ_h $(MPa)^{1/2}$			
Methylene chloride	17	7.3	7.1	+	+	0.309

Table 5-3 continued

Isophorone	17	8	5	+	+	/
Toluene	18	1.4	2	+	+	0.099
1-butanol	16	5.7	15.8	+	+	0.586
Acetonitrile	15.3	18	6.1	+	-	0.46
Tetrahydrofuran	16.8	5.7	8	+	+	0.207
Chlorobenzene	19	4.3	2	+	+	0.188
Dimethylformamide	17.4	13.7	11.3	+	+	0.386
1-propanol	16	6.8	17.4	+	+	0.617
Cyclohexane	16.8	0	0.2	-	+	0.006
Chloroform	17.8	3.1	5.7	+	+	0.259
Pyridine	19	8.8	5.9	+	+	0.302
Methyl ethyl ketone	16	9	5.1	+	+	0.327
Dimethyl sulfoxide	18.4	16.4	10.2	+	-	0.444
Ethyl acetate	15.8	5.3	7.2	+	+	0.228
Water	15.5	16	42.3	+	-	1.0
Formic acid	14.6	10	14	+	-	/
Acetic acid	14.5	8	13.5	+	+	0.648
Ethylene glycol	17	11	26	+	-	0.79
Diethyl ether	14.5	2.9	4.6	+	+	0.117
Styrene	18.6	1	4.1	+	+	/
Acetone	15.5	10.4	7	+	+	0.355
N-hexane	14.9	0	0	-	-	0.009

Table 5-3 continued

Heptane	15.3	0	0	-	-	0.012
Pentane	14.5	0	0	-	-	0.009
P-xylene	17.8	1	3.1	+	+	0.074
Nitrobenzene	20	10.6	3.1	+	+	0.324
Diethyl sulfide	16.8	3.1	2	+	+	/

1 The values for solubility parameters were extracted from HSPiP software.

2. The relative polarity values were reported by Reichardt (Reichardt, 2003).

The solubility spheres of SCP and P-450 on three mutually perpendicular axes are shown in Figure 5-2. The brown circles, inside the solubility spheres, represent polyols soluble in this solvent, while the red triangles, outside the solubility spheres, indicate that the polyols are non-soluble in the solvent. The solubility parameters and the interaction radius for SCP were obtained as 17.58, 4.40, 8.68 (solubility parameters), 9.7 (interaction radius) and for P-450 they were determined as 17.20, 7.80, 13.31, and 13.1, respectively. It can be seen that the Hansen solubility parameters of SCP reside inside the solubility sphere of P-450 and the Hansen solubility parameters of P-450 also reside inside the solubility sphere of SCP, indicating that bio-polyol is compatible with petroleum-based polyol. The calculation results were confirmed by experimental dissolution tests shown in Table 5-4. All polyol blends were compatible in the temperature range between 25 ^{o}C and 90 ^{o}C. Figure 1 showed the homogeneous distribution of SCP in P-450.

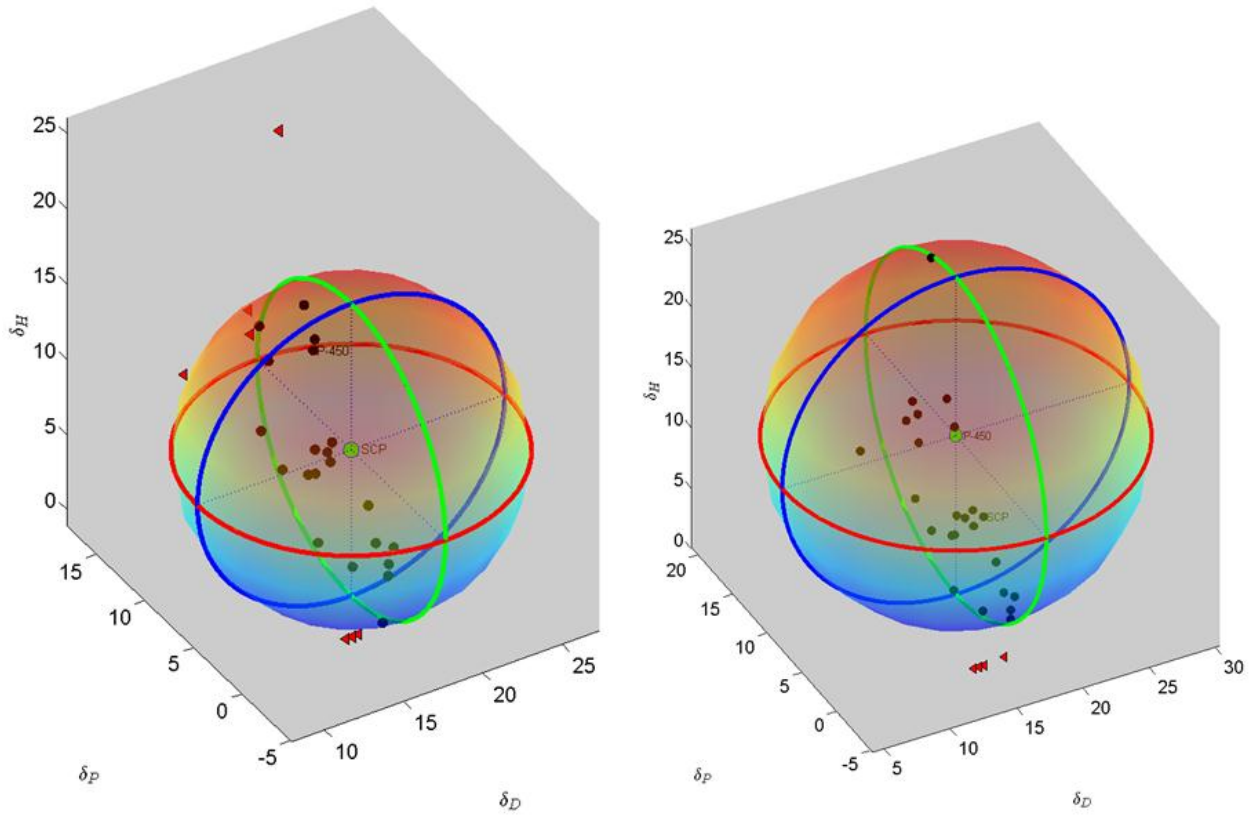

Figure 5-2 Solubility spheres of SCP (left) and P-450 (right), (solubility sphere of SCP: 17.58, 4.40, 8.68, R_1= 9.7; solubility sphere of P-450: 17.20, 7.80, 13.31, R_2 = 13.1. Red triangles represent solvents with Hansen solubility parameter outside solubility sphere, brown circles represent solvents with Hansen solubility parameters inside solubility sphere)

In general, rising time is related to the rate of expansion and gelation. Figure 5-3 shows that with increasing SCP content, the rising time of the respective PU foams increased because of low reactivity OH groups in SCP. The vegetable oil-based SCP contained secondary hydroxyl groups located in the middle of the triglyceride chains, while the petroleum-based P-450 contained highly reactive primary hydroxyl groups and had a much higher hydroxyl number than SCP. The reaction rate of the primary hydroxyl group towards isocyanate is about 3 times higher than that of the secondary hydroxyl group [24, 27].

Table 5-4 Solubility tests of SCP in P-450 (wt.) at different temperatures: soluble (+), and non-soluble (-)

	25 °C	50 °C	70 °C	90 °C
SCP:P-450 = 20:80	+	+	+	+
SCP:P-450 = 40:60	+	+	+	+
SCP:P-450 = 60:40	+	+	+	+
SCP:P-450 = 80:20	+	+	+	+

5.4.2 Characterization of PU Foams

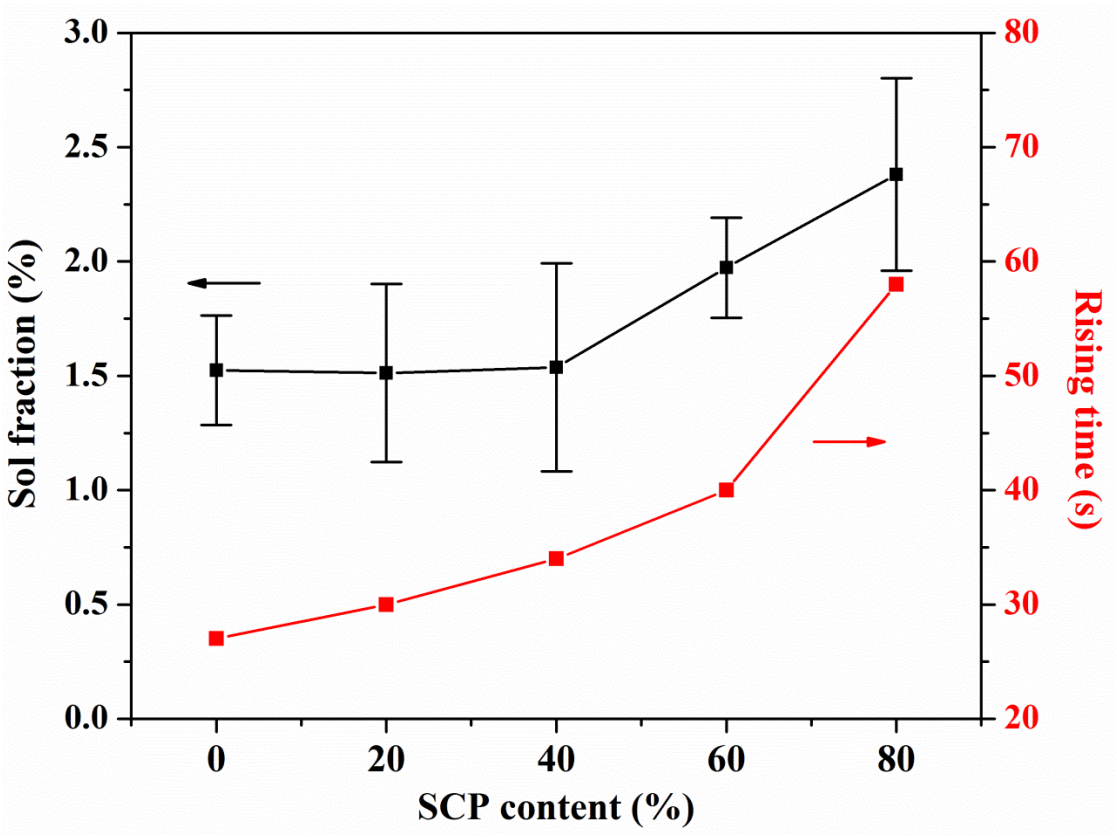

Figure 5-3 Sol fraction and rising time of PU foams prepared from blends with different ratios of P-450 and SCP.

Solvent extraction was conducted to determine the degree of polymerization and polymer network connectivity in the investigated foams. The measured sol fractions of the foams are shown in Figure 5-3. With increasing SCP content, the sol fraction of the resulting PU foams increased, indicating lower reactivity of SCP with isocyanate because of its secondary hydroxyl groups. However, all foams exhibited remarkable low extractable content (less than 3 %), indicating that with long curing times the secondary hydroxyls in SCP had sufficient reactivity to incorporate the polyols into the PU network. Tu [11] reported that 92 % of the polyol reacted with isocyanate within the first 12h in foam containing pure Voranol® 490 (a petroleum-based polyol with terminal hydroxyl groups), while foams containing 50 % soy-polyol (secondary functional groups) and 50 % Voranol® 490 incorporated 80 % of the polyol into the PU network over the same time period. Both systems occurred fully cure after 7 days. The results indicate 8 days was a suitable aging time for foam preparation in the study.

The apparent density of the PU foams prepared from blends with different ratios of P-450 and SCP is shown in Figure 5-4. With increasing SCP content, the density of the PU foams increased. The density of PU foam is determined as its weight to the volume ratio. Here, the weight of the foam matrix includes the weight of the polyols, isocyanates, and all additives, while the weight of air and carbon dioxide (the reaction product of water and isocyanate) trapped in the foam cells is negligible. The measured volume is determined by the foam matrix and the foam cells. Although the weight of the foam matrix decreased because less isocyanate was used with increasing SCP content, the density of the resulting foams increased. This was attributed to the fact that with increasing SCP content, the polymer-forming reaction rate decreased, leading to a weak 3-dimensional PU network. The cell walls were not strong enough to trap the carbon dioxide generated by the blowing reaction, so that the cells ruptured and carbon dioxide was

emitted. The PU matrix expanded less and the volume of the PU foams decreased. These explanations were confirmed by SEM investigations. The thermal conductivity of the PU foam is shown in Figure 5-4. With increasing SCP content, the thermal conductivity of the resulting PU foams increased, because more open and ruptured cell were present in the foam network, leading to more air convection and increased thermal conductivity [24]. Also, the increased density of the foams promoted thermal conductivity [7].

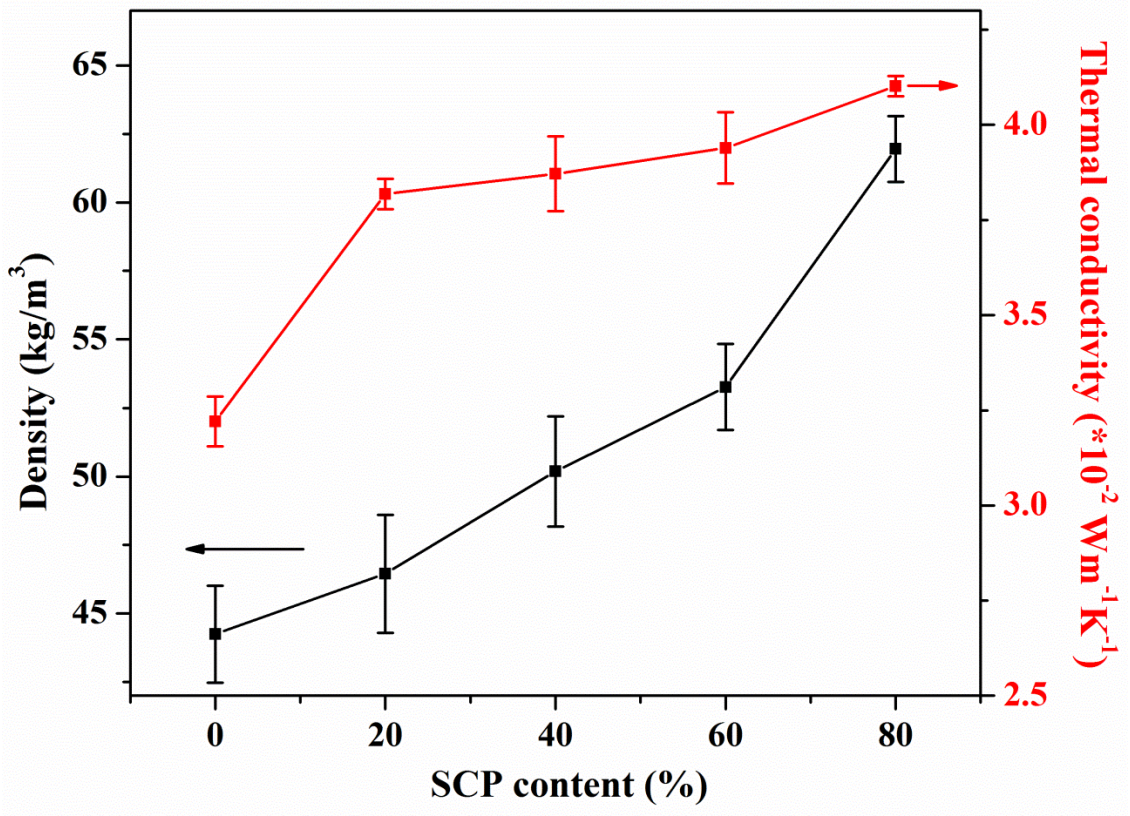

Figure 5-4 Apparent density and the thermal conductivity of PU foams prepared from blends with different ratios of P-450 and SCP.

The cellular structure and morphology of the PU foams were studied by SEM. Figure 5-5 shows SEM micrographs (in the rise direction) of PU foams based on blends of SCP and P-450 in different ratios. The PU foams were composed of various open and closed elliptical cells. With

increasing SCP content, the cell size gradually decreased while the number of cells increased. This was attributed on the one hand to the fact that with increasing SCP content, the viscosity of the reacting liquid mixture increased, because of higher viscosity of SCP than that of P-450 (see Table 5-1), which led to less coalescence among bubbles [28]. On the other hand, the prevalence of pendant groups in the SCP backbone provided more nucleation sites that facilitated the formation of bubbles, as compared to petroleum-based polyol with terminal functional groups [29]. With increasing SCP content, the number of open cells in the PU foams increased and the cell sizes were less uniform. This was attributed to the fact that the low reaction rate between SCP and isocyanate produced weak cell walls during foam reaction, which in turn led to more open cells under the pressure of carbon dioxide inside the cells.

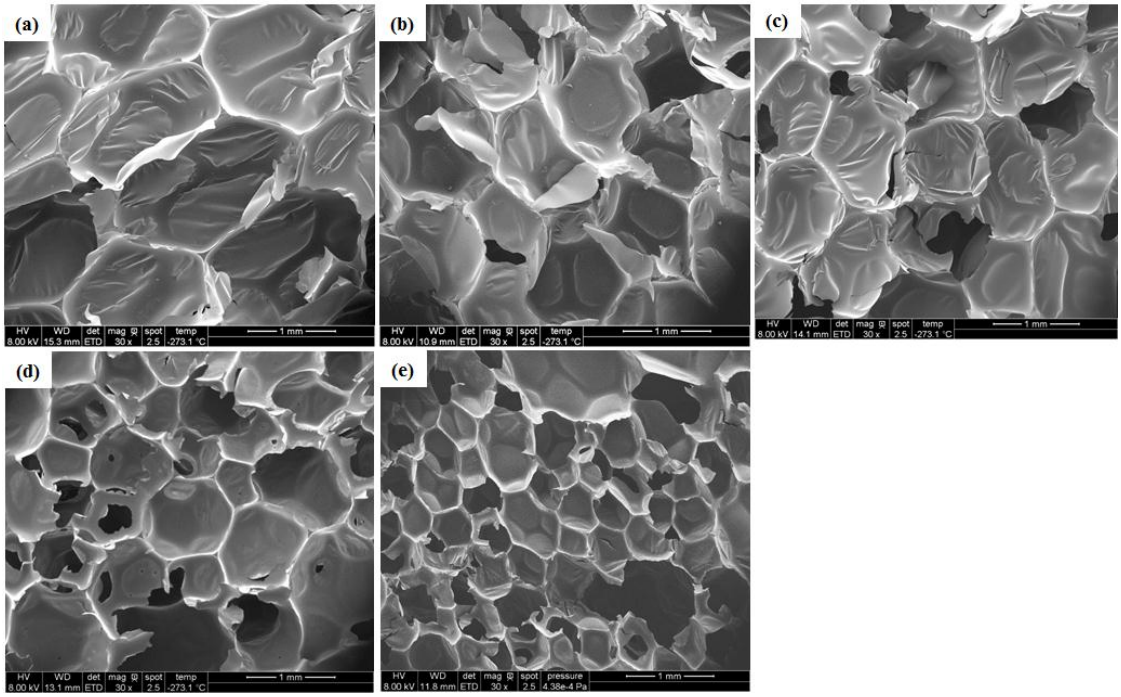

Figure 5-5 Microphotographs of PU foams prepared from blends with different ratios of P-450 and SCP (a) 0% SCP percentage, (a) 0 % SCP, (b) 20 % SCP, (c) 40 % SCP, (d) 60 % SCP, (e) 80 % SCP.

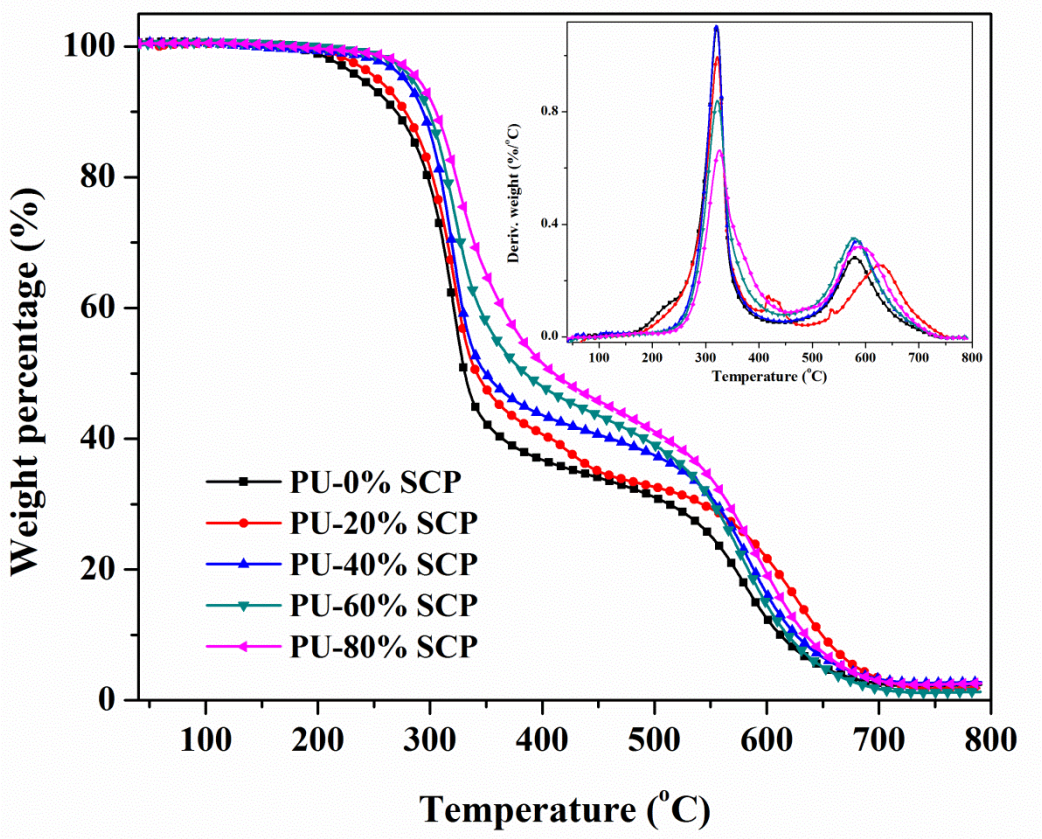

Figure 5-6 Thermo-oxidative behavior of PU foams prepared from blends with different ratios of P-450 and SCP.

The thermo-oxidative behavior of the PU foams prepared from polyol blends with different SCP content is shown in Figure 5-6 and the corresponding data are summarized in Table 5-5. The weight loss derivative curves of the PU foams revealed that all foams underwent three main degradation steps: the initial degradation of PU foams is characteristic of urethane bond decomposition (50 ^{o}C-360 ^{o}C), followed by chain scission of the polyol backbone (360 ^{o}C-520 ^{o}C), and the final degradation region above 500 ^{o}C that is contributed to further thermo-oxidation of the PU foams. Increasing SCP content led to a decrease in the OH number of the polyol blends, resulting in a decreased number of urethane bonds in the PU foam, and therefore improved the thermal stability in the first region. The ether linkages in P-450 are less resistant to

thermal degradation than the ester linkages in SCP [2, 7]. Therefore, the thermal stability of the respective PU foams improved in second step with increasing SCP content.

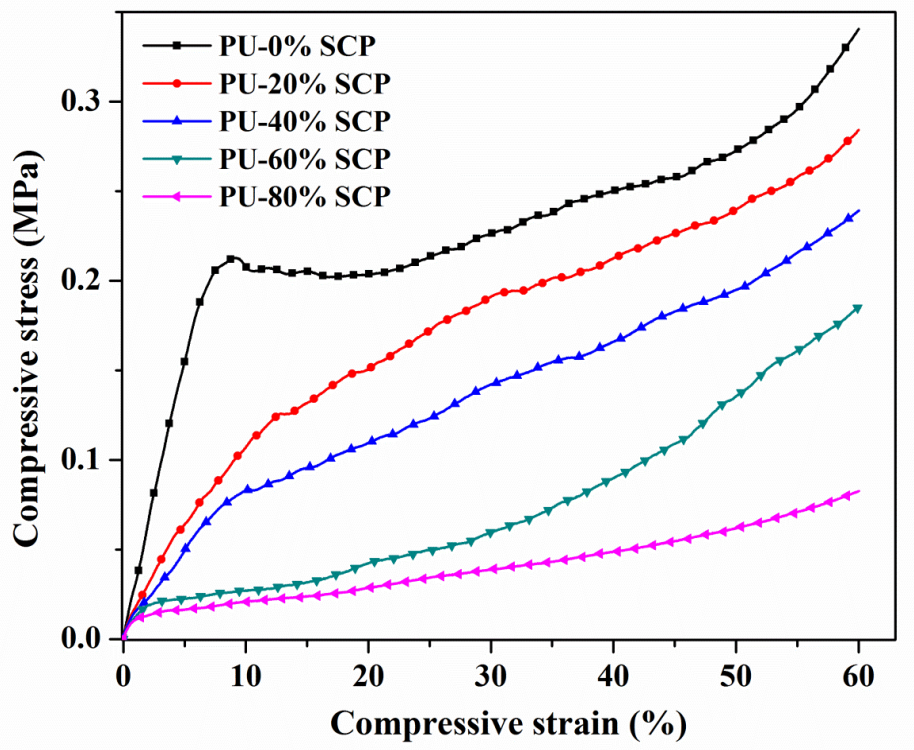

Figure 5-7 Compressive stress-strain curves of PU foams prepared from blends with different ratios of P-450 and SCP.

Figure 5-7 shows compressive stress-strain curves of PU foams prepared from different blends of SCP and P-450. The compression strength (10 % compression strain) of PU foams was summarized in Table 5-5. PU foam prepared from 100 % P-450 showed the typical stress-strain behavior of a rigid foam. Initially, the foam exhibited linear-elastic deformation at low strain, which is then followed by a sustained plateau of deformation-likely a result of bucking plastic yielding and brittle fracture of the cell wall struts. At high strains, the eventual densification of the foam resulting from the compacted structure triggered a steady increase in stress [12]. As the SCP content increased to 60 %, the foams exhibited only two regions, without the plateau of deformation. When the SCP content increased to 80 %, the PU foams showed linear elastic

behavior of a flexible foam. The compressive modulus and the compressive stress decreased with increasing SCP content. SCP with low OH number (compared to P-450) produced PU foams with low cross-linking densities, and therefore decreased mechanical properties of PU foams. Also, the plasticizing effect of dangling chains in the SCP molecule contributed to the inferior mechanical properties.

Table 5-5 Properties of PU foams

	Density (kg/m^3)	Thermal conductivity (10^{-2} $W \bullet m^{-1} \bullet K^{-1}$)	Sol fraction (%)	TGA in air (^oC)		Compression strength (MPa)
				T_{10}	T_{50}	
PU-0 % SCP	44.2±1.8	3.22 ± 0.07	1.52 ± 0.24	270	331	0.210±0.005
PU-20 % SCP	46.4± 2.2	3.82 ± 0.04	1.51 ± 0.39	278	342	0.083±0.025
PU-40 % SCP	50.2 ± 2.0	3.87 ±0.10	1.54 ± 0.46	294	350	0.075±0.007
PU-60 % SCP	53.3 ± 1.6	3.94 ± 0.10	1.97 ± 0.22	299	385	0.060±0.026
PU-80 % SCP	62.0 ± 1.2	4.10 ± 0.03	2.38 ±0.42	305	411	0.025±0.07

5.5 Conclusions

The Hansen solubility parameters of bio-polyol (SCP) and petroleum-based polyol (P-450) and the compatibility of these two polyols were evaluated using dissolution tests. Polyol blends with different ratios were used to prepare PU foam. With increasing SCP content, the number of open cells in the PU foams increased and the cell size became smaller. The thermal stability of the PU foams improved. The thermal conductivity of the PU foams increased and their compression strength decreased because, SCP has a lower hydroxyl numbers (lower reactivity), and higher viscosity of SCP than P-450.

5.6 Acknowledgment

This work was sponsored by Kumho Petrochemical Co.

5.7 References

1. G. Woods, *Flexible polyurethane foams : chemistry and technology*, Applied Science Publishers, London, 1982.

2. M. Szycher, *Szycher's handbook of polyurethanes*, Taylor & Francis, Boca Raton, FL, 2013.

3. R. P. Wool and X. S. Sun, *Bio-based polymers and composites*, Elsevier Academic, Amsterdam ; Oxford, 2005.

4. C. Bonini, M. D'Auria, L. Ernanuele, R. Ferri, R. Pucciariello and A. R. Sabia, *J Appl Polym Sci*, 2005, **98**, 1451-1456.

5. Z. S. Petrovic, *Polym Rev*, 2008, **48**, 109-155.

6. Y. Xia and R. C. Larock, *Green Chem*, 2010, **12**, 1893-1909.

7. A. Guo, I. Javni and Z. Petrovic, *J Appl Polym Sci*, 2000, **77**, 467-473.

8. S. Dworakowska, D. Bogdal and A. Prociak, *Polymers-Basel*, 2012, **4**, 1462-1477.

9. V. B. Veronese, R. K. Menger, M. M. D. Forte and C. L. Petzhold, *J Appl Polym Sci*, 2011, **120**, 530-537.

10. C. S. Lee, T. L. Ooi, C. H. Chuah and S. Ahmad, *J Am Oil Chem Soc*, 2007, **84**, 1161-1167.

11. Y. C. Tu, G. J. Suppes and F. H. Hsieh, *J Appl Polym Sci*, 2008, **109**, 537-544.

12. A. Campanella, L. M. Bonnaillie and R. P. Wool, *J Appl Polym Sci*, 2009, **112**, 2567-2578.

13. L. Zhang, H. K. Jeon, J. Malsam, R. Herrington and C. W. Macosko, *Polymer*, 2007, **48**, 6656-6667.

14. J. H. Tan, X. P. Wang, J. J. Tai, Y. F. Luo and D. M. Jia, *Express Polym Lett*, 2012, **6**, 588-600.

15. J. Argyropoulos, P. Popa, G. Spilman, D. Bhattacharjee and W. Koonce, *J Coat Technol Res*, 2009, **6**, 501-508.

16. T. W. Pechar, G. L. Wilkes, B. Zhou and N. Luo, *J Appl Polym Sci*, 2007, **106**, 2350-2362.

17. T. Wang, X. S. Huang and Y. Z. Zhang, *J Mater Civil Eng*, 2010, **22**, 773-778.

18. P. G. Redelius, *Fuel*, 2000, **79**, 27-35.

19. C. M. Hansen, *Hansen solubility parameters : a user's handbook*, CRC Press, Boca Raton, Fla., 2000.

20. J. H. Hildebrand and R. L. Scott, *The solubility of nonelectrolytes*, Dover Publications, New York,, 1964.

21. C. Hansen and K. Skaarup, *J Oil Colour Chem As*, 1968, **51**, 76-&.

22. D. W. v. Krevelen and P. J. Hoftyzer, *Properties of polymers, their estimation and correlation with chemical structure*, Elsevier Scientific Pub. Co., Amsterdam ; New York, 1976.

23. C. Q. Zhang, Y. Xia, R. Q. Chen, S. Huh, P. A. Johnston and M. R. Kessler, *Green Chem*, 2013, **15**, 1477-1484.

24. Y. C. Tu, P. Kiatsimkul, G. Suppes and F. H. Hsieh, *J Appl Polym Sci*, 2007, **105**, 453-459.

25. M. D. Phaneuf, M. J. Bide, M. Szycher, M. B. Gale, H. X. Huang, C. Q. Yang, F. W. LoGerfo and W. C. Quist, *Asaio J*, 2001, **47**, 634-640.

26. C. Bordes, V. Freville, E. Ruffin, P. Marote, J. Y. Gauvrit, S. Briancon and P. Lanteri, *Int J Pharmaceut*, 2010, **383**, 236-243.

27. R. Herrington, K. Hock and R. Autenrieth, *Flexible polyurethane foams*, Dow Chemical Co., Midland, MI, 1997.

28. P. Mondal and D. V. Khakhar, *Polym Eng Sci*, 2006, **46**, 970-983.

29. H. Y. Fan, A. Tekeei, G. J. Suppes and F. H. Hsieh, *J Appl Polym Sci*, 2013, **127**, 1623-1629.

CHAPTER 6: HIGH BIO-CONTENT POLYURETHANE COMPOSITES WITH URETHANE MODIFIED LIGNIN AS FILLERS

A paper to be submitted to Bioresource Technology

Chaoqun Zhang[a], Hongchao Wu[a], Ying Xia[a], Michael R. Kessler[a,b*]

[a] Dept. of Materials Science and Engineering, Iowa State University, Ames, IA, USA

[b] School of Mechanical and Materials Engineering, Washington State University, Pullman, WA, USA

[*] Author for correspondence

6.1 Abstract

In order to improve the compatibility between lignin fillers and polyurethane matrix, two different chemical strategies were used to modify the lignin macromolecules. Modified lignin was incorporated into vegetable oil-based polyurethanes to produce composites with high bio-contents. It shows that lignin modified with octadecyl isocyanante (lignin urethane) was more compatible with the polyurethane matrix compared to lignin modified by butyric anhydride because of hydrogen bonding and entanglement effects. The effect of lignin urethane loading on the thermo-mechanical properties, thermal resistance, and dielectric properties were investigated. The results showed that the incorporation of lignin urethane as a bio-filler compromised the tensile properties of the obtained composites, while improving the strain properties. High lignin contents (up to 30 wt %) improved the Young's modulus. Lignin urethane lowered the thermal degradation of polyurethanes composites at low temperature but increased thermal resistance at high temperature. Incorporation of lignin urethane did not change the T_g of the polyurethanes

composites significantly, but it greatly improved their dielectric properties compared to PU. This work provides an effective way of curing lignin to utilize this low-cost bio-renewable resource in the polyurethane industry.

6.2 Introduction

Polyurethanes (PUs), synthesized through a polyadddition reaction between polyisocyanate with two or more isocyanate groups and polyol with two or more reactive hydroxyl groups, are among the most versatile polymeric materials and have been widely used as foams, coatings, and sealants[1]. Currently, most of the polyisocyanate and polyols for PU production are derived from petroleum. The increasing concerns regarding the depletion of petroleum resources and environmental problems caused by fossil fuels, have led to considerable efforts to develop materials based on renewable resources, such as natural oils, starch, cellulose, and lignin[2, 3]. For example, vegetable oil based PUs were successfully developed and their structure-property relationships have been extensively investigated[4, 5]. Vegetable oil based PUs exhibit excellent physical and thermal stability properties because of the hydrophobic nature of the triglycerides from which they are derived.

Lignin is second only to cellulose in abundance, and it is composed of three different types of phenylpropane units that form a rigid, three dimensional network[6]. More than 1 million tons lignin and its derivatives are produced annually as byproducts by the paper and pulping industry, and traditionally most of them are used as a low cost fuel[7, 8]. An attractive application of lignin is as economic starting material replacing petroleum stock for various polymer products. Because lignin contains a large amount of hydroxyl groups (phenolic and aliphatic) in its chain, one of most widely studied strategies utilizes lignin as starting material for renewable polyols in the

polyurethane synthesis. This strategy resulted in thermoplastics PU films from polybutadiene diisocyanate and lignin modified by formaldehyde[9], as well as strong thermoset PU films from a three-component system of Alcell® lignin, polyethylene glycol and polymeric methyl-diisocyanate[10]. Lignins from organosolv pretreatment and kraft pulping were evaluated to replace petroleum-based polyols in the production of rigid PU foams[11]. Water-soluble lignosulfonate from sulfite pulping was used to prepare rigid polyurethane foam with glass transition temperature ranging from 80 ^{o}C to 140 ^{o}C[12]. Modified kraft lignin doped with multiwall carbon nanotubes was used to prepare nano-composites for sensor applications[13]. In the application listed above, hydroxyl groups in the lignin were used as reaction sites. However, the structure and functionality of lignin fluctuate depending on its source, processing conditions (humidity, temperature and UV exposure)[14], which in turn influence the properties of the final PU to a large degree. Also, these structure and functionality variations may lead to heterogeneous final products, which is not acceptable for the current commercial polymers that require high-purity starting materials with significant and reproducible reactivities.

Incorporating lignin into PU matrices as non-covalent filler may be a more effective and economically viable approach[15]. Unfortunately, the large number of aromatic and aliphatic hydroxyl groups in lignin makes it highly polar, therefore molecule insoluble in non-polar thermosetting resins. Also, the aromatic hydroxyl groups easily form a stable quinonic structure, which inhibits free radical polymerization. Therefore, the chemical modification of lignin is necessary to synthesize well distributed composites.

In this research, two different chemical modifications of lignin were investigated to improve the interfacial interaction between the PU and the lignin filler. The chemical structure of the modified lignin was characterized by FTIR, elemental analysis and GPC. The modified lignins

were incorporated into vegetable oil based-polyurethane to prepare composites with different filler loadings, and it was shown that the lignin modified with octadecyl isocyanate was better chemically compatible with the PU matrix. Finally, the effect of filler loading on the mechanical, dynamic-mechanical, dielectric properties, and the thermal resistance of the composites were investigated and discussed.

6.3 Experimental

6.3.1 Materials

Epoxidized soybean oil was purchased from Scientific Polymer Inc., New York, NY. Methyl ethyl ketone (MEK), n-hexane, and ethyl ether were purchased from Fisher Scientific Company (Fair Lawn, NJ). Castor oil, sodium hydroxide, hydrochloric acid, butyric anhydride, isophorone diisocyanate (IPDI), and octadecyl isocyanate were obtained from Sigma-Aldrich (Milwaukee, WI). The catalyst for the lignin-anhydride reaction was 1-methyl imidazole (1MI) obtained from Sigma-Aldrich (Milwaukee, WI). Dibutyltin dilaurate (DBTDL), used as the catalyst for hydroxyl group-isocyanate reactions, was purchased from Sigma-Aldrich (Milwaukee, WI). All materials were used as received without further purification.

6.3.2 Synthesis of Vegetable Oils Based Polyols

A soy-castor oil based polyol (SCP) was prepared according to a method developed by Zhang *et al.*[5]. Here, the castor oil was saponified into castor oil fatty acid by sodium hydroxide and hydrochloric acid at 80 ^{o}C. Then, the castor oil fatty acid was used to ring open epoxidized soybean oil to obtain a light reddish/yellow, viscous liquid in 170 ^{o}C. The ratio of carboxyl acid groups to epoxy groups was 0.5:1. The typical properties of SCP are shown in Table 1.

Table 6-1 The properties of SCP

	OH number (mg KOH/g)	Acid number (mg KOH/g)	Number /weight average molecular weight	Polydispersity index
SCP	148	3.7	2611/3442	1.32

6.3.3 Synthesis of Lignin Butyrate

Under vigorous stirring, 100 g lignin, 200 g butyric anhydride, and 1 wt % catalyst 1-MI were added in a flask. The reaction mixture was heated to 50 ^{o}C and reacted overnight. Then, 200 ml ethyl ether was added to reduce the viscosity. The mixture was precipitated with 200ml n-hexane. Finally, the mixture was filtered and washed with n-hexane for at least three times. Lignin butyrate was obtained by drying in a vacuum oven overnight at 60 ^{o}C. The preparation of lignin butyrate is shown in Scheme 6-1.

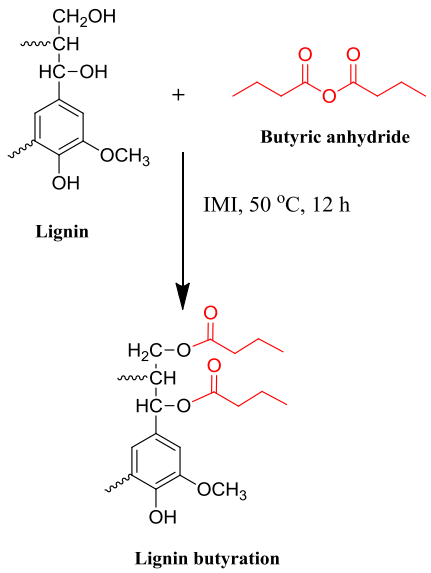

Scheme 6-1 The preparation of lignin butyrate

6.3.4 Synthesis of Lignin Urethane

Under vigorous stirring, 100 g lignin, 150 g octadecyl isocyanate, 1 wt % DBTDL, and 200ml MEK were added in a flask. The reaction mixture was heated to 80 ^{o}C and reacted for 24 h. After

the reaction mixture had cooled down to room temperature, 200ml n-hexane was charged into the mixture under vigorous stirring. Finally, the mixture was filtered, washed with n-hexane for at least three times, and dried in a vacuum oven overnight. The preparation of lignin urethane is shown in Scheme 6-2.

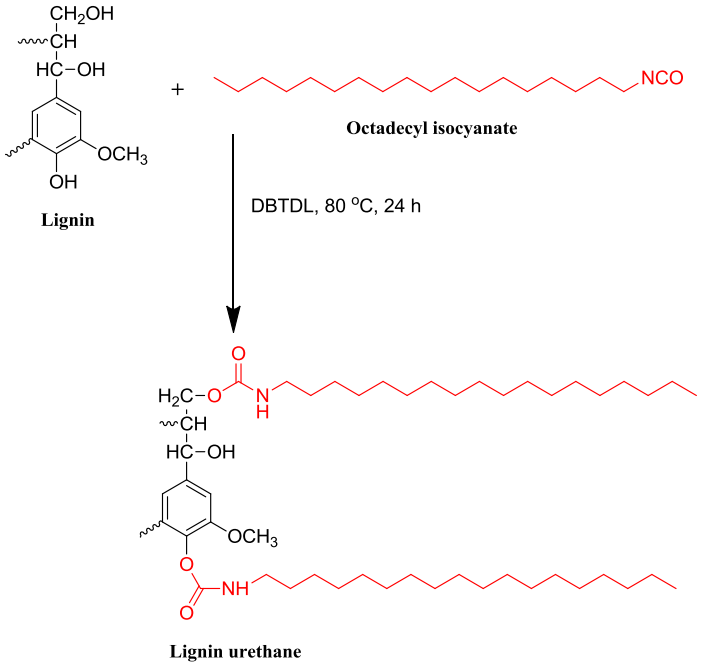

Scheme 6-2 The preparation of lignin urethane

6.3.5 Preparation of PUs Composites

Soy-castor oil based polyol and IPDI were mixed in a flask and stirred vigorously. The ratio of OH groups to NCO groups was 1:1.1. Then, 0.5 wt % DBTDL was added as catalyst. The mixture was heated to 70 ^{o}C and held at this temperature for 1 h. Then, modified lignin at different loadings level was added to the reaction mixture and the reaction continued for another 1 h. Finally, the mixture was poured into a Teflon mold and post-cured in an oven at 80 ^{o}C overnight. Specimens of the PU composites were cut into specific dimensions for thermal, mechanical and dielectric testing.

6.3.6 Characterizations

The FTIR spectra of lignin and modified lignin were recorded on a Nicolet 460 FTIR spectrometer (Madison, WI). The molecular weight distributions of lignin and modified lignin were determined using a THF-eluted GPC equipped with a refractive index detector. Elemental analysis results (%C, %H, %N) were obtained using a PE 2100 Series II combustion analyzer (Perkin Elmer Inc., Waltham, MA).

The distribution of butyrate lignin and urethane lignin in the polyurethane matrix were investigated by scanning electron microscope (SEM, FEI Quanta 250 FEG) coupled with energy-dispersive X-ray spectroscopy (EDS, Oxford Instruments Aztec). The samples were sectioned by blades and examined by elemental mapping methods. Each map was generated by accumulating 40 scans with each scan collecting for 15 seconds at 5000× magnification at 10 kV voltages with an output count rate of 12kcps.

Dynamic mechanical analysis (DMA) of the PU films was conducted with a TA Instruments DMA Q800 dynamic mechanical analyzer using a film-tension mode of 1 Hz. The samples were rectangular with 0.5 thickness, and 8 mm width. The samples were cooled and held isothermally for 3 min at -80 ^{o}C , then they were heated to 140 ^{o}C at a rate of 5 ^{o}C/min.

A TA Instrument Q50 (New Castle, DE) was used to conduct thermogravimetric analyses (TGA) of the 7 mg samples. The samples were heated from room temperature to 800 ^{o}C at a rate of 20 ^{o}C/min in air.

The mechanical properties of the standard dog-bone shape samples were tested using an Instron universal testing machine (model 4502) with a crosshead speed of 50 mm/min. At least four samples were tested to obtain average property values.

The dielectric properties of both composites and neat PU were characterized using a Novocontrol dielectric spectrometer (Novocontrol Technologies, Hundsangen, Germany) with a frequency range from 1 Hz to 1 MHz at room temperature.

6.4 Results and discussion

6.4.1 Characterization of Lignin Butyrate and Lignin Urethane

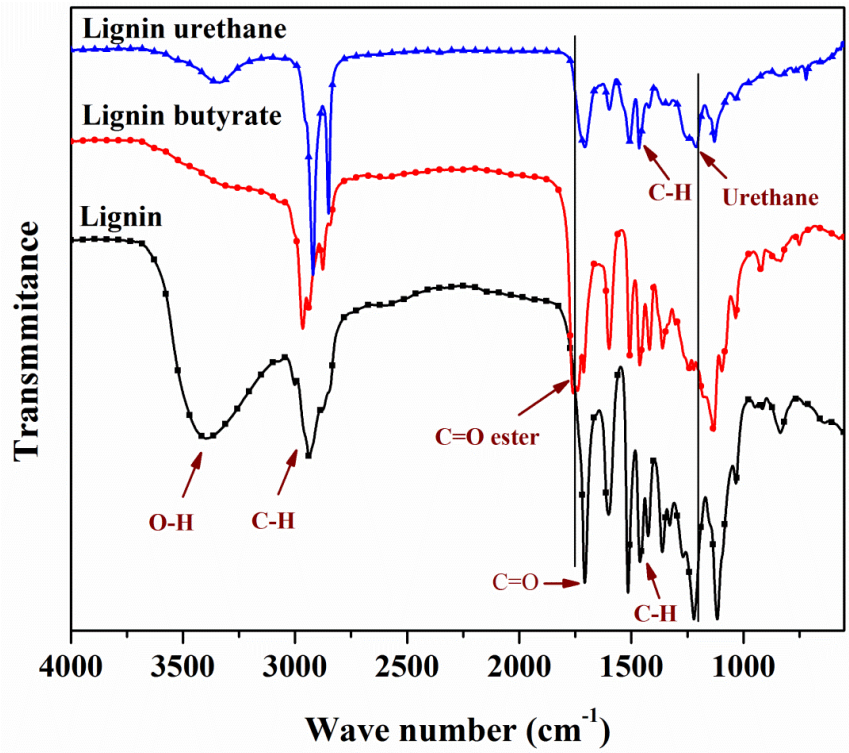

Figure 6-1 FTIR spectra of lignin, lignin urethane, and lignin butyrate.

The FTIR spectra of lignin, lignin urethane, and lignin butyrate are shown in Figure 6-1 where the important peaks have been assigned. Compared to the spectrum of lignin as received, in the spectra of lignin urethane and lignin butyrate the alcohol bands (3300-3700 cm^{-1}) were reduced in size, while the methyl and methylene C-H bands (2880-2966 cm^{-1}) increased, indicating that the hydroxyl groups were consumed during butyration and the formation of urethane linkages. Direct evidence of the successful modification of lignin is the appearance of peaks at 1737 cm^{-1}

corresponding to C=O ester, and the appearance of peaks at 1216 cm^{-1} corresponding to urethane linkages[16]. Elemental analysis was used to determine the composition of the modified lignins, see Table 6-2. Butyration increased the percentage of carbon in lignin butyrate. After modification by octadecyl isocyanate, both the percentage of carbon and nitrogen in lignin urethane increased because of the formation of urethane groups.

Table 6-2 Elemental analysis of lignin, lignin butyrate and lignin urethane

	Lignin	Lignin butyrate	Lignin urethane
C (wt.%)	61.8	64.6	72.6
H (wt.%)	6.4	6.2	11.2
N (wt.%)	0.6	0.7	3.6

6.4.2 Characterization of Polyurethane Composites

Figure 6-2 (a) shows samples of PU composites with different loadings of lignin urethane and lignin butyrate. All samples with lignin urethane exhibited homogenous morphologies, and with increasing lignin urethane loading, the samples became darker. The samples with lignin butyrate exhibited numerous agglomerations. The distribution of lignin butyrate and lignin urethane in the PU matrix were also investigated by SEM as shown in Figure 6-2 (b) and Figure 6-2 (c). The lignin butyrate agglomerated in the PU matrix, leading to the heterogeneity of oxygen content as

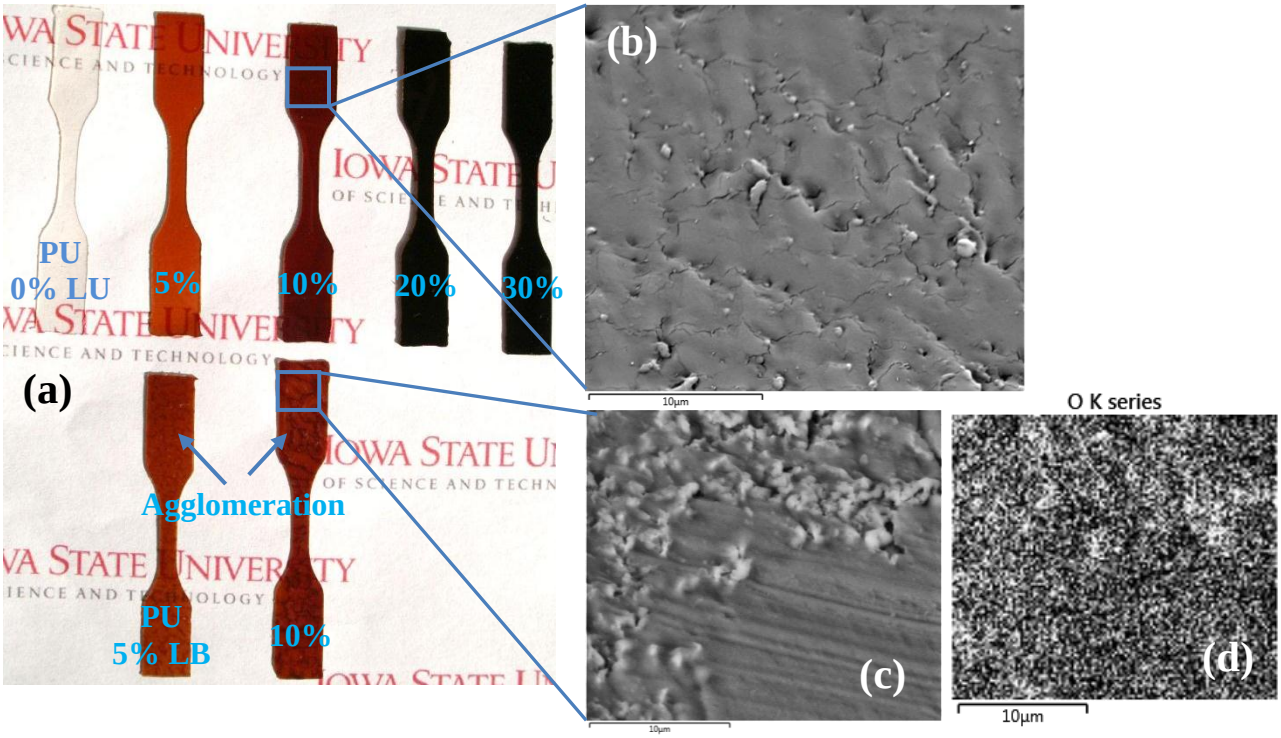

Figure 6-2 Polyurethane composites with different loadings of modified lignin (a) photo of dog-bone samples, (b) SEM microstructure of polyurethane/lignin urethane composites, (c) SEM microstructure of polyurethane/lignin butyrate composites (d) map of oxygen element of polyurethane/lignin butyrate composites.

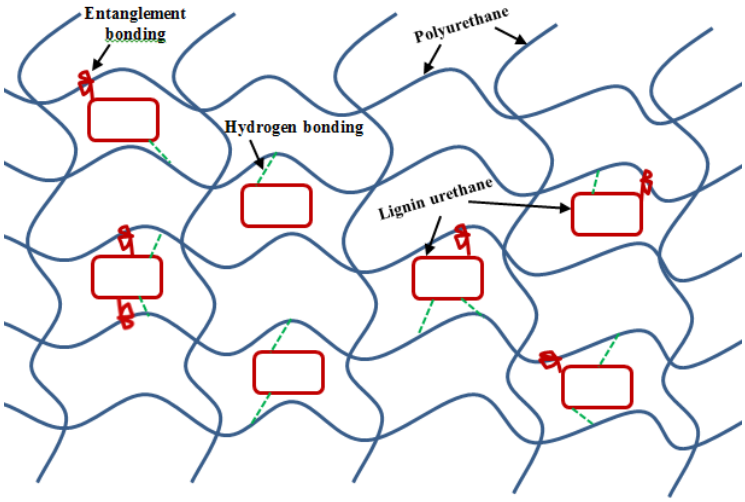

Figure 6-3 Schematic of lignin urethane dispersing in PU matrix

shown in Figure 6-2 (d) (A light area indicates a higher element concentration than a dark area). The urethane lignin disperses homogenously in the matrix. The homogenous distribution of lignin urethane in the PU matrix was attributed to the entanglement effect caused by the long, dangling octadecyl urethane chains and to hydrogen bonding between N-H from octadecyl urethane with C=O from the PU chain[17] as indicated in Figure 6-3. It was concluded that lignin urethane was more compatible with the PU matrix. Therefore, subsequent investigations focused on the effect of lignin urethane on the properties of the composites.

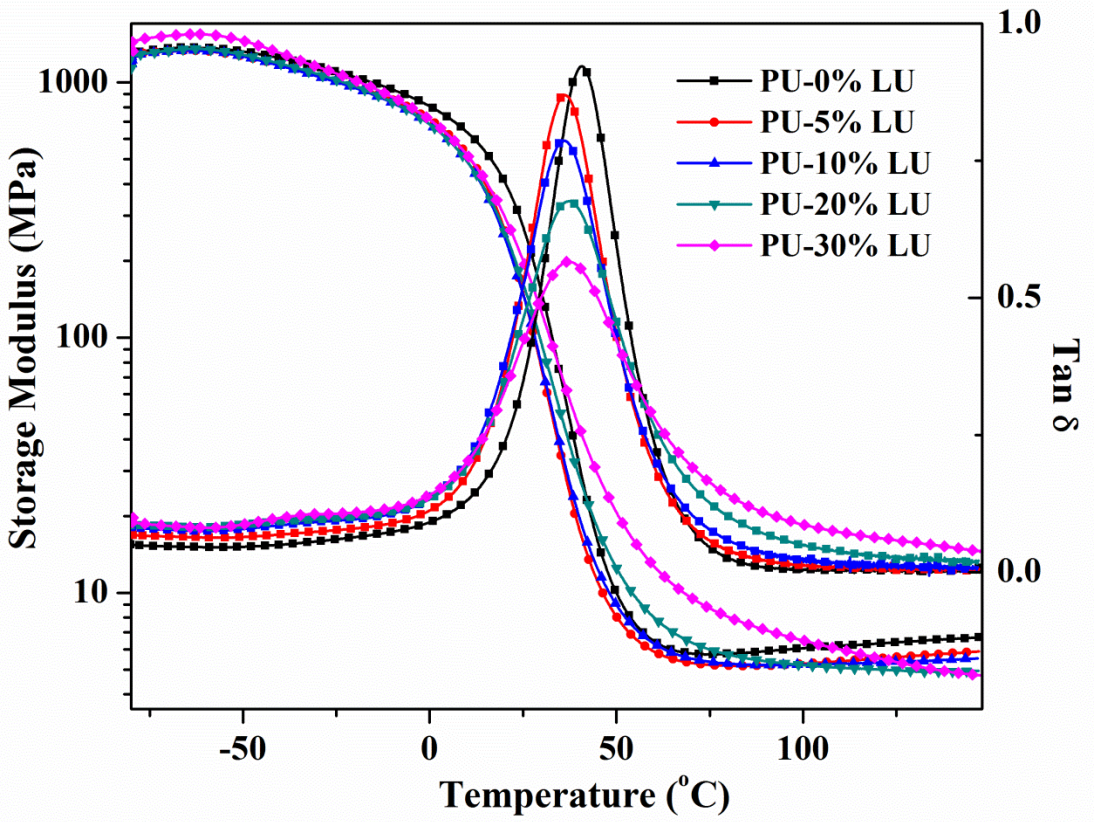

Figure 6-4 Storage modulus and tan δ of PU composites with different levels of lignin urethane as filler (LU-lignin urethane).

Figure 6-4 shows the storage modulus and tan δ of polyurethane composites with different levels of lignin urethane. The glass transition temperature (T_g) was determined from tan δ peaks. All samples exhibited one tan δ peak, confirming the homogeneous nature of the composites. With

increasing lignin urethane loading, the T_g of the PU composites increased slightly (see Table 6-3). However, the T_g of the neat PU was higher than those of the composites. It was concluded that the filler did not significantly affect T_g. At low temperatures, all samples behaved like solids with high storage moduli of 10^3 MPa. As the temperature exceeded T_g, the storage moduli decreased rapidly because of the dramatic increase in molecular motion and then reached a plateau. With increasing loading levels of lignin urethane, the storage moduli of PU composites increased. The storage moduli of the PU composites were typically lower than that of neat PU; however, in certain temperature ranges the composites deviated from this pattern. This negative effect of lignin on the storage modulus of PU composites will be discussed later. In the temperature range from 45-100 ^oC, PU composites with 20 wt % lignin urethane exhibited higher moduli than neat PU; composites with 30 wt % lignin urethane also had higher moduli in the temperature range from 35–120 °C. This behavior was attributed to the fact that in the cross-linked polymer network lignin occupied a certain portion of the free volume and developed positive interfacial interactions with the polymer matrix through effective hydrogen bonding.

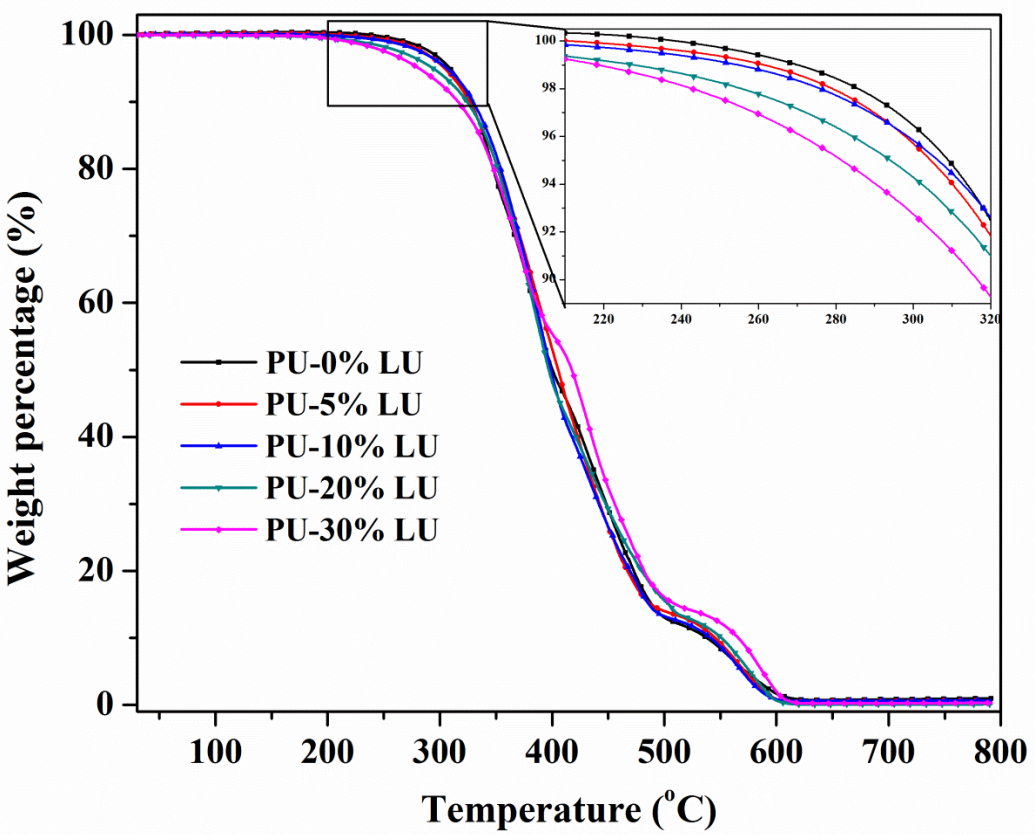

Figure 6-5 TGA curves of polyurethane composites with different loadings of lignin urethane.

The influence of lignin urethane on the thermal stability of polyurethane was studied by TGA. Figure 6-5 shows the weight loss curves in air for polyurethane/lignin urethane composites. Polyurethane/lignin urethane composites underwent thermal degradation in two main stages: The initial degradation stage in the 200-340 ^{o}C temperature range corresponding to the decomposition of unstable urethane bond and cleavage of α- and β-aryl-alkyl-ether linkages of lignin, leading to primary amines, phenols, olefins and carbon dioxide[15]. Table 3 shows the 5% degradation (T_5) temperature for PU composites with 0 %, 5 %, 10 %, 20 %, and 30 % lignin urethane, respectively. The degradation stage above 340 ^{o}C was attributed to the chain scission of the vegetable oils, and the further thermo-oxidation of residual mass. With increasing loading of lignin urethane, the PU composites lost more weight in the first stage because of the increasing number of urethane groups and the unstable ether linkages introduced by the lignin

urethane. The incorporation of lignin improved thermal resistance of polyurethane/lignin urethane composites in the second degradation temperature range, because the increased number of aromatic groups and benzene rings introduced by the lignin urethane enhanced the thermal stabilities to some degree[18].

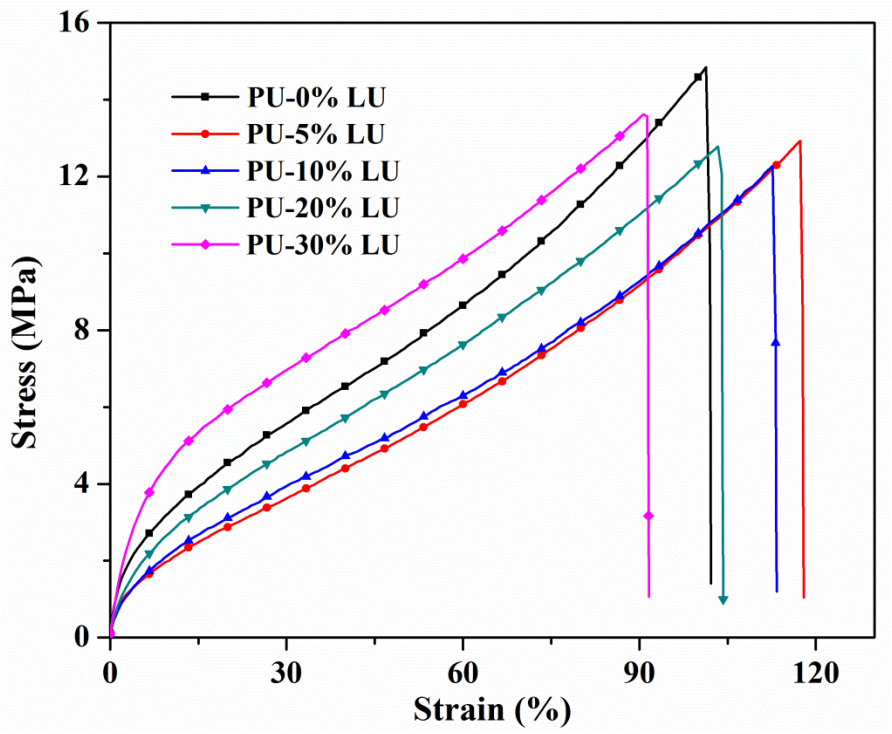

Figure 6-6 Stress/strain curves of polyurethane composites with different loadings of lignin urethane.

Table 6-3 Tensile test of polyurethane/lignin urethane composites

	T_g from DMA (°C)	T_5 (°C)	Tensile strength (MPa)	Elongation at break (%)	Young's modulus (MPa)
PU-0% LU	40.7	310.0	14.5±0.6	96.4±7.5	60.7±1.5
PU-5% LU	36.7	304.5	12.4±0.3	114.2±2.5	34.8±0.7
PU-10% LU	36.9	306.4	12.6±0.3	115.9±5.0	35.6±1.6
PU-20% LU	37.8	294.2	12.5±0.4	101.3±4.3	44.9±4.4
PU-30% LU	38.2	281.5	13.3±0.5	87.6±5.7	80.3±1.1

The results of the tensile tests of PU composites with different lignin urethane loadings are shown in Figure 6-6 and Table 6-3. It shows that the incorporation of lignin urethane slightly decreased the tensile strength of the PU composites. Two reasons were associated with this decrease in the tensile strength: (1) lignin urethane decreases the crosslink density of the matrix material because of the plasticized effect of lignin urethane[19]. (2) PU network near lignin urethane may be disrupted compared with the bulk matrix, and thus lowered the matrix integrity[20]. With 5% lignin urethane content, the Young's modulus of PU composites was lower than that of neat PU. With increasing loading of lignin urethane, the Young's moduli of the PU composites increased and the elongation at break decreased, indicating that the composites became stiffer. At 30% lignin urethane content, the Young's modulus of PU composites was higher than the neat PU. Entanglement of the long urethane dangling chains with the PU matrix may have caused this improvement. On the other hand, the hydrogen bonding effect between -N-H from octadecyl urethane and -C=O in PU chains may have also caused an increase in Young's modulus. Huang *et al.* reported that an increase in hydrogen bonding index resulted in improved phase mixing, which in turn increased modulus and decreased maximum elongation[17].

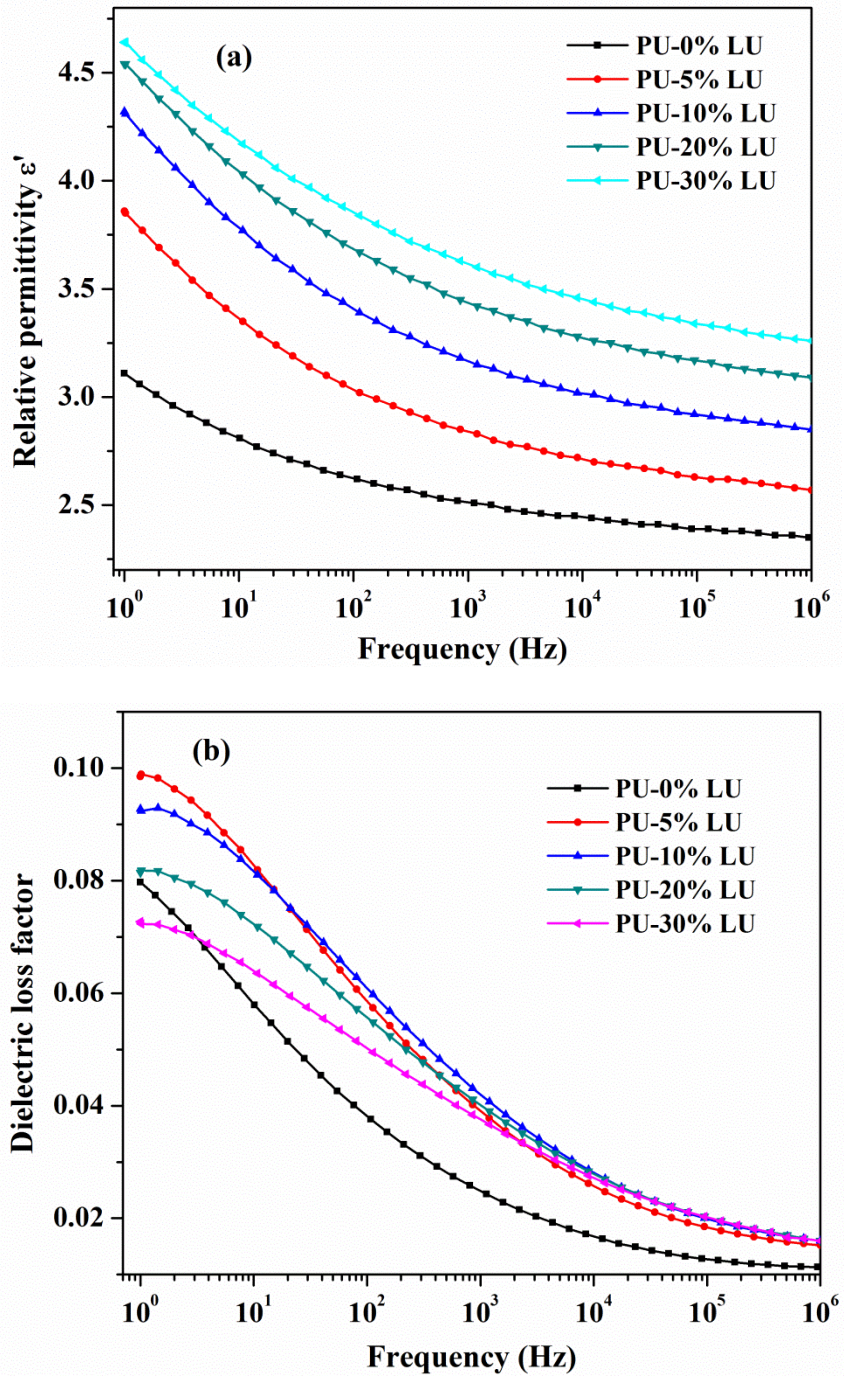

Figure 6-7 Frequency dependence of the permittivity (a), and dielectric loss factor (b) in the polyurethane composites and neat polyurethane.

The dielectric properties of PU composites with different lignin urethane loading levels were studied. As seen in Figure 6-7 (a), both neat PU and its composites exhibited a similar frequency-

dependent permittivity over frequency range between 1 to 10^6 Hz. However, it is interesting to note that the incorporated lignin systematically increased the relative permittivity (ε') of the composites, which may be attributed to the higher ε' of lignin, caused by the dipole orientation and the polarization of the functional groups in lignin molecules. Figure 6-7 (b) shows that the dielectric loss factor of PU composites slightly increased with incorporation of lignin fillers. Although no major difference was observed in loss factor within higher frequency range (10^3-10^6 Hz) at any given loadings, the presence of higher content of lignin resulted in the reduction of dielectric loss factor at lower frequencies. This phenomenon was attributed to the higher dielectric dispersion caused by the lagging behavior of dipoles in the higher frequency field oscillations. Overall, the lignin reinforced PU composites exhibited excellent dielectric properties. It is notable that the polyol used in this study was 100% bio-based and with lignin loading up to 30%, the bio-content of neat PU and PU/lignin composites reached approx. 76 % and 83 %, respectively.

6.5 Conclusion

Two kinds of chemical pathways were used to modify lignin to improve the compatibility of lignin fillers and polyurethane matrix. It was shown that lignin modified with octadecyl isocyanate was better compatible with the polyurethane matrix because of hydrogen bonding and entanglement effects. The influence of lignin urethane loading levels on the mechanical, thermal degradation, and dielectric properties was investigated. The incorporation of lignin urethane as a bio-filler compromised the tensile properties of the obtained composites, while it improved the strain properties. High lignin contents up to 30 wt % improved the composite's Young's moduli. Incorporation of lignin urethane decreased thermal degradation of polyurethanes composites at low temperatures, but increased their thermal degradation at high temperatures. Incorporation of

lignin urethane did not change the T_g of PU composites significantly, but it greatly improved their dielectric properties. This work provides an effective way utilizing lignin, a bio-renewable resource, in the polyurethane industry.

6.6 References

1. M. Ionescu, *Chemistry and technology of polyols for polyurethanes*, Rapra Technology, Shawbury, Shrewsbury, Shropshire, U.K., 2005.

2. A. Gandini, *Macromolecules*, 2008, **41**, 9491-9504.

3. Y. Xia and R. C. Larock, *Green Chem*, 2010, **12**, 1893-1909.

4. D. P. Pfister, Y. Xia and R. C. Larock, *Chemsuschem*, 2011, **4**, 703-717.

5. C. Q. Zhang, Y. Xia, R. Q. Chen, S. Huh, P. A. Johnston and M. R. Kessler, *Green Chem*, 2013, **15**, 1477-1484.

6. R. C. Pettersen, *Advances in Chemistry Series*, 1984, 57-126.

7. Y. Li, J. Mlynar and S. Sarkanen, *J Polym Sci Pol Phys*, 1997, **35**, 1899-1910.

8. R. J. A. Gosselink, E. de Jong, B. Guran and A. Abacherli, *Ind Crop Prod*, 2004, **20**, 121-129.

9. T. Saito, J. H. Perkins, D. C. Jackson, N. E. Trammel, M. A. Hunt and A. K. Naskar, *Rsc Adv*, 2013, **3**, 21832-21840.

10. R. W. Thring, M. N. Vanderlaan and S. L. Griffin, *Biomass Bioenerg*, 1997, **13**, 125-132.

11. X. J. Pan and J. N. Saddler, *Biotechnol Biofuels*, 2013, **6**.

12. T. Hatakeyama, Y. Matsumoto, Y. Asano and H. Hatakeyama, *Thermochim Acta*, 2004, **416**, 29-33.

13. F. A. C. Faria, D. V. Evtuguin, A. Rudnitskaya, M. T. S. R. Gomes, J. A. B. P. Oliveira, M. P. F. Graca and L. C. Costa, *Polym Int*, 2012, **61**, 788-794.

14. H. Y. Chung and N. R. Washburn, *Acs Appl Mater Inter*, 2012, **4**, 2840-2846.

15. C. Ciobanu, M. Ungureanu, L. Ignat, D. Ungureanu and V. I. Popa, *Ind Crop Prod*, 2004, **20**, 231-241.

16. Y. Kurimoto, M. Takeda, A. Koizumi, S. Yamauchi, S. Doi and Y. Tamura, *Bioresource Technol*, 2000, **74**, 151-157.

17. S. L. Huang and J. Y. Lai, *Eur Polym J*, 1997, **33**, 1563-1567.

18. M. Shao, Z. Q. Liu, D. Li, Y. Zhao, N. Ozkan and X. D. Chen, *Int J Food Eng*, 2012, **8**.

19. W. Thielemans and R. P. Wool, *Compos Part a-Appl S*, 2004, **35**, 327-338.

20. K. W. Putz, M. J. Palmeri, R. B. Cohn, R. Andrews and L. C. Brinson, *Macromolecules*, 2008, **41**, 6752-6756.

CHAPTER 7: REDUCTION OF EPOXIDIZED VEGETABLE OILS: A NOVEL METHOD TO PREPARE BIO-BASED POLYOLS FOR POLYURETHANE

A paper published in Macromolecular Rapid Communications, 2014,

DOI: 10.1002/marc.201400039

Chaoqun Zhang, Rui Ding, Michael R. Kessler*

C. Q. Zhang, R. Ding, Prof. M. R. Kessler
Dept. of Materials Science and Engineering, Iowa State University, Ames, IA, 50011, USA
Prof. M. R. Kessler, Author for correspondence

School of Mechanical and Materials Engineering, Washington State University, Pullman, WA, 99164-2920, USA
Email: michaelr.kessler@wsu.edu

7.1 Abstract

A novel method, epoxidation/reduction of vegetable oils, is developed to prepare bio-based polyols for the manufacture of polyurethanes (PUs). These polyols are synthesized from castor oil, epoxidized soybean oil, and epoxidized linseed oil and their molecular structures are characterized. They are used to prepare a variety of PUs, and their thermo-mechanical properties are compared to those of PU made with petroleum-based polyol (P-450). It is shown that PUs made with polyols from soybean and linseed oil exhibit higher glass transition temperatures, tensile strength and Young's modulus and PU made with polyol from castor oil exhibits higher elongation at break and toughness than PU made with P-450. However, PU made with P-450 displays better thermal resistance because of tri-ester structure and terminal functional groups. The method provides a versatile way to prepare bio-polyols from vegetable oils, and it is expected to partially or completely replace petroleum-based polyols in PUs manufacture.

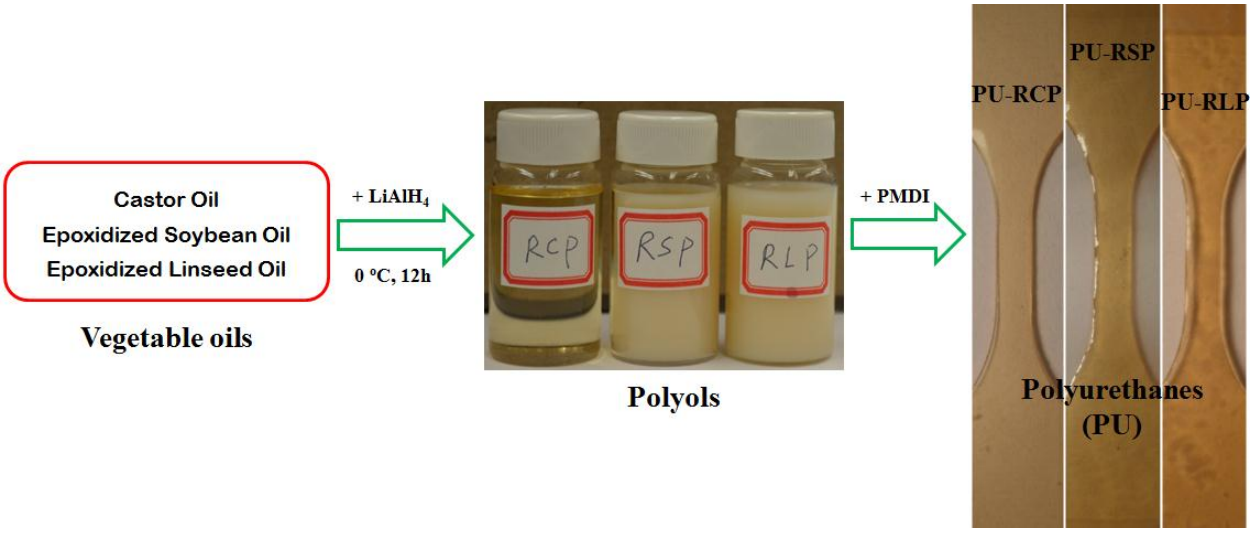

7.2 Introduction

Vegetable oil-based polyols enjoy significant interest worldwide because they are considered promising candidates for green monomers to synthesize PUs, which are typically prepared by polyaddition of diisocyanates and polyols that contain at least two hydroxyl groups.[1-3] The exploitation of petrochemical resources increasingly triggers concerns regarding environmental pollution, unsustainable depletion, and the rising price of petroleum; therefore, there is increasing demand for bio-based polyols that can replace petroleum-based polyols in PU production in the near future. Recently, industrial corporations such as Huntsman, BASF, Cargill, Atofina and Oleon have developed more than 20 types of vegetable oil-based polyester polyols that are currently available on the market.[4, 5]

Vegetable oils are triglyceride of fatty acid that usually contains 12 to 22 carbon atoms and 0 to 3 carbon-carbon double bonds. Except for castor oil, most triglyceride oils do not contain the hydroxyl groups necessary in polyols for PU synthesis. The reactive chemical sites present in vegetable oils, however, offer several routes to introduce hydroxyl groups to the triglyceride molecule.

Depending on the structure and the reactive sites in a vegetable oil, specific methods have been developed to transform an inexpensive, readily available natural feedstock into a valuable monomer. Epoxidation of carbon-carbon double bonds, followed by ring opening with amines, carboxylic acids/halogenated acids, or alcohols has been widely investigated for the preparation of commercial vegetable-based polyols for PUs in recent years.[6-9] Ozonolysis of vegetable oil into ozonides, followed by reduction to aldehyde and finally to alcohol creates polyols that contain primary hydroxyl groups that are far more reactive towards isocyanates than secondary hydroxyl groups. In addition, the hydroxyl groups of polyols prepared using this method are located at the end of the fatty acid chains, which make all the aliphatic chains in the macromolecular network resulting in rigid PUs.[10] Primary hydroxyl groups can also be introduced by hydroformylation/reduction with syngas (CO/H_2) catalyzed by rhodium or cobalt carbonyl complexes.[1, 11, 12] Vegetable oil-based polyols can also be prepared by transesterification of vegetable oils with alcohols or by amidation with amines.[13, 14] Although transesterification and amidation allow for the incorporation of several functionalities based on the choice of alcohol or amine, the absence of hydroxyl groups in the fatty acid chains (unless castor oil is used) results in long fatty acid chains acting as elastic, unreactive chains. The recent development of thiol-ene click reactions offers promising routes for the preparation of polyols for polyurethane technology.[15] Based on these routes, several research groups are dedicated to combine the advantages offered by the modification of carbon-carbon double bonds and those offered by the modification of esters to develop high functionality polyols. For example, Kong used 1, 3-propanediol for ring-opening of epoxidized vegetable oils and transesterification with the triglycerides.[16] Lligadas developed oligomeric polyether polyols by ring-opening polymerization of epoxidized methyl oleate followed by reduction of the ester groups.[17]

In this paper, a novel method will be proposed to prepare high functionality polyols by epoxidation of vegetable oils, followed by reduction of the epoxy groups and ester. Lithium aluminum hydride, as a conventional strong reducing agent, was chosen to validate this idea. Recently, several catalytic hydrogenations were developed and investigated as the replacement of $LiAlH_4$. In further research, other mild catalytic alternatives will be considered and investigated to extend the application of this approach. For example, the reactivity of sodium borohydride can be enhanced for reducing ester and epoxy group in the presence of certain additives, such as iodine, $ZnCl_2$, MeOH.[18, 19] Also, other green reductants, such as ammonia borane also can be used in neat water as strong reducing agent to improve atom efficiency and decrease the amount of inorganic salt residues.[20] For possible future industrial applications, hydrogen (with ruthenium hydride complexes as catalyst) offers a promising and efficient reductant to be used in mass production.[6, 21, 22]

The current work is devoted to developing a one-pot process for preparing PUs from novel polyols possessing themo-mechanical properties comparable to that of petroleum-based polyols. The structures of these polyols produced from vegetable oils were characterized by proton nuclear magnetic resonance (^{1}H NMR), Fourier transform infrared spectroscopy (FTIR), and gel permeation chromatography (GPC). PUs produced using these polyols were prepared and characterized by dynamic mechanical analysis (DMA), differential scanning calorimetry (DSC), thermogravimetric analysis (TGA) and tensile testing. Finally, the thermal and mechanical properties of PUs from bio-based polyols were compared with that from petroleum-based polyol.

7.3 Experimental Section

7.3.1 Materials

Polyol 450 (P-450) prepared by reacting propylene oxide with glycerin, and polymeric diphenylmethane-4, 4'-diisocyanate (PMDI, NCO content: 31 wt.%) were provided by Kumho Petrochemical Co. Commercial epoxidized linseed oil (ELO) and epoxidized soybean oil (ESBO), obtained from Scientific Polymer Inc. (New York, NY), were used to assess the validity of the epoxidation/reduction method. Castor oil (CO), dibutyltin dilaurate (DBTDL), lithium aluminum hydride ($LiAlH_4$), magnesium sulfate ($MgSO_4$), methyl ethyl ketone (MEK), hydrogen chloride (HCl), ethyl acetate, and tetrahydrofuran (THF, HPLC grade), were purchased from Sigma-Aldrich (Milwaukee, WI). All materials were used as received without further purification.

7.3.2 Preparation of Polyols from Vegetable Oils

200 ml THF was charged to $LiAlH_4$ (14.72 g for castor oil, 18.45 g for ESBO, and 22.23 g for ELO)in a 1000 ml two-neck round bottom flask at 0 ^oC. 100 g vegetable oil (castor oil, ESBO, and ELO) dissolved in 200 ml THF was added drop wise to the $LiAlH_4$ suspension. The reaction mixture was maintained at 0 ^oC with vigorous mechanical stirring overnight. After the reaction was finished, 1 M HCl aqueous solution was added slowly to the reaction mixture and cooled by iced water until the solution was clear. Then ethyl acetate was added to extract the polyols and the organic layer was washed with water at least six times, dried with $MgSO_4$ and filtered. Finally, the polyols derived from reduced castor oil (RCP), from reduced epoxidized soybean oil (RSP), and from reduced epoxidized linseed oil (RLP) were obtained after removal of the organic solvent by rotary evaporation and drying in the vacuum oven. The trace amounts of Al

and Li in the polyols were only present in negligible amounts as shown in supporting information. The representative preparation routine for RSP is shown in Figure 1.

7.3.3 Preparation of PU from Polyols and PMDI

2.2 g polyol (P-450, RCP, RSP, and RLP) were dissolved in MEK, and then PMDI was added at a ratio of OH to NCO of 1:1.05. The precursor solution was allowed to react at 70 ^{o}C for 2 hours. Then, one drop of DBTDL was added to the reacting solution and stirred for 5 minutes. Finally, the solution was poured into a Teflon mold to form a 50 × 50 mm (length × width) sheet and post-cured at 80 °C in an oven overnight. The solvent was removed completely during the post-cure. The resulting PU films were cut into specific dimensions for thermo-mechanical testing.

7.3.4 Characterization of Polyols and PUs

The chemical structure of the vegetable oils and their derived polyols were analyzed by ^{1}H NMR spectroscopy using a Varian spectrometer (Palo Alto, CA) at 300 MHz and by FT-IR spectroscopy using a Nicolet 460 FT-IR spectrometer (Madison, WI). The OH values of the polyols were titrated according to the Unilever method.[23] The acid numbers of the polyols were determined by AOCS Official Method Te 1a-64. The molecular weight of the vegetable oils and polyol derivatives were determined using a Thermo Scientific Dionex Ultimate 3000 THF-eluted GPC (Sunnyvale, CA) equipped with a Shodex Refractive Index detector. Thermal and mechanical properties of the resulting PU films were characterized using a TA Instruments Q800 DMA with a film-tension mode of 1 Hz. Rectangular specimens of 0.6 × 10 mm (thickness × width) were used for the analysis. The samples were cooled and held isothermally for 3 min at –80 ^{o}C before the temperature was increased to 160 ^{o}C at a rate of 3 ^{o}C/min. A TA Instrument Q2000 DSC was used to examine the glass transition temperature (T_g). Samples of approx. 5 mg were heated from room temperature to 110 ^{o}C at 20 ^{o}C/min to erase their thermal history. Then

the samples were equilibrated at –60 ^{o}C, followed by a second heating cycle to 110 ^{o}C at a heating rate of 20 ^{o}C/min. A TA Instrument Q50 TGA was used to evaluate the thermal stability of the PU films. Samples of approx. 10 mg were heated from room temperature to 700 ^{o}C at a heating rate of 20 ^{o}C/min in nitrogen. The tensile properties of the PU films were measured using an Instron universal testing machine (model 4502) with a crosshead speed of 5 mm/min. ASTM standard dog-bone samples were used. Average values of at least three replicates of each sample were taken. The toughness of the polymer was obtained from the area under the corresponding tensile stress/strain curves.

7.4 Results and Discussion

7.4.1 Characterization of Polyols

The ^{1}H NMR spectra of vegetable oils and polyols derived from them are shown in Figure 7-1 and 7-2. The disappearance of peaks at 2.8-3.2 ppm in RSP indicated the removal of epoxy groups, and the disappearance of peaks at 5.2-5.3 ppm (-$CH_2C\mathbf{H}CH_2$-) and 4.1-4.4 ppm (-$C\mathbf{H_2}$-$CHCH_2$-) in RSP demonstrated the removal of ester groups. The appearance of peaks in RSP at 3.5-3.8 ppm indicated the formation of OH functional groups. These results confirmed that the epoxy and ester groups were successfully reduced into hydroxyl groups. Using the area for peaks at 0.8-0.9 ppm (the terminal-$C\mathbf{H_3}$) of RSP for normalization (with an integrated value of 3), the functionalities of the polyol can be determined, see Table 1. Similar results were found for the reduction process of castor oil and epoxidized linseed oil into corresponding polyols, as shown in Figure 7-2.

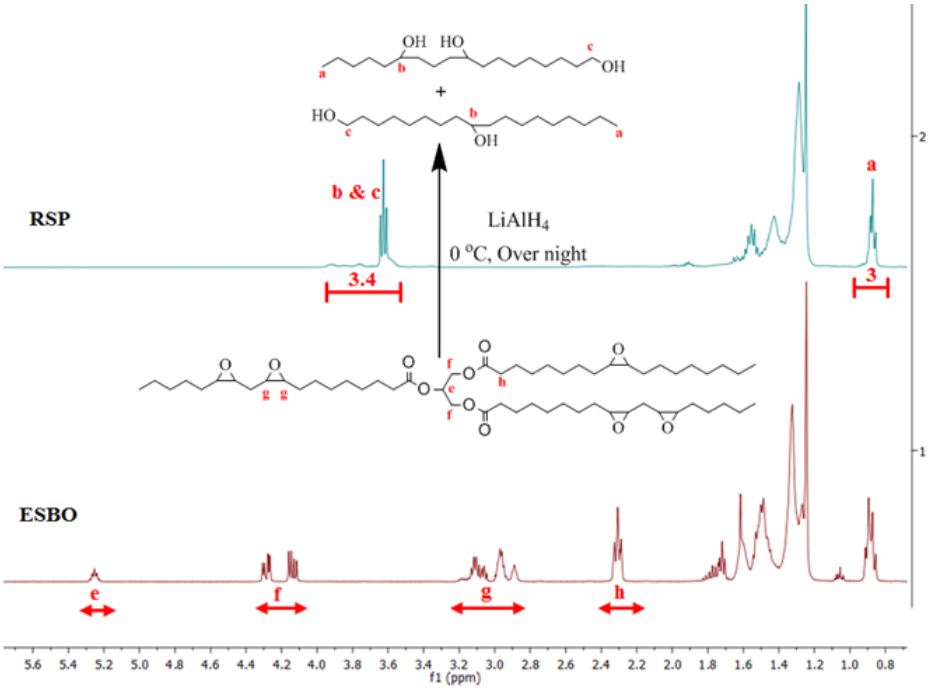

Figure 7-1 ^{1}H-NMR spectra and structures of polyols for ESBO and RSP.

The reduction from epoxy and ester to hydroxyl functionality was also confirmed by the FTIR spectra shown in Figure 7-3. The disappearance of the peak at 1746 cm^{-1} for bio-polyols compared to that of corresponding epoxidized vegetable oils, indicating the removal of ester groups. In addition, the absorbance increase at 3380 cm^{-1} and decrease at 821 cm^{-1} indicated the formation of new hydroxyl groups and the removal of epoxy groups, respectively. The molecular weights of the polyols are summarized in Table 1. After the reduction of ester and epoxy groups into hydroxyl groups, the molecular weights of the resulting polyols was approximate ⅓ the molecular weight of vegetable oils (The number average molecular weight of ESBO by GPC is 1420[24]).

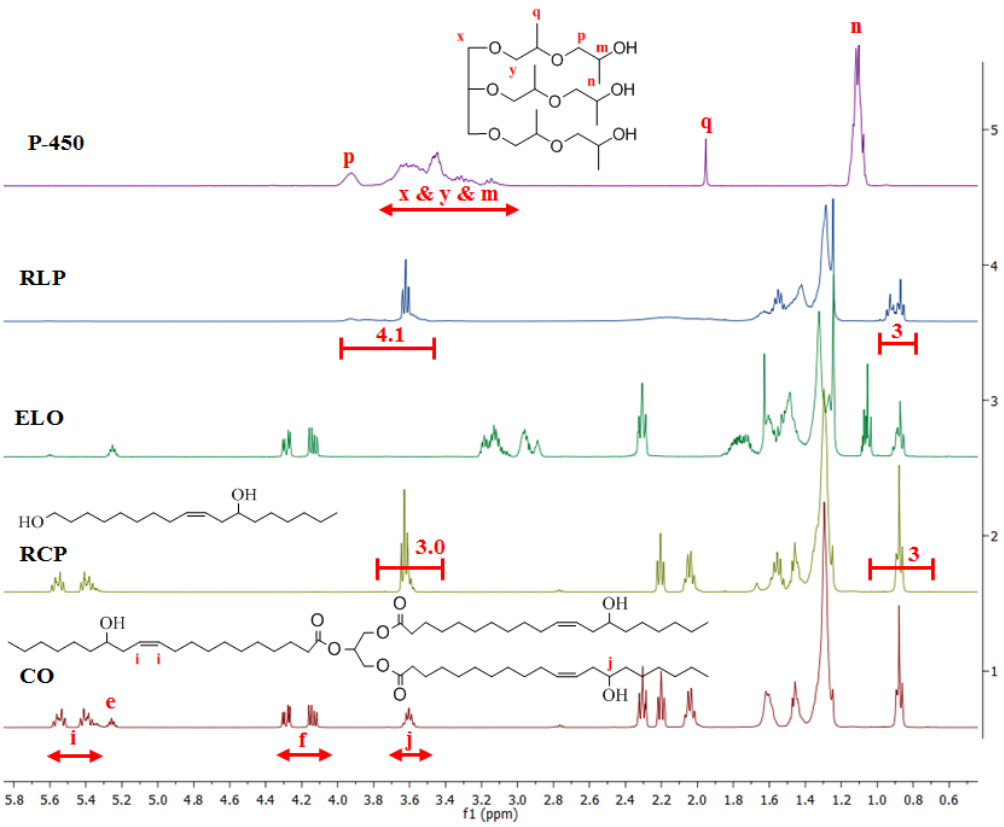

Figure 7-2 ^{1}H-NMR spectra and structures for epoxidized oils, bio-polyols and petroleum-derived polyol.

Table 7-1 The properties of bio-derived and petroleum-derived polyols.

	Functionality	OH number (mg KOH/g)	Acid number (mg KOH/g)	Number average molecular weight by GPC	PDI[×]	State at room temperature
P-450	3	355	-	702	1.05	Liquid
RCP	2	353.1±0.8	0.8	498	1.02	Liquid
RSP	2.4	377.0±0.6	0.6	533	1.05	Wax
RLP	3.1	434.0±0.8	0.8	562	1.04	Wax

× Polydispersity index

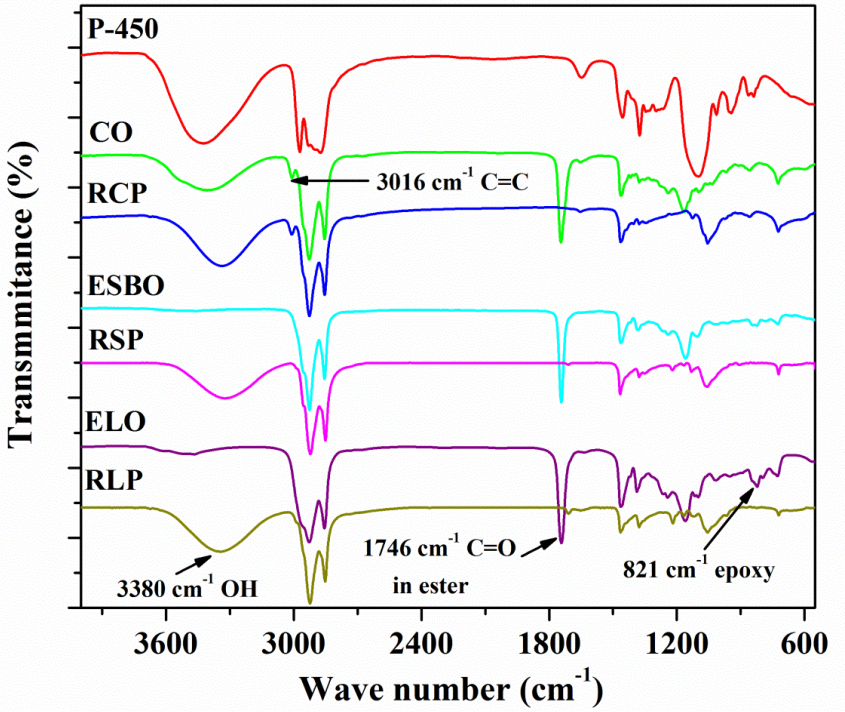

Figure 7-3 FTIR spectra of epoxidized vegetable oils and polyols.

7.4.2 Characterization of PUs

The thermomechanical properties of the PUs derived from P-450, RCP, RSP, and RLP were investigated using DMA within a temperature range of -80 ^{o}C to 150 ^{o}C. As shown in Figure 7-4, it was observed that in bio-polyols an increase in OH number resulted in respective PUs an amplitude decrease of the tan δ peak and a shift to higher temperatures. The corresponding storage modulus measured in the rubbery state increased from PU-RCP to PU-RSP to PU-RLP, indicating an increase in the degree of cross-linking caused by an increase in hard segments. The T_g was determined by the peak maximum of tan δ, see Table 7-2. Although the OH number of P-450 was similar to that of RCP, PU-450 exhibited a higher T_g and storage modulus than PU-RCP at both high and low temperatures, which was attributed to the tri-ether groups in P-450. These glycerin-propylene oxide based polyether groups allow for pre-crosslinking of the polyol. On the other hand, the hydroxyl groups in P-450 are terminal, making the whole polyether chain part of

the network. In contrast, the hydroxyl groups in RCP are positioned in the middle of the fatty acid chains. A portion of the chains was therefore not included in the network and left acting as plasticizers. In addition, the tan δ curve of PU-RLP exhibited multiple transitions surrounding the T_g region, showing behavior similar to PUs from soybean phosphate ester polyol and PMDI reported by Mohanty.[25] This phenomenon may be the result of the complicated composition of the polyols, including mono-ol, diol, and triol derived from oleic, linoleic and linolenic fatty acid.

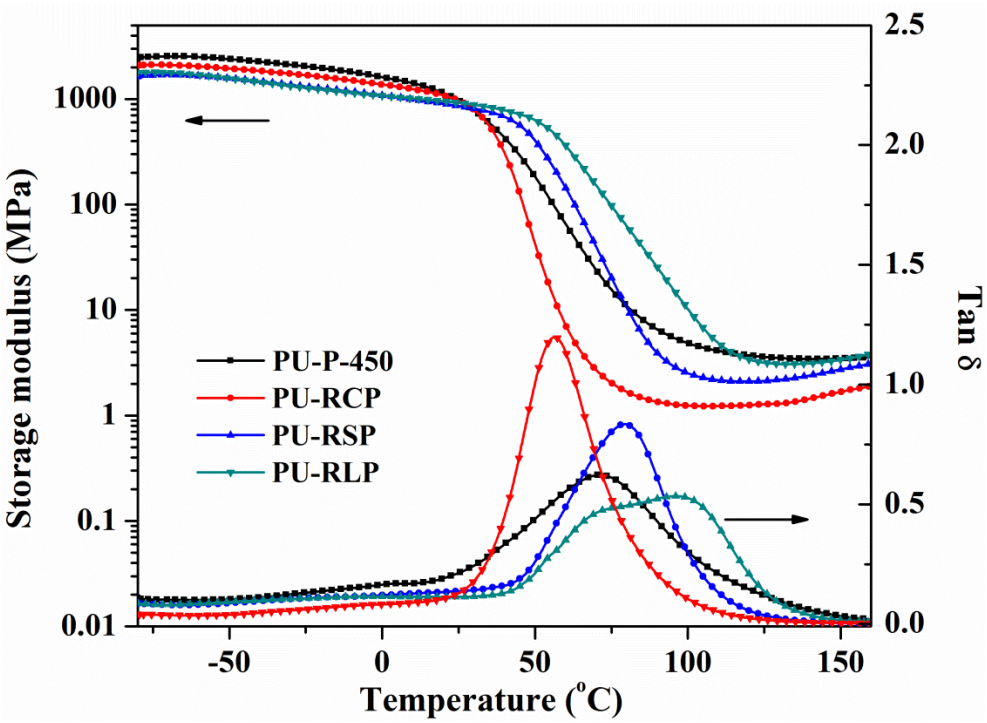

Figure 7-4 Storage modulus and tan δ of PUs derived from P-450, RCP, RSP, and RLP.

DSC scans of the PUs are shown in Figure 5. The T_g values were determined by the midpoint temperature between the slope of the heat capacity change and are summarized in Table 2. The DSC results confirmed the T_g determined by DMA in dependence of the structures of polyols. PU-RLP exhibited the highest T_g, while PU-RCP exhibited the lowest T_g.

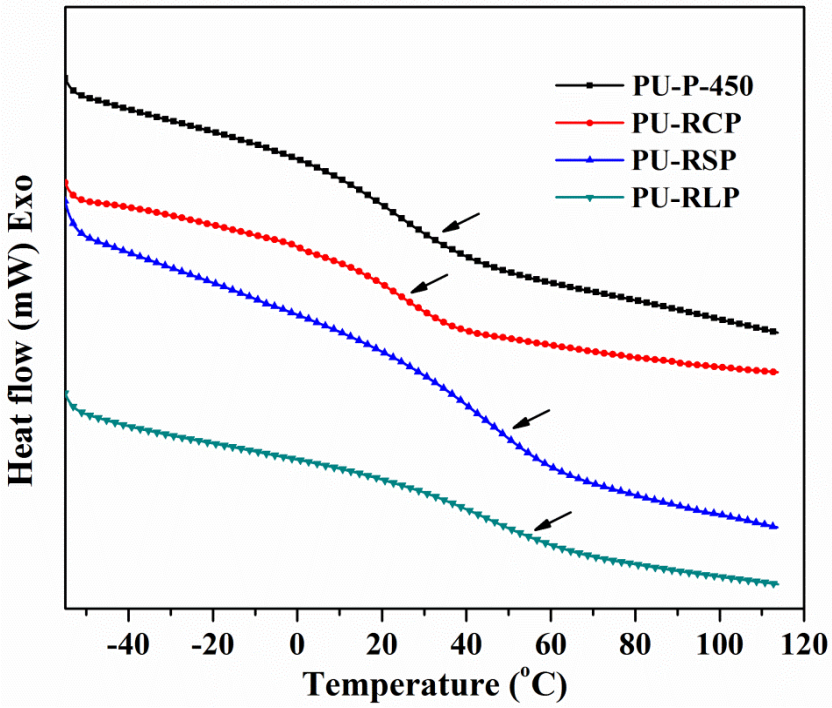

Figure 7-5 DSC scans of PUs (20 °C/min) derived from P-450, RCP, RSP, and RLP.

Table 7-2 Thermal and mechanical properties of PUs based on P-450, RCP, RSP, and RLP.

	DMA T_g (°C)	DSC T_g (°C)	TGA in nitrogen (°C)		Tensile strength (MPa)	Young's modulus (GPa)*	Elongation at break (%)	Toughness (MPa)
			T_{10}	T_{50}				
PU-P-450	69.8	26.6	318	366	19.7±1.7	0.36±0.04	69.3±1.3	8.8
PU-RCP	55.6	23.7	315	347	20.1±0.7	0.42±0.05	90.4±6.7	13.8
PU-RSP	79.7	45.5	313	355	26.1±0.1	0.55±0.08	9.5±2.1	1.64
PU-RLP	97.0	52.3	305	350	35.1±5.9	1.19±0.25	11.9±3.8	4.1

*Modulus calculated from the initial slope of the stress-strain curve

TGA weight loss curves in nitrogen for PU films are shown in Figure 6 and the corresponding data are summarized in Table 7-2. The decomposition of the PUs occurred in three stages: dissociation of the unstable urethane bond between 150 and 330 °C, decomposition of the soft polyol segments between 330 and 400 °C, and the further degradation of fragments produced after the second stage.[26] The OH numbers increased from RCP to RSP to RLP, resulting in an increase in urethane bond formation; therefore, the thermal stability of the respective PUs decreased in the first stage. The thermal stability of PU-P-450 and PU-RCP were similar during

the first stage because of their similar OH numbers. In the second stage, the described cross-linking structure caused by tri-esters in P-450 resulted in a thermal stability of PU-P-450 that was higher than the stabilities of the bio-PUs. PU-RCP exhibited the lowest thermal stability, as reported by others,[27] which may be the result of degradation induced by carbon-carbon double bonds in castor oil fatty acids.

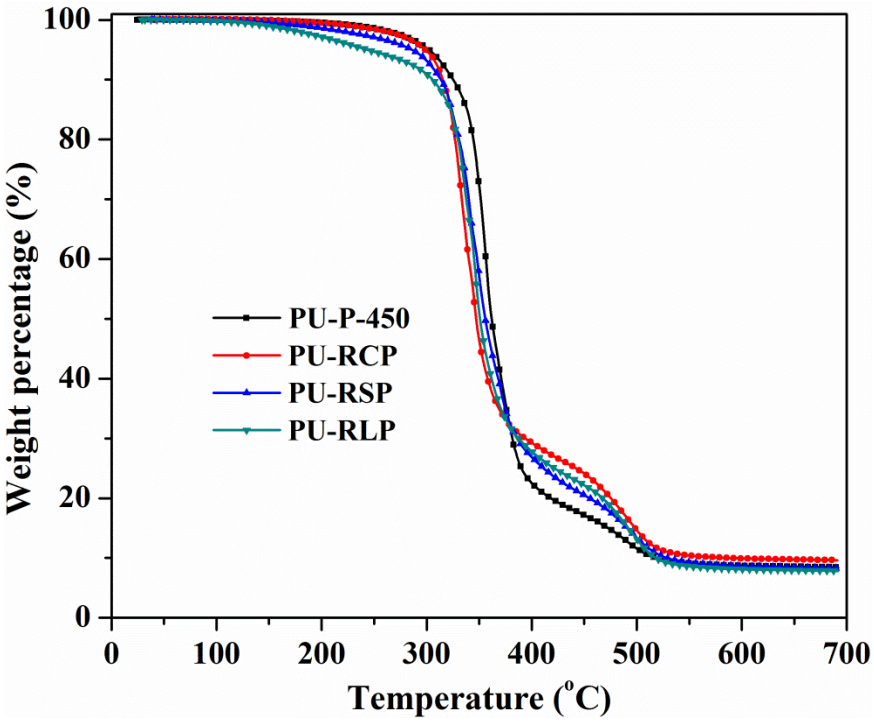

Figure 7-6 TGA weight loss curves in nitrogen for PUs derived from P-450, RCP, RSP, and RLP.

The stress-strain curves of PUs from P-450, RCP, RSP, and RLP are shown in Figure 7-7. Young's modulus, tensile strength, elongation at break, and toughness of PU films are summarized in Table 7-2. The glass transition temperatures for PUs derived from P-450 and RCP determined by DSC indicated that these PUs were in an elastomeric state at tensile testing condition of room temperature, displaying large elongation at break, while PUs derived from RSP and RLP exhibited brittle behavior in the glassy state indicated by their higher T_gs. As the

hydroxyl numbers of RCP, RSP, and RLP increased, the tensile strength of the corresponding PUs increased because of their increasing cross linking density, as discussed in the section on thermomechanical properties. The tensile strength of PUs derived from P-450 and RCP were almost identical because of the similar OH number of their respective polyols. The latter exhibited higher elongation at break because of the flexible chains in RCP, leading to higher toughness of the PU derived from RCP.

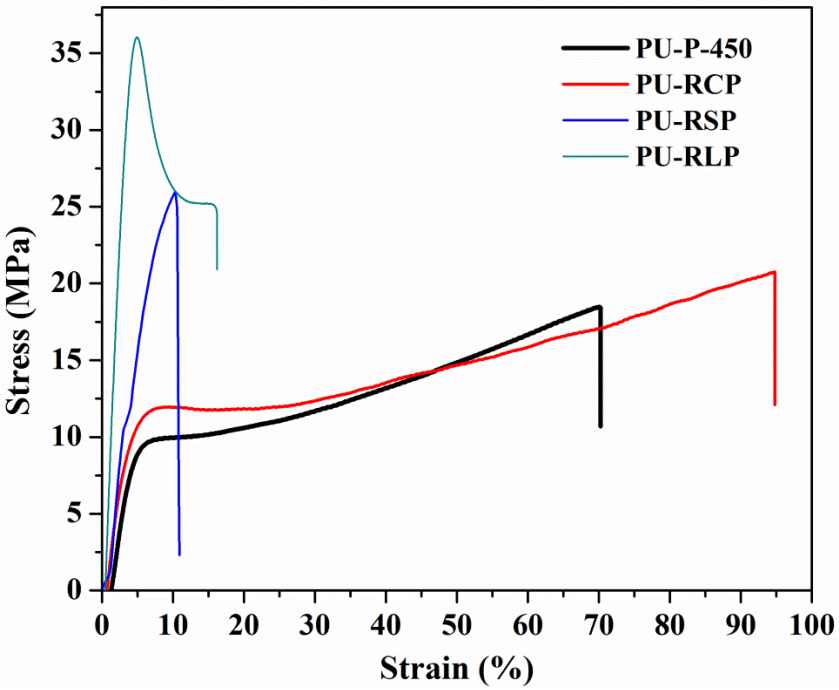

Figure 7-7 Stress-strain curves of PUs derived from P-450, RCP, RSP, and RLP.

7.5 Conclusions

A novel method was developed to prepare polyols for PU application from vegetable oils. The molecular structures of the resulting polyols were characterized and the respective PUs derived from bio-polyols were prepared and characterized. The properties of the PUs of bio-polyols were compared with those of petroleum-based polyol. It was shown that PUs from soybean and linseed oil exhibited higher T_g, tensile strength and Young's modulus and PUs from castor oil exhibited higher elongation at break and toughness than PUs derived from petroleum-based

polyol. However, PUs derived from petroleum-based polyol (P-450) displayed better thermal resistance and storage modulus at high and low temperatures because of their tri-ester structure and terminal functional groups. This new method provides a versatile way to prepare bio-polyols for PUs with promising properties and is expected to partially or completely replace petroleum-based polyols in the PU industry.

7.6 Acknowledgements

All authors would like to give special thanks to Hongyu Cui at the Dept. of Materials Science and Engineering at Iowa State University for her assistance with mechanical testing of the PUs.

Keywords: Biopolymers; polyurethanes; vegetable oil; green monomer; mechanical properties

7.7 References

1. D. P. Pfister, Y. Xia and R. C. Larock, *Chemsuschem*, 2011, **4**, 703-717.

2. Z. S. Petrovic, *Polym Rev*, 2008, **48**, 109-155.

3. M. Ionescu, *Chemistry and technology of polyols for polyurethanes*, Rapra Technology, Shawbury, Shrewsbury, Shropshire, U.K., 2005.

4. M. Desroches, M. Escouvois, R. Auvergne, S. Caillol and B. Boutevin, *Polym Rev*, 2012, **52**, 38-79.

5. B. Nohra, L. Candy, J. F. Blanco, C. Guerin, Y. Raoul and Z. Mouloungui, *Macromolecules*, 2013, **46**, 3771-3792.

6. A. Guo, Y. J. Cho and Z. S. Petrovic, *J Polym Sci Pol Chem*, 2000, **38**, 3900-3910.

7. X. Pan and D. C. Webster, *Chemsuschem*, 2012, **5**, 419-429.

8. C. S. Wang, L. T. Yang, B. L. Ni and G. Shi, *J Appl Polym Sci*, 2009, **114**, 125-131.

9. D. S. Tathe and R. N. Jagtap, *J Am Oil Chem Soc*, 2013, **90**, 1405-1413.

10. Z. S. Petrovic, W. Zhang and I. Javni, *Biomacromolecules*, 2005, **6**, 713-719.

11. U. Biermann, W. Friedt, S. Lang, W. Luhs, G. Machmuller, J. O. Metzger, M. R. Klaas, H. J. Schafer and M. P. Schneider, *Angew Chem Int Edit*, 2000, **39**, 2206-2224.

12. A. Guo, D. Demydov, W. Zhang and Z. S. Petrovic, *J Polym Environ*, 2002, **10**, 49-52.

13. A. Fridrihsone, U. Stirna, B. Lazdina, M. Misane and D. Vilsone, *Eur Polym J*, 2013, **49**, 1204-1214.

14. S. D. Miao, S. P. Zhang, Z. G. Su and P. Wang, *J Appl Polym Sci*, 2013, **127**, 1929-1936.

15. G. Lligadas, J. C. Ronda, M. Galia and V. Cadiz, *J Polym Sci Pol Chem*, 2013, **51**, 2111-2124.

16. X. H. Kong, G. G. Liu, H. Qi and J. M. Curtis, *Prog Org Coat*, 2013, **76**, 1151-1160.

17. G. Lligadas, J. C. Ronda, M. Galia, U. Biermann and J. O. Metzger, *J Polym Sci Pol Chem*, 2006, **44**, 634-645.

18. N. Boechat, J. C. S. da Costa, J. D. Mendonca, P. S. M. de Oliveira and M. V. N. de Souza, *Tetrahedron Lett*, 2004, **45**, 6021-6022.

19. A. Saeed and Z. Ashraf, *J Chem Sci*, 2006, **118**, 419-423.

20. L. Shi, Y. Y. Liu, Q. F. Liu, B. Wei and G. S. Zhang, *Green Chem*, 2012, **14**, 1372-1375.

21. J. Zhang, G. Leitus, Y. Ben-David and D. Milstein, *Angew Chem Int Edit*, 2006, **45**, 1113-1115.

22. E. Balaraman, C. Gunanathan, J. Zhang, L. J. W. Shimon and D. Milstein, *Nat Chem*, 2011, **3**, 609-614.

23. M. D. Phaneuf, M. J. Bide, M. Szycher, M. B. Gale, H. X. Huang, C. Q. Yang, F. W. LoGerfo and W. C. Quist, *Asaio J*, 2001, **47**, 634-640.

24. C. Q. Zhang, Y. Xia, R. Q. Chen, S. Huh, P. A. Johnston and M. R. Kessler, *Green Chem*, 2013, **15**, 1477-1484.

25. J. P. L. Dwan'isa, A. K. Mohanty, M. Misra, L. T. Drzal and M. Kazemizadeh, *J Mater Sci*, 2004, **39**, 2081-2087.

26. E. Hablot, D. Zheng, M. Bouquey and L. Averous, *Macromol Mater Eng*, 2008, **293**, 922-929.

27. I. Javni, Z. S. Petrovic, A. Guo and R. Fuller, *J Appl Polym Sci*, 2000, **77**, 1723-1734.

7.8 Supporting Information

for *Macromol. Rapid Commun.*,

Reduction of epoxidized vegetable oils: A Novel Method to Prepare Bio-based Polyols for Polyurethanes

Chaoqun Zhang, Rui Ding, Michael R. Kessler*

The trace amounts of Li and Al in polyols were directly measured by inductively coupled plasma-mass spectrometry (ICP-MS). They were also indirectly measured by testing the Li and Al in the polyurethane (prepared with the same method discussed in manuscript) using energy-dispersive X-ray spectroscopy (EDS).

1. ICP-MS test

RSP, RLP, and RCP samples were analyzed for trace amounts of Li and Al by ICP-MS. Samples were dissolved in chloroform and extracted with 3% aqueous hydrochloric acid (HCl) in polypropylene 15 mL centrifuge tubes (Corning 430052). HCl was used to ensure the extraction of Al/Li. The 3% hydrochloric acid layer was collected for analysis. Calibration standards were prepared in 3% HCl at Li and Al concentrations of 0.5, 5, and 50 ppb. The standards and samples were analyzed by ICP-MS (Bruker Aurora Elite). The instrument was optimized for maximum sensitivity and minimal oxide and doubly charged ratios ($CeO^+/Ce^+ < 2\%$, and $Ba^{2+}/Ba^+ < 3.5\%$ respectively) (Table 1). Signals for m/z values of Li and Al in the samples were blank subtracted and the concentrations were determined with Li and Al calibration curves created from the standards.

As shown in Table 2, a very small amount of Li and Al was detected in RCP, RSP, and RLP samples. The high standard deviations of the Li concentrations in all three samples are due to the variability in the measured signal at the respective m/z values. The variability of the signal is increased due to the measured values falling near the limit of detection.

Table 1. Instrument parameters for the analysis of Li and Al in RCP, RSP, and RLP samples.

Argon Gas Flow ((L/min))	Plasma	18
	Auxiliary	1.80
	Sheath	0.30
	Nebulizer	0.98
RF Power (kw)		1.40
Sampling Depth (mm)		6.50
Pump Rate (rpm)		5.00

Table 2. Concentrations of Li and Al in RCP, RSP, and RLP samples. (Concentrations calculated from the concentration of the diluted samples measured on the ICP-MS).

	RCP	RSP	RLP
Al (ppb)	27.0 $\pm$ 1.1	110.0 $\pm$ 3.2	51.0 $\pm$ 1.5
Li (ppb)	0.5 $\pm$ 1.1	0.9 $\pm$ 2.9	1.1 $\pm$ 1.4

2. EDS test

The residual aluminum in the polyols (RCP, RSP, RLP) was indirectly studied by determining the elemental composition of the polyurethanes from these polyols using a scanning electron microscope (FEI Quanta 250 FEG) coupled with EDS system (Oxford Instruments Aztec). EDS spectra were collected for 50 seconds at 500× magnification at 10 kV voltage with an output count rate of 12kcps. Three analysis points were tested for every sample as shown in Table 3. From the EDS analyses, a very small amount of aluminum was detected for all three polyurethane samples with a maximum of 0.03 wt%. The aluminum content was even less than that of Sn, which was introduced by the DBTDL catalyst for the polyurethane preparation. This demonstrates that the trace amount of Al in the polyols (i.e. the starting material for the polyurethane) themselves are also very small.

Table 3 EDS analyses results (wt%) on the polyurethanes surface

		C	N	O	Al	Si	Cl	Sn
	1	80.98	6.46	12.37	0.02	0.01	0.06	0.06
PU-RCP	2	80.44	7.32	11.95	0.03	0.01	0.07	0.13
	3	82.34	5.83	11.64	0.00	0.03	0.04	0.08
	1	79.30	6.97	13.45	0.02	0.00	0.13	0.14
PU-RSP	2	79.70	6.60	13.57	0.01	0.02	0.09	0.00
	3	79.64	6.76	13.37	0.00	0.01	0.06	0.16
	1	78.13	7.87	13.75	0.00	0.02	0.10	0.14
PU-RLP	2	78.37	7.51	13.96	0.00	0.02	0.12	0.03
	3	79.13	6.98	13.75	0.02	0.01	0.09	0.01

Overall, we can conclude that the Al and Li in the polyols are only present in negligible amounts. They were largely removed during the work-up process in preparation of the polyols.

CHAPTER 8: IN-SITU SYNTHESIS OF BIO-POLYURETHANE NANOCOMPOSITES REINFORCED WITH MODIFIED CARBON NANOTUBES

A paper to be submitted to Composites Science and Technology

Chaoqun Zhang[a], Danny Vennerberg[a], Michael R. Kessler[a,b]

[a] Dept. of Materials Science and Engineering, Iowa State University, Ames, IA, USA

[b] School of Mechanical and Materials Engineering, Washington State University, Pullman, WA, USA

8.1 Abstract

Bio-polyurethane (PU) nanocomposites reinforced with modified multiwall carbon nanotubes (CNT) were successfully prepared. The surface of CNT was introduced a functional amine group via ozone oxidation followed by silanization. The structure of the modified carbon nanotube was characterized by FTIR, XPS and TGA. The modified CNT was incorporated into polymer network via covalent bondings to prepare PU nanocomposites. The effect of CNT loading on the morphologies, thermo-mechanical, tensile properties of PU nanocomposites were studied. It showed that modified carbon nanotube can be dispersed effectively and improve the interfacial strength between it and polymer matrix. Therefore, the storage modulus, glass transition temperature, the Young's modulus, and tensile strength were increased with increasing CNT loading to 0.8%. When the loading of CNT continued to increase to 1.2%, the properties of the PU nanocomposites decreased because the high amounts of hydroxyl groups in high loading carbon nanotube compete for the isocyanate groups with hydroxyl groups in polyols, leading to decreasing integrity of the PU matrix.

Keywords: Nanocomposite; Carbon nanotube; Polyurethane

8.2 Introduction

Polyurethane (PU) is one of the most versatile polymetric materials with excellent properties [1-3] and has been widely used in industry and daily life as coating, adhesives, foams, and sealants [4, 5]. In order to tailor the properties of PU and endow new functional properties to extend its application, two strategies can be utilized. The first and directly one is by the selection of starting materials (polyols, isocyanates, chain extender) and the ratios of the starting materials. Vegetable oil-based polyols as sustainable building blocks have gained increasing attention worldewide to partially or totally substitute the counterparts from petroleum crude oil and coal [6, 7] because of the increasing concerns toward depletion of nonrenewable resources and environment issues. The structure-property relationships of these novel polyols have been extensively investigated. It is found that the hydrophobic nature of triglyceride structures of vegetable oils render the final PU excellent physical and thermo-mechanical properties [8, 9]. Guo reported that rigid PU foams prepared from methoxylated soybean oil polyol exhibited comparable mechanical, and insulating properties, and better thermal resistance properties than foams from petrochemical feedstocks [10]. Petrovic found that glass reinforced PU composites using Soypolyol 204 derived from soybean oil showed better oxidative and hydrolytic stability than petrochemical based ones [11].

Another strategy to improve the mechanical, thermal, and electrical properties is to incorporation of functional fillers or fibers into PU matrix. For example, short banana fiber (treated and untreated) was used to improve the tensile strength and dynamic mechanical properties of vegetable oil-based PUs [12, 13]. Long glass fiber could improve the physic-mechanical and thermal stability properties of bio-based PU [14]. Attapulgite particle was incorporated in PU matrix to prepare porous materials with a strong dye adsorption function for wastewater treatment [15].

Carbon nanotubes (CNT) have been extensively investigated as reinforcement in various matrixes due to its high aspect ratio, excellent mechanical strength, electrical and thermal conductivity [16, 17]. To increase the interfacial adhesion between CNT and matrix, which is critical for load transfer and overcome the easily aggregates of CNT in matrix, which leads to heterogeneous structure and lowers the mechanical properties of resulting composites, many efforts have been made to explore novel methods to disperse carbon nanotube homogenous throughout polymer matrix. Qian reported the homogenous distribution of 1 wt% multiwall CNT homogenous in polystyrene matrix by a ultrasonic assisted solution-evaporation method and the elastic modulus and break stress of resulted composites increased 36-42%, and 25%, respectively through load transfer across the nanotube-matrix interface [18]. Zhu found that the functionalized CNT using the acid treatment and subsequent fluorination can be integrated into epoxy matrix through strong covalent bonds, resulting in 30% increase in modulus and 18% increase in tensile strength of nanocomposites containing 1 wt% carbon nanotube [19]. Liu reported that CNT functionalized with terminal amino groups dispersed better in low viscosity rubber epoxy resin than in high viscosity glassy epoxy, leading to 28% increase in tensile Young's modulus in rubbery system and no improvement in modulus in glassy system containing 1 wt% CNT [20]. Kuan prepared amine-functioned CNT which was compatible with waterborne PU matrix via ionic bonding, leading to 370% increase in tensile strength of nanocomposites with 4% CNT content [21].

In this paper, the surface of CNT was introduced a functional amine group via ozone oxidation followed by silanization. The amine functionalized CNT could react with isocyanates to form urethane linkage. The residue NCO groups were reacted with castor oil-based polyols to prepare PU matrix. Therefore, castor oil-based PU nanocomposites were prepared through covalent

bonding between polymer matrix and CNT with loading ranging from 0.2 wt% to 1.2 wt%. The effect of CNT loadings on the thermal-mechanical properties of PU composites were investigated and discussed.

8.3 Materials and Methods

8.3.1 Materials

The polyols derived from reduced castor oil (RCP) was prepared by a reported method. Polymeric diphenylmethane-4, 4'-diisocyanate (PMDI, NCO content: 31 wt.%) were provided by Kumho Petrochemical Co. Dibutyltin dilaurate (DBTDL), methyl ethyl ketone (MEK) were purchased from Sigma-Aldrich (Milwaukee, WI). All materials were used as received without further purification.

8.3.2 Fluidized Ozone Treatment and Amine Functionalized of CNT

The oxidation of multiwall carbon nano-tube (o-MWCNTs) was conducted to obtain primarily hydroxyl functionality using fluidized ozone treatment. Briefly, 100 mg of pristine MWCNTs were placed into an empty gas purifier flask, which is shown schematically in Figure 8-1. An O_2/O_3 mixture containing 6% (wt/wt) O_3 was then flushed through the glassware from the lower insertion at a flow rate of 3 scfh, causing the MWCNTs to mix in a partially fluidized state. A porous membrane affixed to the top of the reactor allowed venting of excess gas, which was scrubbed into iodide solution to remove any remaining O_3 before discharging to atmosphere in a fume hood. The MWCNTs were treated for 10-90 min at a relative humidity of about 50%.

The amine functionalization of multiwall carbon nano-tube (s-MWCNTs) with N-(2-aminoethyl)-3-aminopropylmethyldimethoxysilane (ADMS) was shown Figure. Reactions were conducted by dispersing o-MWCNTs in millipore water via bath sonication for 10 min. ADMS were subsequently added to the solution in concentrations of 1.0 wt%. The solution was stirred at

room temperature for 20 min, after which the MWCNTs were filtered and washed copiously with water. The resulting filtrate was heated to 110 ^{o}C in an oven and held isothermally for 30 min to promote condensation of the silanols with hydroxyl groups on the nanotube surface.

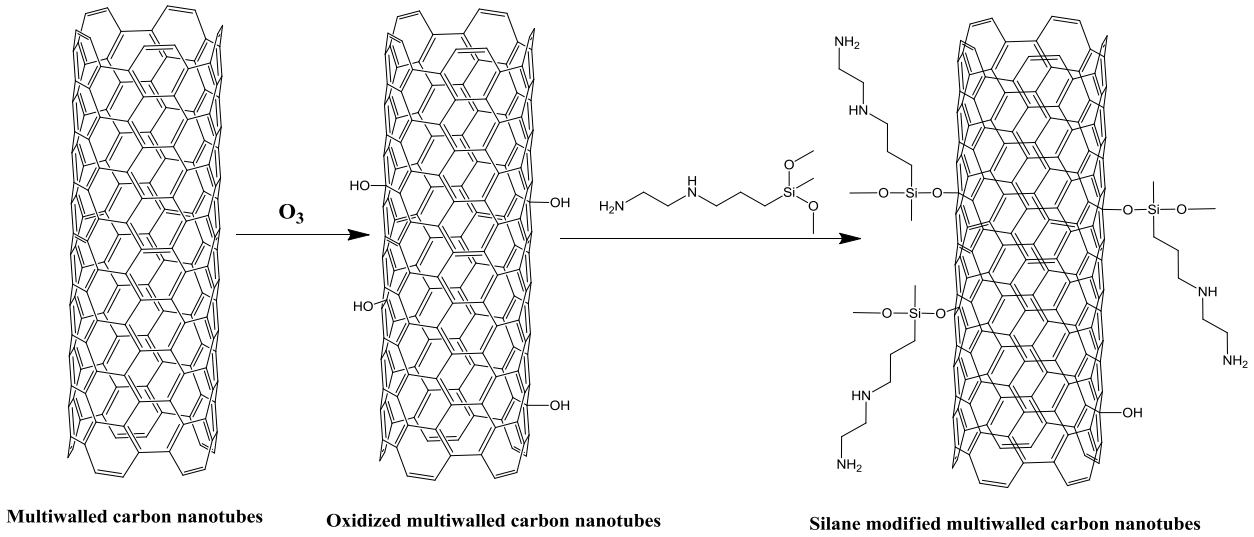

Figure 8-1 Modification of multiwall carbon nanotube

8.3.3 Preparation of PU Composites

The preparation of PU composites was shown in Figure 8-2. s-MWCNTs (0 wt. %, 0.2 wt. %, 0.4 wt. %, 0.8 wt. %, 1.2 wt. %) was charged into MEK in a small vial, and then PMDI was added. The mixture was sonicated at 70 ^{o}C for 1 h. RCP was added into the mixture and the reaction solution was sonicated at 70 ^{o}C for 2 h. The ratio of OH in RCP to NCO in PMDI was fixed at 1:1.1. Then 1% of DBTDL was mixed with the reaction solution in sonication bath for 3 minutes. Finally, the solution was poured into Teflon mold to form a 50 × 50 mm (length × width) sheet and post-cured at 80 °C in an oven overnight. The preparation of PU composites was shown in Figure 2. The resulting PU films were cut into specific dimensions for thermo-mechanical testing.

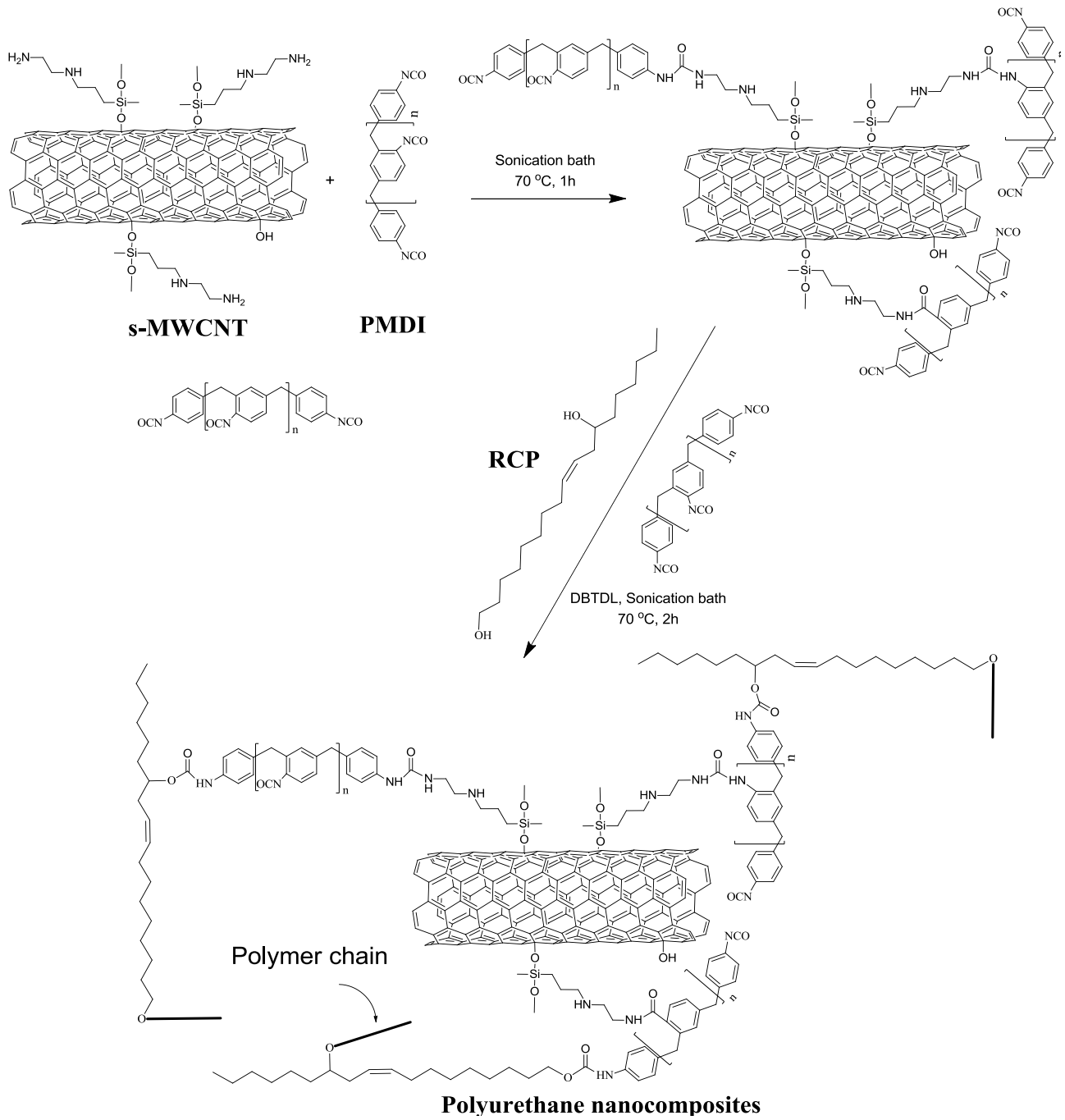

Figure 8-2 Preparation of polyurethane composites

8.3.4 Characterizations

A Nicolet 460 Fourier transform infrared spectroscopy (FTIR) spectrometer (Madison, WI) was used to investigate functional groups in p-MWCNT, o-MWCNT, and s-MWCNT as well as neat PU and PU composites. The samples were prepared by mixing CNT or polymer powders with potassium bromide following by pressed into a pellet using a Michelson interferometer. The element composition on the surface of CNT were measured by X-ray photoelectron spectroscopy (XPS) using a Physical Electronics 5500 Multitechnique system with a monochromatic Al Kα radiation source, and CasaXPS software was employed for data processing. The modification on the surface of CNT was studied by thermogravimetric analysis (TGA, Q50, TA Instruments) in air from room temperature to 700 ^{o}C at 20 C/min heating rate. 6mg samples were used for each test.

The morphology of the fracture surface of neat PU and PU composites were investigated by scanning electron microscope (SEM, FEI Quanta 250 FEG).

Thermal and mechanical properties of the resulting PU films were characterized using a TA Instruments Q800 DMA with a film-tension mode of 1 Hz. Rectangular specimens of 0.4 × 7 mm (thickness × width) were used for the analysis. The samples were cooled and held isothermally for 2 min at –80 ^{o}C before the temperature was increased to 170 ^{o}C at a rate of 3 ^{o}C/min. The tensile properties of the PU films were measured using an Instron universal testing machine (model 4502) with a crosshead speed of 5 mm/min. ASTM standard dog-bone samples were used. Average values of at least three replicates of each sample were taken.

8.4 Results and Discussion

8.4.1 Characterization of Modified Carbon Nanotube

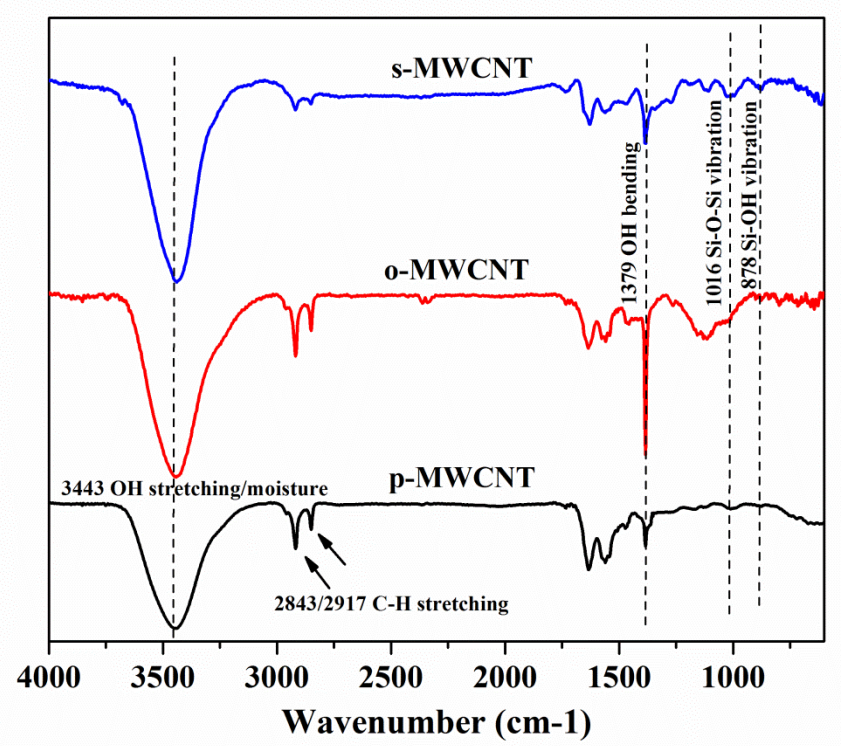

Figure 8-3 FTIR spectra of p-MWCNT, o-MWCNT, and s-MWCNT.

The change of function groups on the surface of carbon nanotube after ozone and subsequent silane treatment was studied by FTIR as shown in Figure 8-3. The broad peak at 3443 cm^{-1} corresponds to OH stretching and ambient moisture absorbed on the surface of CNT. The characteristic of C-H stretching is shown at 2843 and 2917 cm^{-1}. The peak at 1379 corresponding to OH bending increased after ozone treatment and decreased after the following silane treatment. It indicates that the ozone treatment introduced new OH groups on the surface of CNT and the sialne treatment consumed partially the OH groups. The appearance of peaks at 1016 and 878, corresponding to Si-O-Si and Si-OH vibration confirms that the silane was successfully grafted on the surface of CNT.

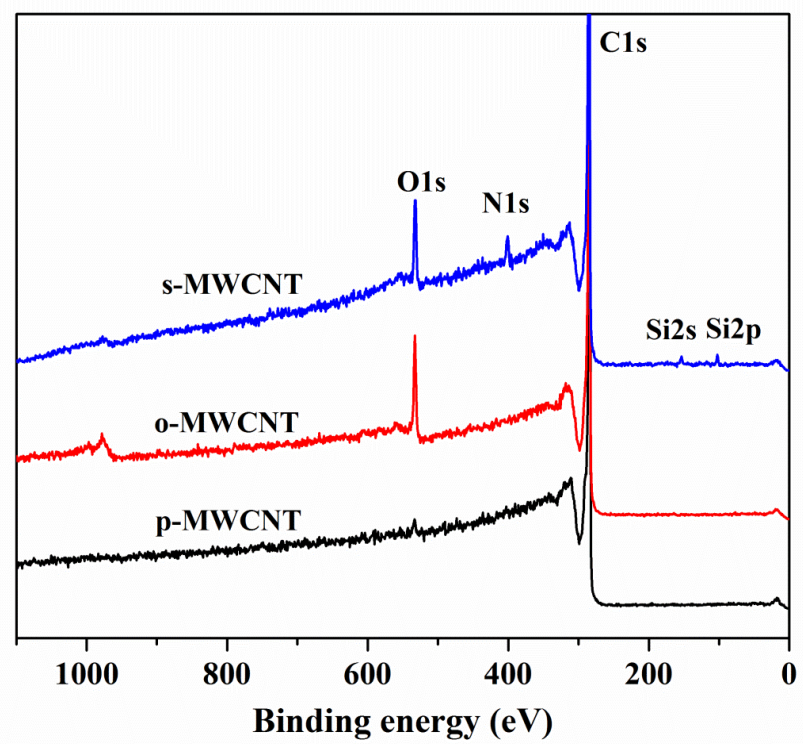

Figure 8-4 XPS survey scans of p-MWCNT, o-MWCNT, and s-MWCNT.

Figure 8-4 shows the survey spectra of p-MWCNT, o-MWCNT, and s-MWCNT. The peaks at 533, 401 286, 154, and 103 eV correspond to O1s, N1s, C1s, Si2s, and Si2p electrons, respectively [22]. Clearly, the intensities of the O1s increase greatly after ozone treatment compared to p-MWCNT. The intensities of O1s decrease while the new peak corresponding to the N1s, Si2s and Si2p appear in the speactra after silane treatment, indicating that the silane molecules successfully grafted to the surface of MWCNT.

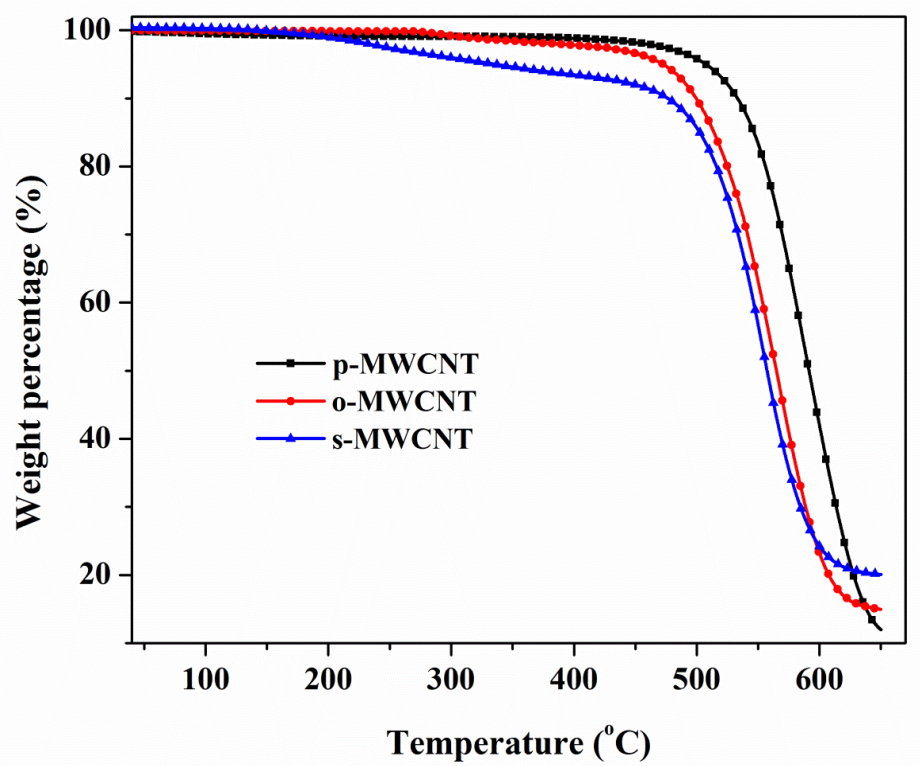

Figure 8-5 TGA weight loss curves of p-MWCNT, o-MWCNT, and s-MWCNT

TGA weight loss curves of p-MWCNT, o-MWCNT, and s-MWCNT are shown in Figure 8-5. p-MWCNT did not show obvious weight loss up to 500 ^{o}C, while o-MWCNT exhibited a minor weight loss due to the decomposition of the associated organic groups [23]. As compared to p-MWCNT and o-MWCNT, The low onset degradation temperature and the rapid degradation behavior in the temperature range of 25-500 ^{o}C of s-MWCNT turned up because of the decomposition of grafted silane. Furthermore, the higher char residue from decomposition of s-MWCNT above 600 ^{o}C also confirmed that the silane was successfully grafted onto the surface of CNT.

8.4.2 Characterization of PU Nano-composites

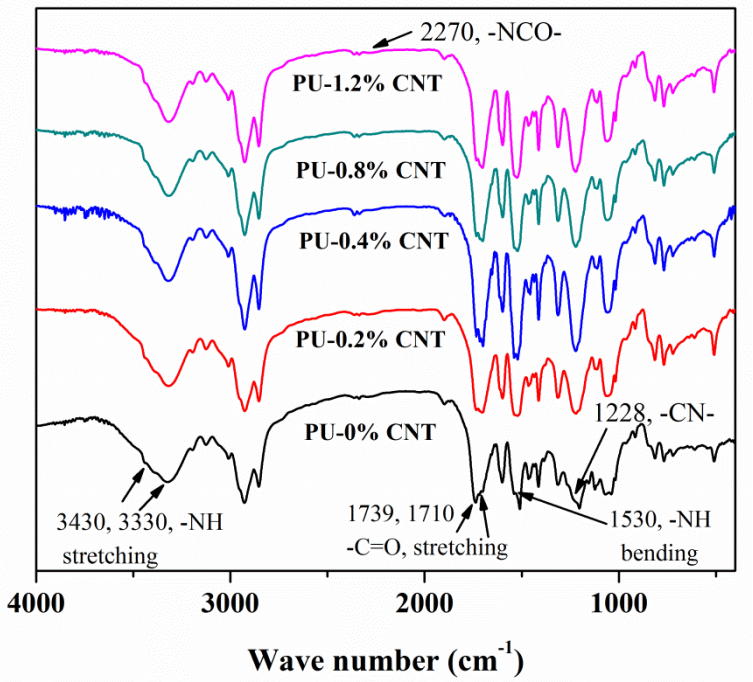

Figure 8-6 FTIR spectra of neat PU and PU nanocomposites

The FTIR spectra of PU nanocomposites are shown in Figure 8-6. The almost disappearance of isocyanate groups at 2270 cm^{-1} indicates that most of NCO groups in PMDI have reacted. Meanwhile, the strong peak of hydrogen bonder –NH (stretching) at 3330 cm^{-1} and very weak peak of non-hydrogen bonder –NH (stretching) at 3430 cm^{-1}indicates that most of the amide groups are involved hydrogen bonding [24]. As the s-MWCNT loading increased, the peaks of PU nanocomposites corresponding to –NH (bonding) at 1530 cm^{-1} and -CH- at 1228 cm^{-1} increased clearly, indicating that the amine groups in s-MWCNT reacted with isocyanate groups [21, 25]. The resulting –NH groups provides more hydrogen bonding sites to –C=O, leading to a decrease peaks of non-hydrogen bonder –C=O at 1739 cm^{-1} and an increase of hydrogen bonder –C=O at 1710 cm^{-1}. This spectrum clearly shows that s-MWCNT has been successfully grafted to PU networks.

Figure 8-7 PU and PU/ s-MWCNT composites

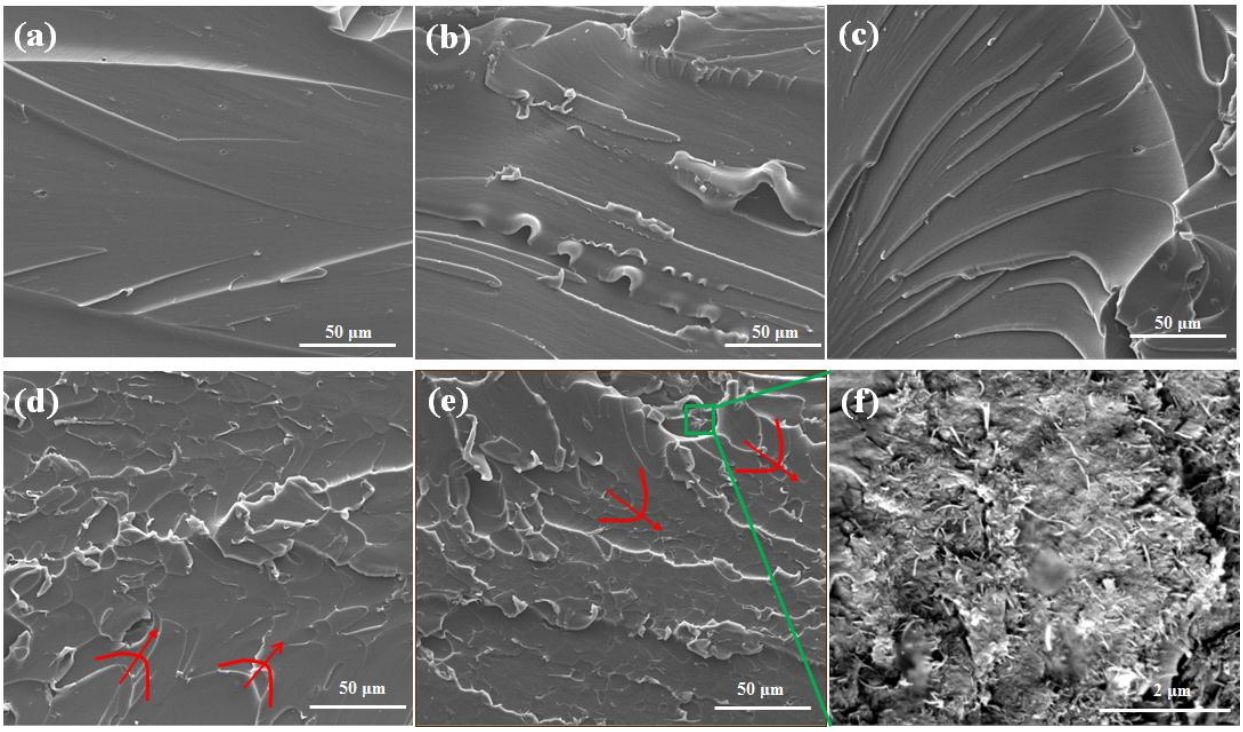

Figure 8-8 SEM images of the fracture surfaces of (a) neat PU, and PU nanocomposites (b) 0.2 wt % s-MWCNT, (c) 0.4 wt % s-MWCNT, (f) 0.8 wt % s-MWCNT, (e) 1.2 wt % s-MWCNT (f) enlarged figures of local area in image (e).

The morphology of PU composites were observed by SEM as shown in Figure 8-8. Neat PU demonstrated a flat fracture surface and showed limited river markings with the shape of linear stripes, indicating a brittle failure. With increasing loadings of s-MWCNT in PU matrix, the density of river markings increased and the river markings curved as arrows showed, indicating the cracks deflected during propagation because of the reinforcing effect of s-MWCNT. As shown in Fig. 8 (f), CNT dispersed homogenous into matrix without any obvious agglomeration.

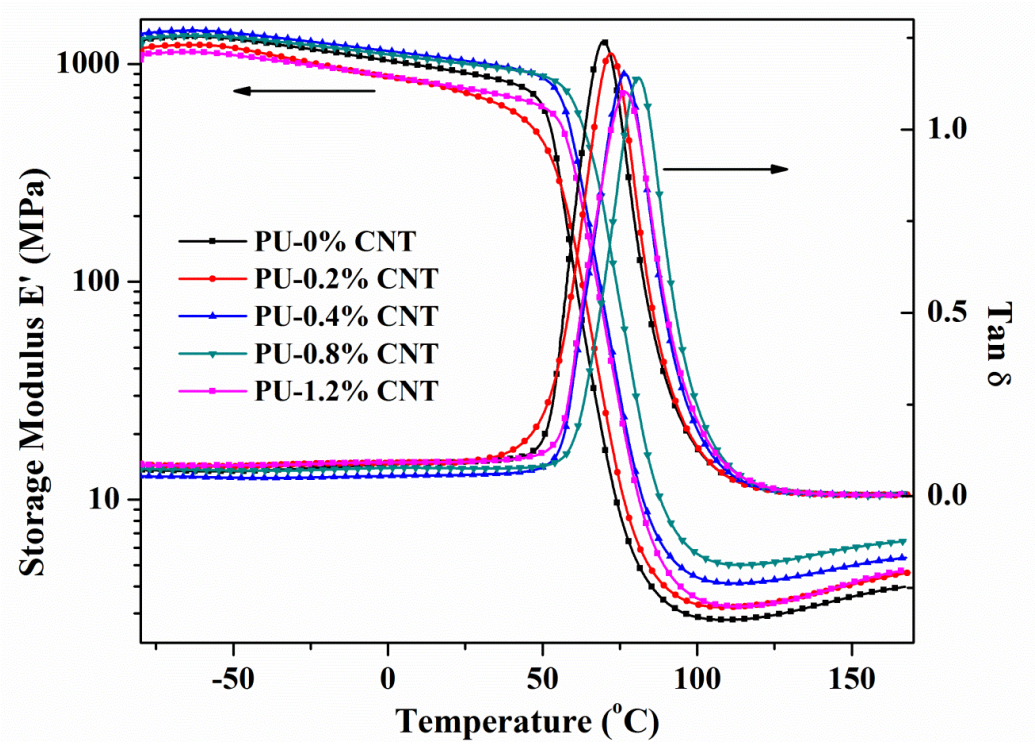

Figure 8-9 Temperature dependence of storage modulus and tan δ for PU and PU/ s-MWCNT composites

The storage modulus and tan δ of PU nanocomposites with different loading of s-MWCNT are shown in Figure 8-9. The T_g associated with α relaxation of PU and nanocomposites determined by the peak maximum of tan δ were shown in Table 8-2. At low temperature, all samples show the glassy state with typical E' values of polymer on the order of 1000 MPa. As temperature

increased, the storage modulus of all samples decreased gradually in the initial stage. After the temperature exceeded the T_g, the storage modulus of all samples shows a very strong decay, indicating PU and nanocomposites transited from glassy to rubber state. As the s-MWCNT loading increased to 0.8%, the storage modulus of PU nanocomposites increased, and then decreased when the loading reached 1.2%. Also, as the s-MWCNT loading increased, the peak of tan δ for PU nanocomposites decreased, indicating increased constraint of polymer chains motion by strong interfacial interactions. The T_g for PU nano-composites first increased and then decreased as the loading of s-MWCNT increased. In the composites, s-MWCNT functioned as the reinforcement and PU served as the matrix. The incorporation of s-MWCNT (low loading) in the PU network stiffened the polymer and constrain the polymer chain, leading to enhanced storage modulus and T_g. However, as s-MWCNT loading exceeded a threshold value and reached to 1.2%, the large amounts amine groups induced by s-MWCNT consume the large proportion of isocyanate and therefore make disconnect of PU matrix and less integrity of the films, resulting in decreased storage modulus and T_g.

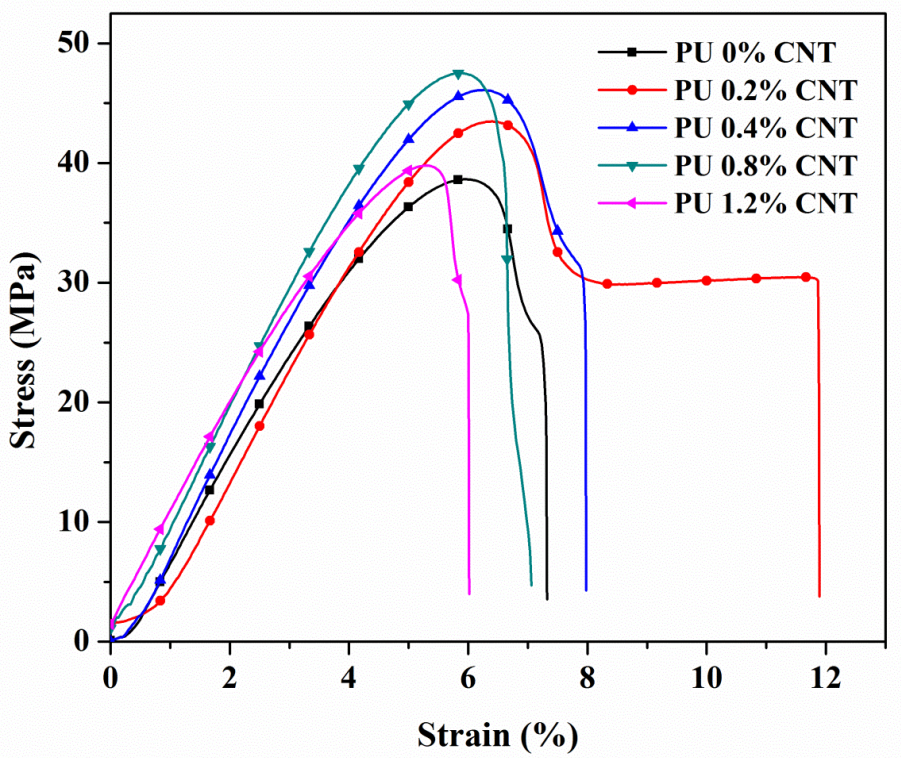

Figure 8-10 Stress-strain curves of PU and PU/ s-MWCNT composites

Table 8-2 Properties of PU nanocomposites

	Storage modulus (MPa) at 60 ^{o}C	T_g from DMA (^{o}C)	Tensile strength (MPa)	Elongation at break value (%)	Young's modulus (MPa)
PU-0% CNT	115	69.6	39.1±0.6	6.5±1.0	1000.8±5.7
PU-0.2% CNT	157	71.9	44.3±1.1	10.6±1.9	1043.5±20.7
PU-0.4% CNT	428	76.6	46.4±0.4	8.0±0.3	1100.4±37.3
PU-0.8% CNT	661	81.0	47.8±0.8	7.0±0.4	1102.8±17.2
PU-1.2% CNT	340	76.7	43.4±3.8	6.3±0.3	1039.3±75.2

Figure 8-10 shows the stress-strain curves of PU and PU/ s-MWCNT composites. The tensile strength, elongation at break value, Young's modulus were summarized in Table 8-2. As s-MWCNT loading increased from 0 to 0.8%, the tensile strength of the nanocomposite films were increased from 39.1 MPa to 47.8 MPa, corresponding to an increase ratio of 22%. Also, the Young's modulus of the nanocomposites films increased and the elongation at break value

decreased. The enhancement of the mechanical properties of PU composites is due to the reinforcing effect of CNT which provide constraints of the polymer chains motion and favors efficient load transfer from matrix to s-MWCNT [26]. However, as the s-MWCNT loading continued to increase to 1.2%, the tensile strength and Young's modulus started to decrease, because the large amounts amine groups induced by high loading s-MWCNT consume the large proportion of isocyanate, leading to disconnect of PU matrix and less integrity of the films, under the condition that the NCO group was fixed at 1.1 times of OH in RCP.

8.5 Conclusions

The surface of CNT was introduced a functional amine group via ozone oxidation followed by silanization. The amine functionalized CNT was incorporated into the castor oil-based PU matrix via strong covalent bondings. It showed that carbon nanotube can be dispersed effectively and improve the interfacial strength between it and polymer matrix. The thermo-mechanical properties (storage modulus, glass transition temperature, the Young's modulus, and tensile strength) of PU nanocomposites were increased with increasing CNT loading to 0.8%. When the loading of CNT continued to increase to 1.2%, the properties of the PU nanocomposites decreased because the high amounts of amine groups in high loading carbon nanotube compete for the isocyanate groups with hydroxyl groups in polyols, leading to decreasing integrity of the PU matrix.

8.6 Reference

1. Z. S. Petrovic, *Polym Rev*, 2008, **48**, 109-155.

2. Y. Xia and R. C. Larock, *Green Chem*, 2010, **12**, 1893-1909.

3. M. Ionescu, *Chemistry and technology of polyols for polyurethanes*, Rapra Technology, Shawbury, Shrewsbury, Shropshire, U.K., 2005.

4. D. P. Pfister, Y. Xia and R. C. Larock, *Chemsuschem*, 2011, **4**, 703-717.

5. L. Zhang, H. K. Jeon, J. Malsam, R. Herrington and C. W. Macosko, *Polymer*, 2007, **48**, 6656-6667.

6. C. K. Williams and M. A. Hillmyer, *Polym Rev*, 2008, **48**, 1-10.

7. M. Desroches, M. Escouvois, R. Auvergne, S. Caillol and B. Boutevin, *Polym Rev*, 2012, **52**, 38-79.

8. Y. S. Lu and R. C. Larock, *Chemsuschem*, 2010, **3**, 329-333.

9. G. Lligadas, J. C. Ronda, M. Galia and V. Cadiz, *Biomacromolecules*, 2007, **8**, 686-692.

10. A. Guo, I. Javni and Z. Petrovic, *J Appl Polym Sci*, 2000, **77**, 467-473.

11. S. Husic, I. Javni and Z. S. Petrovic, *Compos Sci Technol*, 2005, **65**, 19-25.

12. C. Merlini, S. D. A. S. Ramoa and G. M. O. Barra, *Polym Composite*, 2013, **34**, 537-543.

13. C. Merlini, V. Soldi and G. M. O. Barra, *Polym Test*, 2011, **30**, 833-840.

14. J. P. L. Dwan'isa, A. K. Mohanty, M. Misra, L. T. Drzal and M. Kazemizadeh, *J Mater Sci*, 2004, **39**, 2081-2087.

15. K. Dong, F. X. Qiu, X. R. Guo, J. C. Xu, D. Y. Yang and K. C. He, *J Appl Polym Sci*, 2013, **129**, 1697-1706.

16. P. Calvert, *Nature*, 1999, **399**, 210-211.

17. T. Kashiwagi, E. Grulke, J. Hilding, R. Harris, W. Awad and J. Douglas, *Macromol Rapid Comm*, 2002, **23**, 761-765.

18. D. Qian, E. C. Dickey, R. Andrews and T. Rantell, *Appl Phys Lett*, 2000, **76**, 2868-2870.

19. J. Zhu, J. D. Kim, H. Q. Peng, J. L. Margrave, V. N. Khabashesku and E. V. Barrera, *Nano Lett*, 2003, **3**, 1107-1113.

20. L. Q. Liu and H. D. Wagner, *Compos Sci Technol*, 2005, **65**, 1861-1868.

21. H. C. Kuan, C. C. M. Ma, W. P. Chang, S. M. Yuen, H. H. Wu and T. M. Lee, *Compos Sci Technol*, 2005, **65**, 1703-1710.

22. K. Peng, L. Q. Liu, H. C. Li, H. Meyer and Z. Zhang, *Carbon*, 2011, **49**, 70-76.

23. F. A. Abuilaiwi, T. Laoui, M. Al-Harthi and M. A. Atieh, *Arab J Sci Eng*, 2010, **35**, 37-48.

24. Y. S. Lu and R. C. Larock, *Biomacromolecules*, 2008, **9**, 3332-3340.

25. T. L. Wang, C. C. Yu, C. H. Yang, Y. T. Shieh, Y. Z. Tsai and N. F. Wang, *J Nanomater*, 2011.

26. D. X. Yan, L. Xu, C. Chen, J. H. Tang, X. Ji and Z. M. Li, *Polym Int*, 2012, **61**, 1107-1114.

CHAPTER 9: GENERAL CONCLUSIONS

This dissertation presents two novel methods to prepare vegetable oil-based polyols for PU production. The resulting polyurethane films and foams were characterized and compared with that from a petroleum-based polyol. Also, PU nanocomposites reinforced with modified lignin and carbon nanotube were prepared and characterized. These two methods reported in this dissertation provided versatile ways to prepare vegetable oil-based polyols for PUs with promising properties, and, as a result, is likely to be of immediate practical interest to academic researchers, industrial scientists, and engineers. The bio-PU films, foams and nanocomposites may find applications in protective coatings, construction application as a replacement of petroleum-based counterparts.

Firstly, a solvent-free/catalyst-free method to prepare 100% bio-based polyols for PU production were developed by ring opening reaction of epoxidized soybean oil initiated with castor oil fatty acid. Reaction temperature of 170 ^{o}C and reaction time of 7 hs were found to be the optimized parameters to promote the completion of the ring opening reaction. When the stoichiometry of ratios between carboxyl to epoxy groups reached at 0.5:1, the functional groups in ESBO and castor oils fatty acid were totally consumed. In the synthesis, OH groups in COFA and newly formed OH groups were also involved into ring opening reaction with carboxyl group acting as catalyst. It is also found that PU based on the polyols prepared by this method exhibited higher glass transition temperature, tensile strength, and Young's modulus and better thermal stability compared with that from CO and MSOL. Pre-crosslinking in the SCP backbone chain could correspond to the better thermal and mechanical properties of the final PU.

This method was further applied to other vegetable oil systems, resulting in bio-polyurethanes with different crosslinking densities which exhibited a wide range of thermophysical and mechanical properties from soft and flexible elastomer to hard and rigid plastics. Increasing hydroxyl numbers of the polyols resulted in an increase in crosslinking densities of the resulting PUs, leading to increasing glass transition temperatures, Young's modulus, and tensile strength. Also, the value of rate of recovery of PUs, an indication of shape memory property, decreased with increasing crosslinking densities of the corresponding polyols.

Kinetic investigation confirmed that the ring opening reaction between ESBO and COFA included two sub-reactions: acid initiating ring opening, and hydroxyl initiating ring opening. Furthermore, DBU not only accelerated the ring opening reaction and decreased reaction temperature, but also depressed the hydroxyl initiating ring opening, leading to less oligomerization and a homogenous structure. The homogenous structure of polyols prepared with DBU as catalyst increased the glass transition temperature and Young's modulus of final PUs.

The blends of polyols prepared with solvent-free/catalyst-free method (SCP) and a petroleum-based polyol (P-450) were used to prepare PU foams. The dissolution test and Hansen solubility parameters prediction demonstrated that SCP is compatible with P-450 with different ratios in the temperature range of 25-90 ^{o}C. With increasing SCP content, the number of open cells in PU foam increased, the cell size became smaller, the compression strength of PU foam decreased while the thermal conductivity and the thermal stability increased.

Two kinds of chemical modification on lignin molecules were conducted to improve the compatibility of this bio-filler with PU matrix for production of bio-composites. It was shown that lignin modified lignin was better compatible with PU matrix because of the hydrogen bonding and entanglement effects of fillers with PU. The incorporation of lignin compromised the tensile properties of the obtained composites, while it improved the strain properties. Incorporation of lignin urethane did not change the T_g of PU composites significantly, but it greatly improved their dielectric properties.

Another novel method was developed to prepare polyols for PU production by reduction of epoxidized vegetable oils. The ether groups and epoxy groups were reduced into hydroxyl groups that are necessary for polyols. It was shown that PUs from soybean and linseed oil exhibited higher T_g, tensile strength and Young's modulus and PUs from castor oil exhibited higher elongation at break and toughness than PUs derived from petroleum-based polyol. However, PUs derived from petroleum-based polyol (P-450) displayed better thermal resistance and storage modulus at high and low temperatures because of their tri-ester structure and terminal functional groups.

Finally, carbon nanotubes were successfully modified with a functional amine group, which subsequently reacted with isocyanates in PU matrces to form nanocomposite. It is found that with increasing carbon nanotube loading to 0.8%, the storage modulus, glass transition temperature, Young's modulus, and tensile strength of PU nanocomposites were increased. However, when the loading continued to increase to 1.2%, the properties of the PU nanocomposites decreased because the high amounts of amine groups in high loading carbon nanotube compete for the isocyanate groups with hydroxyl groups in polyols, leading to decreasing integrity of the PU matrix.